Institut für Organische Chemie und Biochemie
Lehrstuhl für Biotechnologie

Characterization of the DnaK-DnaJ-GrpE system under oxidative heat stress

Katrin Linke

Vollständiger Abdruck der von der Fakultät für Chemie der Technischen Universität München zur Erlangung des akademischen Grades eines

Doktors der Naturwissenschaften (Dr. rer. nat.)

genehmigten Dissertation.

Vorsitzende: Univ.-Prof. Dr. S. Weinkauf

Prüfer der Dissertation: 1. Univ.-Prof. Dr. J. Buchner
2. Asst.-Prof. U. Jakob, Ph.D., University of Michigan, USA

Die Dissertation wurde am 17.01.2005 bei der Technischen Universität München eingereicht und durch die Fakultät für Chemie am 17.02.2005 angenommen.

Contents

1 Summery

Under heat shock conditions in *E. coli*, a large number of proteins are protected against irreversible heat-induced aggregation by the joint action of the DnaK/DnaJ/GrpE chaperone system. Surprisingly, in an environment of combined heat and oxidative stress, however, the majority of these proteins are no longer protected against aggregation by this chaperone system (1).

We propose that the dramatic decrease in the cellular ATP concentration upon oxidative stress in combination with the elevated temperature conditions causes the reversible inactivation of DnaK. In the absence of bound nucleotides, DnaK's N-terminal ATP binding domain is thermolabile and unfolds at heat shock temperatures both *in vitro* and *in vivo*. After return to non-oxidative stress conditions, cellular ATP levels increase, the N-terminus of DnaK refolds and DnaK's chaperone function is restored. We discovered that a highly conserved cysteine (Cys15) present in the N-terminal ATP binding site becomes exposed and oxidatively modified upon oxidative heat stress treatment. This modification, which locks DnaK's N-terminus in its unfolded inactive conformation, appears not to be important for DnaK's inactivation and reactivation *in vivo.* Substitution of Cys15 by alanine did not influence DnaK's chaperone activity in supporting cells upon exposure to stress and non-stress conditions. Chaperone activity assays performed *in vitro*, however, revealed impaired chaperone activity of the $DnaK_{cys15ala}$ mutant protein.

We show that oxidation of DnaJ *in vitro* causes thiol modification and zinc release of DnaJ's two highly conserved zinc centers. This appears to increase DnaJ's autonomous, DnaK-independent chaperone activity, turning oxidized DnaJ into a very efficient holdase. In contrast, the activity of oxidized DnaJ in cooperation with the DnaK/DnaJ/GrpE refolding machine appears to be impaired. Zinc release studies revealed that oxidation of only one zinc center appeared to be sufficient for the detected shift in DnaJ's activity.

To investigate the function of the two highly conserved zinc centers in DnaJ, we constructed two DnaJ mutants that were separately missing the cysteines of either zinc center I or zinc center II. Our studies revealed that zinc center I plays an important role in the DnaK-independent chaperone activity of DnaJ. Zinc center I mutant proteins show a significantly reduced ability to interact with unfolded proteins and to prevent their irreversible aggregation. At the same time, however, these mutant proteins are fully able to cooperate with DnaK and GrpE in the refolding of denatured substrate proteins *in vitro*. This explains why zinc center I appears to be largely dispensable for DnaJ's *in vivo* function and suggests

that the DnaK-independent chaperone activity of DnaJ can be disconnected from its DnaK-dependent chaperone activity. DnaJ's zinc center II, on the other hand, is crucial for the refolding activity of the DnaK/DnaJ/GrpE chaperone machine *in vitro* and for DnaJ's function *in vivo*. Importantly, zinc center II mutants do not show any defect in substrate binding or inability to stimulate the ATPase activity of DnaK-ATP-substrate protein complexes. Our studies reveal, however, that zinc center II provides a previously unidentified additional interaction site between DnaJ and DnaK-substrate complexes. This interaction appears to be essential for "locking-in" substrate proteins in DnaK, and therefore for the successful refolding of proteins by the DnaK/DnaJ/GrpE foldase machine.

2 Introduction

2.1 About the Ups and Downs of proteins

2.1.1 Protein folding *in vivo*

All known life forms utilize proteins as structural and functional cellular components. The information for *de novo* protein synthesis is encoded in the nucleotide sequences of the corresponding DNA (gene), which is converted by controlled transcription into mRNA followed by translation into proteins. Even though the resulting polypeptide chains are determined by a very specific primary structure, the amino acid sequence, they lack defined structural elements such as α-helices or β-sheets, which are referred to as secondary structure. Adoption of a defined three-dimensional structure, which is based on specific intermolecular amino acid interactions, is crucial for the functionality of most proteins. Only correctly folded polypeptides show their specific activity, reveal stability in the crowded environment of the cell and are able to interact selectively with their native partners.

How a protein matures from an unstructured random coil state to its defined three-dimensional native state is not exactly understood. With the amino acid sequence, a newly synthesized protein contains all necessary information to reach its final conformation (2). Local elements like α-helices and β-sheets can be generated very rapidly and independently from the remainder of the polypeptide (3, 4). These secondary structure elements are stabilized by hydrogen bonding between amide and carbonyl groups of the main chain. This is followed by the formation of three-dimensional structures that are stabilized by long-range interactions. The folding of larger proteins appears to occur in form of independent modules (domains) (5), which undergo long-range interactions to form the correct overall structure (6, 7).

Most of the recent knowledge about protein folding origins from the comparison of computer stimulation data with experimental observations using small proteins as folding models. To better explain the folding scenario, the energy landscape of a folding protein has been described as a folding funnel (8). The surface of the wide funnel opening stands for all the countless possibilities of amino acid interactions in any given unfolded amino acid sequence. Due to the evolutionary particular development of polypeptide chains, only certain contacts between residues are actually favored, leaving a much smaller number of pathways down the now narrower getting folding funnel (5, 9, 8). These particular amino acid

interactions yield in rudimentary, native-like transition states of folding intermediates, also called the saddle points of the folding funnel. Being past that critical region of the energy surface of the folding funnel, only few key interactions within amino acids remain. Are they possible, the protein has passed the quality control and rapidly condenses to its final native structure (10).

In vivo, many proteins are unable to reach their native states without additional help (11-13). In their search for a thermodynamically stable conformation, these proteins end up in slow folding or non-productive, folding intermediates that are trapped in local energy minima. The tendency to remove hydrophobic side chains from the aqueous solution to form a hydrophobic core seems to be a driving force in this process (for review see Ref. 14). Unfolded or incorrectly folded proteins characteristically expose hydrophobic side chains, which have a high tendency to interact with exposed hydrophobic surfaces of other non-native proteins. This yields in the formation of growing protein agglomerates and causes finally the irreversible precipitation of non-soluble protein aggregates. The formation of large deposits of aggregated proteins can impair specific organs or neuronal tissues and has recently been shown to accompany and might even cause diseases like Alzheimers and Parkinson disease, Spongiform encephalitis or type II diabetes (15-18).

2.1.2 Chaperones – Helpers in hard times

Many growing polypeptide chains that emerge from ribosomes need to be protected against the spontaneous and premature hydrophobic collapse as well as against nonspecific interactions with other nascent polypeptides (for review see Ref. 19, 20). Often, only the full-length protein is capable of being folded into the proper active conformation (21). Properly folded native proteins may then encounter similar problems for a second time after their partial unfolding caused by environmental influences like heat shock or oxidative stress. In either case, these non-native polypeptides are prone to irreversible aggregation. To prevent the loss of newly synthesized or damaged proteins, cells have evolved complex machineries, the molecular chaperones (11, 12). The task of chaperones is to prevent protein aggregation and to assist protein folding *in vivo.* Because aggregation is a very concentration dependent process, binding of folding intermediates that expose hydrophobic surfaces is efficient to minimize the otherwise fatal effects of aggregation in cells (22). Controlled binding and release of these folding polypeptides allows then the refolding of these intermediates to the native state. In addition to their function in protein folding, molecular chaperones also participate in other important cellular tasks such as protein translocation, degradation or

protein complex assembly. For all this processes, chaperones need to be able to recognize unfolding proteins and interact with them by controlled substrate binding and release.

The fate of bound substrate proteins depends largely on the type of molecular chaperone. It can either lead to the subsequent refolding of the substrate, to the transfer to other molecular chaperones or to extended interaction with chaperones until conditions improve (for review see Ref. 11). Proteins that are "beyond help" are targeted for degradation by proteases. Based on this, chaperones can be categorized in protein foldases and holdases. Foldases not only bind to non-native proteins and prevent their aggregation but they also provide a folding environment that allows proper folding of the proteins. In the case of the Hsp70 (DnaK) chaperones, this can be achieved, for instance, by the unfolding of incorrect conformations, in which the folding intermediates have been trapped (for review see Ref. 23). Upon substrate release, the unfolded proteins have a new chance to fold properly or, if necessary, rebind to Hsp70 and go through another round of unfolding. Other chaperones like the cylindrical chaperonines of the Hsp60 family (GroEL) (for review see Ref. 14) use a central cavity, which encloses the substrate proteins in a protected hydrophilic environment that allows them to fold (Anfinsen cage). For these processes, foldases require energy in form of ATP. Holdases, on the other hand, work usually ATP independent. They bind to unfolding proteins to prevent their aggregation and maintain a stable chaperone-substrate complex until more favorable conditions are restored. Then, proteins can be released, transferred to foldases for proper refolding (24) or presented to proteases for degradation (25). Here, other factors such as temperature (small heat shock proteins), co-chaperones (DnaJ) or redox conditions (Hsp33) regulate the substrate release (for review see Ref. 26).

2.1.3 The many classes of molecular chaperones

Small heat shock proteins (sHsps) - sHsp are 15 – 42 kDa proteins, which typically assemble into large oligomeric structures of 9 to more than 32 subunits (for review see Ref. 27, 28). Some of these oligomers have been shown to dissociate into suboligomeric species, which represent the actual substrate binding state (for review see Ref. 26, 27). As chaperone holdases, they bind to unfolding polypeptides and prevent protein aggregation. Upon return to non-stress conditions, they provide a pool of substrates available for subsequent refolding by the Hsp70-system (29, 30).

Hsp33 – Hsp33 functions as a chaperone holdase, which uses redox conditions of the environment as regulatory switch (for review see Ref. 32, 31). Once activated by oxidative stress, Hsp33 binds in an ATP independent manner to a large variety of different unfolding

proteins to prevent their aggregation (1). Long-term incubation studies with model substrates showed the efficiency of this chaperone holdase. For substrate release, return to non-stress conditions and availability of the active DnaK-system is necessary. This allows the refolding of substrate by the DnaK-system (for review see Ref. 24).

Hsp60 (GroEL) - GroEL in *E. coli* is a well-investigated member of the Hsp60 family (for review see Ref. 14). It consists of 14 identical subunits that form two stacked rings. Each subunit is characterized by an equatorial ATP binding domain, a central hinge-like domain and an apical substrate binding domain, which harbors a number of highly conserved amino acids (33). The latter are responsible for binding to the substrate proteins as well as for interacting with the co-chaperone GroES. GroES also consists of a ring of 7 identical subunits (34). In the presence of ATP, GroES binds to the GroEL-substrate complex. This causes a significant conformational change in the apical domain of GroEL As a result, ATP is hydrolyzed and the substrate protein is released into the central cavity (35). It remains there for approximately 15 seconds to get a chance for proper folding. ATP binding to the other ring of GroEL causes conformational changes that result in the dissociation of GroES and the substrate (36).

Hsp70 (DnaK) - Members of the highly conserved Hsp70 family are present in prokaryotes and all compartments of the eukaryotic cell, often represented by several homologues. In concert with its co-chaperones DnaJ (Hsp40) and GrpE, DnaK forms a major chaperone machinery that refolds unfolded substrate proteins in an ATP-dependent manner (for review see Ref. 23, 37). In the presence of substrate proteins, DnaJ stimulates ATP hydrolysis by DnaK and triggers conformational changes in the foldase DnaK (38, 39). As a result, DnaK's substrate binding domain has an increased affinity and binds tightly to substrate proteins (40, 41). Substrates remain bound to DnaK with high affinity until the nucleotide exchange factor GrpE replaces ADP by ATP (42). Then, substrates are released and can either refold or undergo a further DnaK-binding cycle. Upon nucleotide exchange and substrate release, DnaK changes back to its low affinity conformation, ready to enter a new cycle. The functional mechanism of this major foldase machine is discussed in detail in chapter 2.3.

Hsp90 (HtpG) – Hsp90 is a very abundant protein (1-2%) in eukaryotic cells and has been shown to be essential for growth in yeast. Its *E. coli* homologue HtpG, on the other hand, is not essential for cell growth and in archaea, no homologue of Hsp90 has been identified (for review see Ref. 43). Hsp90 forms a multi-chaperone complex together with the Hsp70-system and Hop (Hsp70-Hsp90 organizing protein), which is involved in folding and

maturation of key regulatory proteins like steroid receptors, transcription factors and kinases (for review see Ref. 43). There is also evidence that Hsp90 works as molecular chaperone on its own and a growing number of client proteins have been described in the literature (43). Hsp90 comprises of three domains, the N-terminal highly conserved ATPase domain, a middle domain and the C-terminal dimerization domain (44-46). The middle domain is suggested to be involved in nucleotide- and substrate binding, while the dimerization domain connects to chaperone partners and forms the Hsp90 homodimer (47).

Hsp100 (ClpB) – Members of the Hsp100 family catalyze locomotion, unwinding, disassembly and unfolding of macromolecules (for review see Ref. 48). They are AAA+ proteins and form ring-shaped oligomers enclosing domains for target binding and ATP hydrolysis. Sub-stoichiometric amounts of ClpB (Hsp104) together with the DnaK-system have been shown to efficiently catalyze the disaggregation of stable protein aggregates in *E. coli* (49, 50). The authors propose a mechanism by which ClpB is responsible for the initial recognition and binding to the aggregates. This results in the partial unfolding and exposure of new hydrophobic side chains, which can be bound by the DnaK-system for refolding (50). By a similar mechanism, other Clp family members (ClpA, ClpC, ClpX, HslU) appear to stimulate ATP-dependent protein degradation, catalyzed by proteases such as ClpP and HslV.

2.2 Heat shock response and its regulation

Different types of environmental and physiological stress conditions constantly challenge all living organisms. Exposure of cellular polypeptides to such stress conditions may cause their unfolding, often followed by irreversible aggregation. Especially microorganisms have to face a highly variable environment and appropriate reactions are very important. It is, therefore, not surprising that cells have developed a rapid molecular response system that repairs stress-induced damage and protects against further exposure. One of these rapid responses is the heat shock response, which is characterized by the up-regulation of a group of highly conserved proteins, the heat shock proteins (Hsps), that constitute a system for folding, repair and degradation of thermally damaged proteins (51, 52). Despite their name, many heat shock proteins are also induced upon exposure to other environmental stresses besides high temperatures including oxidative stress or viral infection (53). What all of these stress conditions have in common is the accumulation of unfolded proteins in the cell. It has been shown that even small changes in the protein-folding status of the cell can be sensed and converted to the initiation of heat shock protein expression (54). The most important heat shock proteins are molecular chaperones like the small Hsps (IbpA/IbpB),

Hsp60 (GroEL), Hsp70 (DnaK) and Hsp90 (HtpG) (section 2.1.3) or proteases like Clp and FtsH (25).

The heat shock sigma factor 32 (σ^{32}) is the central player in this process. As subunit of the heat shock promoter specific RNA polymerase, it positively regulates the heat shock response on transcriptional level (55,56). When present, σ^{32} forms a complex with the RNA polymerase holoenzyme, which specifically initiates the transcription of heat shock proteins. Because σ^{32} is constitutively expressed in cells, its complex formation with the RNA polymerase under non-stress conditions needs to be prevented. The DnaK chaperone system has been shown to control the availably of σ^{32} by tightly binding to the heat shock transcription factor (57, 58). To maintain an overall low σ^{32} level, DnaK triggers its degradation by FtsH, an ATP-dependent metallo-protease of the AAA+ family (59). The level of heat shock gene expression is therefore indirect controlled by the DnaK-system. During normal growth conditions, the amount of DnaK is sufficient to suppress the heat shock response. In stress situations that lead to the accumulation of misfolded proteins, however, the DnaK-system binds to unfolding polypeptides, titrating away available DnaK (55, 60). That leaves σ^{32} uncomplexed and ready to trigger the heat shock response. This yields in the expression of a large amount of heat shock proteins and molecular chaperones, including the DnaK-system. Once the overwhelming number of non-native proteins is reduced due to Hsp-mediated repair and degradation, the DnaK-system becomes available again, binds to σ^{32} and shuts down the heat shock response (55, 60). In case of non-lethal temperatures, the shut-off phase of the heat shock starts after only five to ten minutes of induction. This makes the DnaK-system a highly sensitive stress indicator that regulates the expression of heat shock genes directly in response to protein misfolding.

2.3 The DnaK/DnaJ/GrpE-system

The DnaK-system, which consists of the heat shock proteins DnaK, DnaJ and GrpE, represents one of the major chaperone machineries in the cytosol of *E. coli*. Similar to its eukaryotic homologues Hsp70, Hsp40 and Mge1p/Bag-1, it is involved in important cellular processes including protein folding, translocation, degradation as well as assembly and disassembly of protein complexes (for review see Ref. 11, 23).

Surprisingly, DnaK and its co-chaperones appear not to be essential for the cell under normal growth conditions (61, 62). Backup-systems seem to compensate for the activity of the DnaK-system and only upon exposure of cells to stress conditions such as elevated

temperature does the chaperone machine become indispensable for the cell (63). Triggered by increased levels of unfolding polypeptides, the DnaK-system indirectly induces the heat shock response and thereby its own up-regulation (section 2.2).

2.3.1 The molecular chaperone DnaK

DnaK was originally discovered because of a mutation in one of the λ-replication genes (λP) that was suppressed in a *dnaK* deletion strain (64). Further investigations revealed that DnaK supports the replication of λ-phage by dissociating a complex consisting of λP, λO, DNA helicase DnaB and λ*ori*. Release of λP results in free helicase DnaB, which is now able to unfold the DNA double helix (64), thereby initiating replication.

DnaK functions as an ATP-dependent molecular chaperone. It possesses a low intrinsic ATPase activity (65) and its nucleotide state plays a crucial role in the regulation of DnaK's activity (for review see Ref. 23). In the ATP-bound state (T-state), DnaK reveals a fast rate of substrate binding and release and, therefore, a low affinity for target polypeptides. ATP hydrolysis by DnaK, which is accelerated by the interaction with the co-player DnaJ and substrate proteins, changes DnaK's conformation (38, 39). The resulting ADP-bound state (R-state) shows a significantly higher substrate affinity and lower on/off rates, which enables DnaK to stably bind to unfolding proteins (40, 66). The nucleotide exchange factor GrpE initiates the replacement of ADP by ATP, which triggers substrate release and prepares DnaK for a new cycle of substrate binding and release (67).

DnaK is composed of two functional domains, the N-terminal highly conserved 42 kDa ATPase-domain and the C-terminal variant 25 kDa substrate-binding domain (Figure 1). The X-ray structure was solved for both domains independently and provided together with mutation studies important insights into DnaK's function (69, 70). The ATPase domain (amino acids 1-385) of DnaK binds ATP with a very high affinity (K_d = 1 nM) in a K^+ and Mg^{2+} dependent manner (Figure 1B) (71). It consists of two large domains I and II, each of which is composed of two subdomains. While IA and IIA lie at the base of the deep nucleotide-binding cleft, IB and IIB make up the sides of the nucleotide-binding site (69). DnaK's substrate binding domain (amino acids 393-638) consists of two structural elements: an 8-stranded antiparallel β-sandwich with the hydrophobic central substrate-binding pocket (amino acids 393-537) and the α-helical lid domain (amino acids 509-638) (Figure 1C) (70). Both elements contribute to the stability of the DnaK-substrate complex in DnaK's ADP-bound state (68). The substrate-binding cavity is formed by two pairs of inner and outer loops

and protrudes upwards from a β-sandwich (70). The lid opens and closes continuously via a hinge region (amino acids 536-538) in both ATP and ADP-liganded states of DnaK. However, the transition between the closed and opened cavity is much faster in the ATP-bound state, which is the reason for the observed higher on/off rates of substrate binding (68). The activities of both ATPase domain and substrate binding domain are coupled and ligand-induced conformational changes are transmitted between the domains. While ATP binding to DnaK's N-terminus triggers rapid substrate release by the C-terminal peptide-binding domain, DnaK's ATP hydrolysis is stimulated by substrate binding.

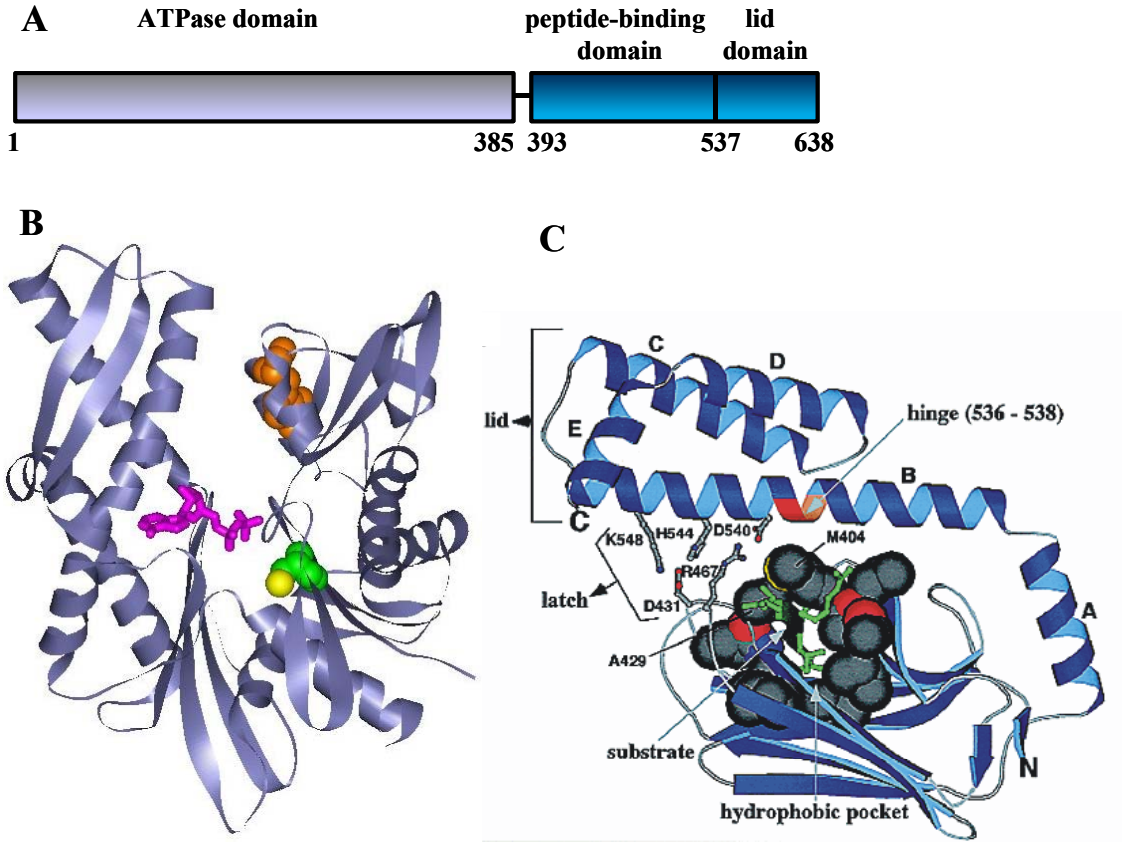

Figure 1 Structure of DnaK

A. Schematic domain structure of DnaK. B. Structure of the N-terminal ATPase domain of the DnaK homologue Hsc70 with bound ATP (pink). Shown in green/yellow and orange are the only cysteine and tryptophan residues, respectively. The image was created using PyMOL. C. Structure of the C-terminal polypeptide-binding domain of DnaK with a bound peptide shown in green (from Ref. 68). Important amino acids for substrate binding are emphasized in space-filling representation (C in gray, N in blue, O in red and S in yellow). The five helices that constitute the lid are marked A–E.

2.3.2 The molecular chaperone DnaJ

DnaJ, the Hsp40 homologue in *E. coli*, plays an essential role as co-chaperone in the DnaK/DnaJ/GrpE system. DnaJ is crucial for many cellular processes including protein

folding, translocation and degradation. Deletion or mutation of the *dnaJ* gene leads to bacterial growth arrest at heat shock temperatures, demonstrating a functional role of DnaJ in the protection against heat stress (72). As part of the DnaK-system, DnaJ interacts directly with substrate proteins, transfers the substrates to DnaK and is responsible for the stimulation of DnaK's ATPase activity, which results in DnaK's conversion into its high affinity binding state (66, 73, 74). DnaJ possesses furthermore autonomous chaperone activity *in vitro*. As a holdase, it binds tightly to unfolding proteins, thus preventing their irreversible aggregation *in vitro* (75).

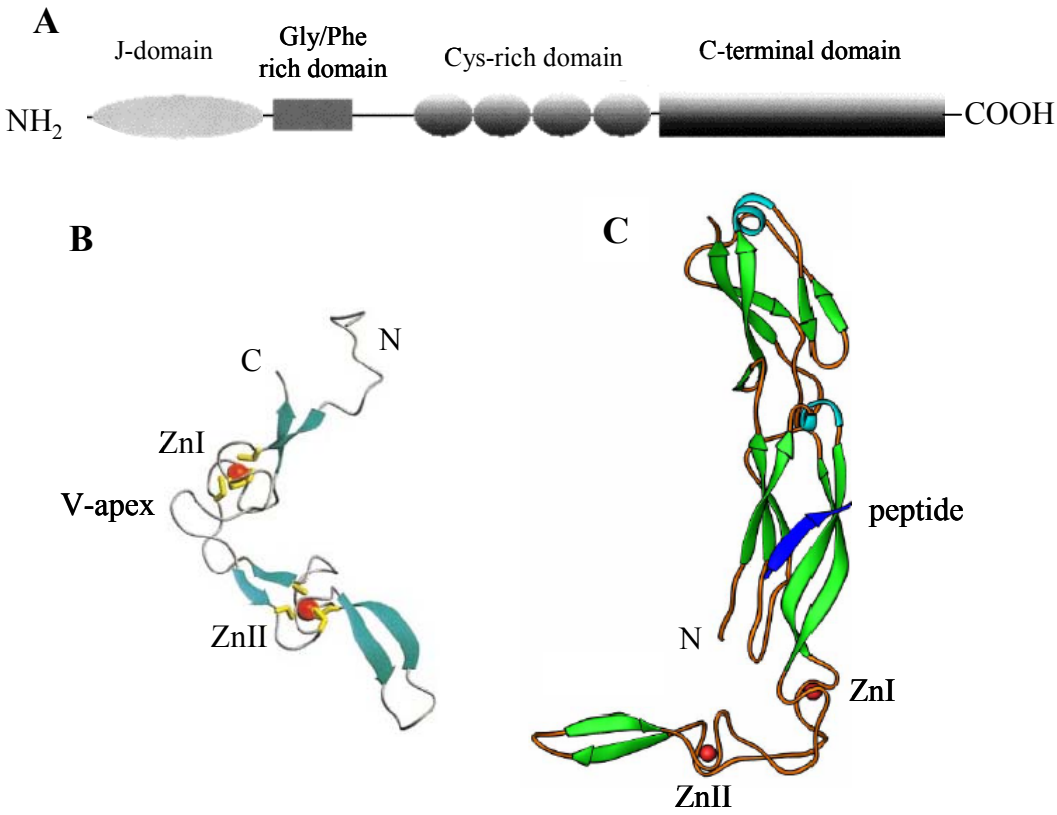

Figure 2 Structure of DnaJ

A. Schematic domain structure of DnaJ. B. Ribbon diagram of the structure of DnaJ's cysteine rich domain (from Ref. 83). β-strands are shown as blue arrows, the zinc atoms as red spheres and the cysteine residues as yellow sticks. The two zinc clusters ZnI and ZnII are labeled. C. Structure of the DnaJ homologue Ydj1p in yeast (from Ref. 4). Ydj1p is shown in complex with the peptide GWLYEIS (red) in ribbon drawing. α-helices are shown in light blue and the β-strands are shown in green. Zinc center I and II are labeled and the zinc ions are shown in dark blue spheres.

Monomers of the homodimer DnaJ are structured into four domains, a N-terminal J-domain, followed by a G/F motif, a zinc binding domain and a C-terminal domain (Figure 2). Only full length DnaJ is able to work cooperatively with the DnaK-system in refolding of non-native proteins (76, 77). Based on their domain composition, Hsp40 homologues are

grouped into three classes. Class I homologues contain all four domains. Class II homologues lack the central zinc binding domain but harbor two C-terminal domains instead. Hsp40 homologues that have only the J-domain in common belong to the class III homologues.

The J-domain (amino acid 1-76 in DnaJ) is the signature motif of all Hsp40 homologues (78). It contains the absolute conserved tripeptide His-Pro-Asp, which has been shown to be a crucial interaction site with DnaK's ATPase domain (79-81). The DnaJ259 mutant protein, which harbors a point mutation in this sequence (His33Gln), has been shown to be unable to stimulate ATP hydrolysis of DnaK and, therefore, DnaK's binding to substrate proteins (82). In class I and II Hsp40 homologues, the so-called G/F motif (amino acid 77-107 in DnaJ) is located directly downstream of the J-domain. The name reflects the high content of glycine and phenylalanine residues in this conserved sequence (77). The G/F motif is essential for the maximal stimulation of DnaK's ATPase activity and the subsequent conversion of DnaK into its high affinity binding state *in vitro.* It has also been shown to be required for the down regulation of the heat shock response *in vivo* (73, 77).

The zinc binding domain (amino acids 144-200 in DnaJ), also referred to as the cysteine rich (CR) domain, is characterized by four repeated Cys-X-X-Cys-X-Gly-X-Gly motifs that are invariable to all class I homologues (83, 85). These highly conserved cysteine residues are involved in the coordination of two zinc ions per DnaJ monomer. Each zinc center is formed by four thiols that tetrahedrally coordinate one zinc ion (76, 86). Lacking structural data, it was originally assumed that the two zinc centers in DnaJ are formed by the two adjacent cysteine motifs. Recent NMR structure data of the isolated cysteine rich domain revealed, however, that zinc center I is formed by cysteine motif 1 (Cys144, Cys147) and cysteine motif 4 (Cys197, Cys200) while zinc center II is formed by cysteine motif 2 (Cys161, Cys164) and cysteine motif 3 (Cys183, Cys186) (Figure 2) (83). The two zinc centers I and II form the "wings" of a V-shaped structure. Two antiparallel β-strands form the outside of each zinc center. In zinc center II, the β-strands are connected by a β-hairpin loop, while in zinc center I the N-and C-terminal strands approach each other to form the β-strands (83). The zinc binding domain and the less conserved C-terminus have been suggested to be involved in substrate binding (76, 87). While the deletion of the CR-domain did not affect the DnaJ-induced acceleration of DnaK's ATP hydrolysis, it blocks the conformational transition of DnaK into its high affinity binding state (86).

2.3.3 Mechanism of the DnaK/DnaJ/GrpE-system

Several models have been proposed in order to describe the mechanism of the DnaK-system and the involved interactions of DnaK with its co-chaperone and substrate proteins. One model suggests that DnaK binds to unfolding polypeptides independently of DnaJ (68, 88) while the other model favors DnaK's binding via a preformed DnaJ-substrate complex (38, 66, 89). A targeting action of DnaJ has been suggested also by the observation that DnaJ shares its substrate-binding motif with DnaK and has high substrate affinity (90). DnaJ might bind substrates that DnaK is unable to bind on its own and might subsequently present it to DnaK. More recent investigations showed that DnaK's intrinsic affinity for substrate proteins is crucial for its chaperone activity and that both chaperones bind simultaneously to the same polypeptide chain. Proximity of the co-chaperones would then facilitate the interaction between the J-domain and DnaK's ATPase domain (88). The interaction of the highly conserved tripeptide His-Pro-Asp of DnaJ's J-domain with the ATPase domain of DnaK leads then to the acceleration of DnaK's ATP hydrolysis and to the conversion of DnaK into the high affinity binding state for unfolding polypeptides (40, 41). The cleavage of γ-phosphate by DnaK is therefore controlled by the simultaneous presence of DnaJ and substrate.

Binding of polypeptides into the hydrophobic cavity of DnaK's C-terminal substrate binding domain involves inter-domain communication with the N-terminal ATPase domain of DnaK (91). It has been shown that the 13 amino acid long linker region between both domains is responsible for this communication, because DnaK mutant proteins with point mutations in this sequence are not able to hydrolyze ATP when exposed to substrate proteins and DnaJ (92). After ATP hydrolysis and substrate binding by DnaK, DnaJ dissociates from the DnaK-substrate complex. The stable binding of ADP-DnaK to polypeptides is maintained until GrpE induces the nucleotide exchange and, therefore, the transition to the low affinity state (T) (42). DnaK is immediately ready to start a new cycle of substrate binding of either the same polypeptide or a different non-native protein (Figure 3).

Interestingly, certain eukaryotic Hsp70-systems do not require a nucleotide exchange factor. Because DnaK and Hsp70 possess different nucleotide binding and hydrolysis properties, ADP release is the rate-limiting step for the prokaryotic DnaK-system (39), while ATP hydrolysis appears to be the rate-limiting step in eukaryotic Hsp70-systems (93, 94). This makes a nucleotide exchange factor obsolete. So far, an eukaryotic GrpE homologue has only been found in yeast mitochondria (Mge1p) (95). The eukaryotic protein Bag-1 has been

shown to possess nucleotide exchange activities although it lacks sequence homology with GrpE (96).

To assist the refolding of newly synthesized proteins *in vivo*, the DnaK-system cooperates with the ribosome associated peptidyl cis-trans-isomerase trigger factor (TF) (97, 98). TF binds to emerging nascent polypeptide chains and prevents their premature incorrect folding. Once protein translation is completed, TF transfers the bound polypeptides to the DnaK-system for chaperone assisted folding.

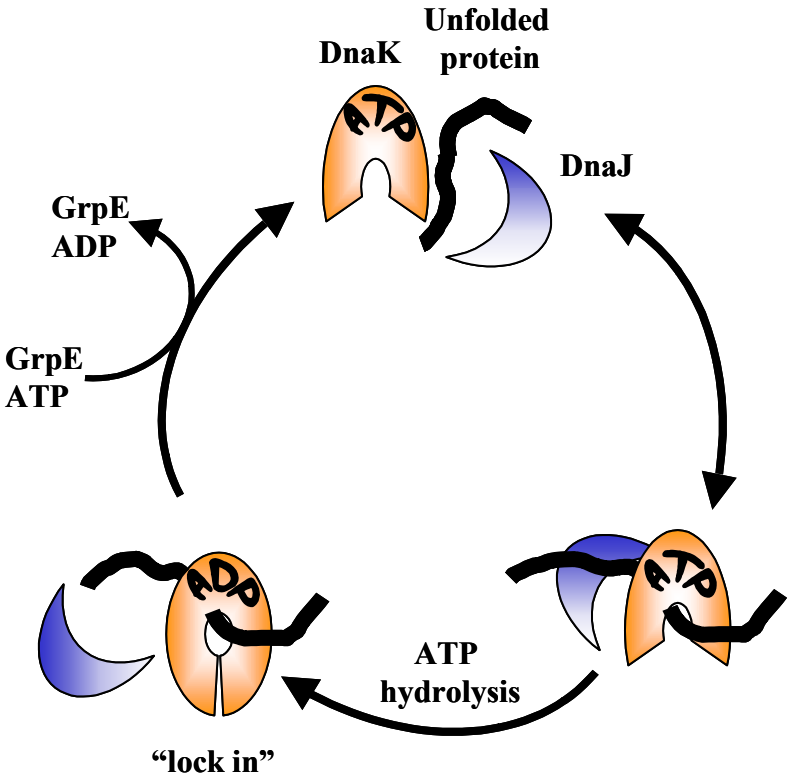

Figure 3 The refolding cycle of the DnaK-system

DnaK in its ATP-bound state possesses low substrate-binding affinity. Simultaneous interaction of DnaK-ATP with DnaJ and unfolding proteins accelerates DnaK's intrinsic ATPase activity. Hydrolysis of ATP leads to major conformational rearrangements. DnaK-ADP has a higher substrate affinity and is able to lock unfolded polypeptides in its substrate-binding cavity. The nucleotide exchange factor GrpE then exchanges ADP with ATP and unlocks DnaK.

2.4 Aerobic life and oxidative stress

In addition to stress caused by extreme temperatures, cells are also endangered by a variety of other stress conditions. All aerobic living organisms, for instance, are constantly exposed to the toxic byproducts of respiration and other oxidation reactions. These so-called reactive oxygen species (ROS) represent a major risk for cells because of their ability to

damage proteins, nucleic acid, lipids and other macromolecules (for review see Ref. 99). Superoxide anions (O_2^-) oxidatively destroy iron-sulfur-clusters of proteins. This not only affects the activity of the damaged protein but also frees iron, which in turn is able to react with hydrogen peroxide (H_2O_2) to form hydroxyl radicals (•OH) via the Fenton reaction (100). Hydroxyl radicals directly damage most biomolecules and cause side chain oxidation, disulfide bond formation, thermal instability and finally protein aggregation (101) (Figure 4).

Even though evolution has selected for protein structures that are relatively well protected against oxidation (102), ROS can cause thiol-modification and nonspecific disulfide bond formation, which often leads to irreversible protein damage (99). Hydrogen peroxide (H_2O_2) can oxidize thiols to sulfenic acid (R-SOH), which is relatively unstable and is then further oxidized to sulfinic acid (R-SO_2H) and sulfonic acid (R-SO_3H). Additionally, sulfenic acids will attack vicinal thiol groups and form non-native disulfide bonds in polypeptides (103) (Figure 4). Similarly, reactive nitrogen species like nitric oxide (NO) or peroxynitrite (NO_3) can oxidize exposed thiol residues to S-nitrosothiol (R-SNO) and S-nitrothiol (R-SNO_2), respectively.

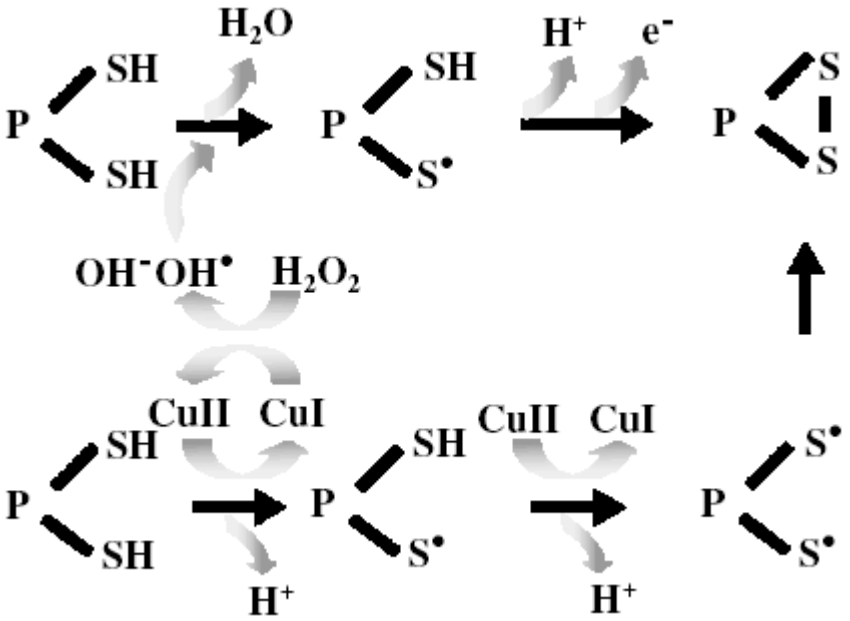

Figure 4 Thiol modification induced by Fenton reaction (32)

Transition metals like Cu(I) or Fe(II) are able to cleave hydrogen peroxide (H_2O_2) via the Fenton reaction. The resulting hydroxyl radicals then attack thiol groups and form the even more reactive thiyl radicals that quickly form intra- and intermolecular disulfide bonds with other thiol groups. What feeds this vicious cycle is the direct reaction of oxidized Cu(II) and Fe(III) with thiols, a reaction that regenerates the Fenton reagents while forming more thiyl radicals on cysteines.

Not surprisingly, organisms have evolved systems to eliminate ROS and repair the damage. Enzymes such as catalase, peroxidase and superoxide dismutase are highly efficient to degrade ROS or to convert them into less aggressive molecules (104). Furthermore, redox buffers comprised of the glutathione system as well as redox balancing systems such as the thioredoxin-system help to maintain the reducing environment of the cytosol and reduce non-native disulfide bonds *in vivo* (for review see Ref. 105). The thioredoxins Trx1 and Trx2 are able to reduce disulfides by direct thiol-exchange reactions. Oxidized thioredoxin is restored by thioredoxin reductase (TrxB), which in turn withdraws electrons from NADPH (106). The redox buffer in the cytosol is comprised of oxidized and reduced glutathione, which is a very abundant molecule (cellular concentration 5 mM). The ratio of the reduced (GSH) to the oxidized (GSSG) glutathione species is 200:1 under normal conditions in the cytosol (107). This translates into a redox potential of –260 to –280 mV (108). GSH reduces disulfides by attacking a protein disulfide and forming a mixed disulfide intermediate. This is resolved by one of the glutaredoxins Grx1-3. The glutathione oxidoreductase (GOR) ensures a constant GSH:GSSG ratio (109).

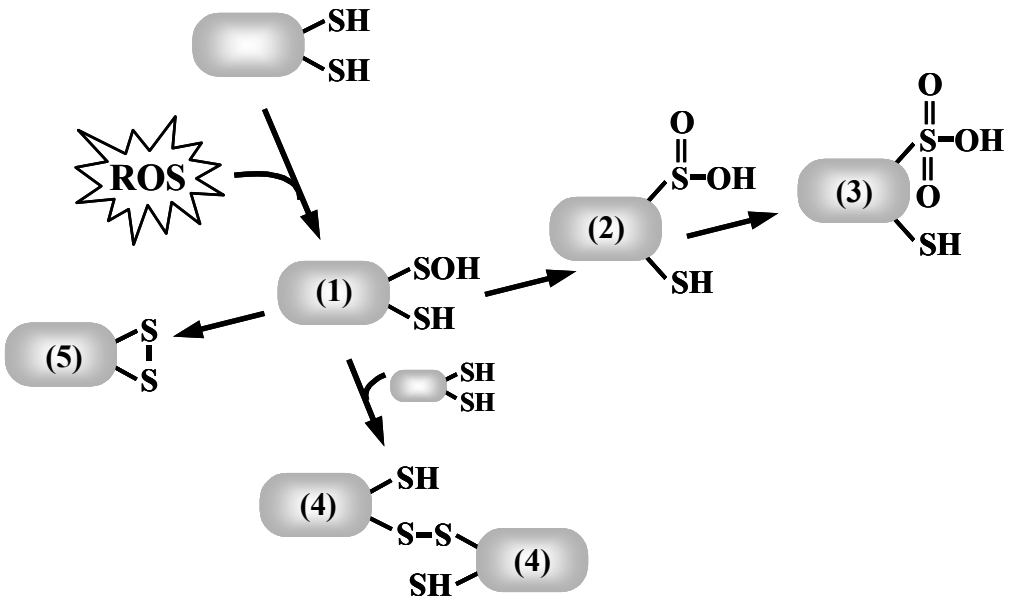

Figure 5 Chemical modifications of cysteine residues

Oxidation of cysteine residues in proteins by ROS leads to the formation of sulfenic acid (1), which can react further to sulfinic acid (2) and sulfonic acid (3) derivatives. Reaction of sulfenic acid (1) with thiol groups in the vicinity can furthermore result in intermolecular (4) or intramolecular disulfide bond (5).

The production and removal of ROS is well balanced under normal physiological growth conditions and prevents the accumulation of unwanted disulfide bonds in cytosolic proteins. However, when ROS-reducing systems are no longer able to sufficiently eliminate

ROS, the ROS concentration raises and the cells reach a state of oxidative stress (110). This can be due to environmental influences or cellular defects. Activated macrophages and neutrophiles, for instance, release high concentrations of superoxide as a first line of defense against invading pathogenic bacteria (111). The combined activity of NADPH-oxidase and myeloperoxidase in neutrophiles leads to the production of hypochlorous acid (bleach), which is one of the strongest physiological oxidants and a powerful antimicrobial agent (112, 113). Exposure of cells and organisms to such harsh oxidative stress conditions induces a very efficient cellular defense system, the oxidative stress response. In *E. coli*, the redox regulated transcription factors OxyR and SoxR are mainly responsible for the induction of the oxidative stress response (for review see Ref. 114, 115). They are able to sense hydrogen peroxide and superoxide anion, respectively, and respond with the induction of their target genes (section 2.4.1). This leads then to the rapid overexpression of ROS scavenging molecules as well as chaperones, proteases and DNA repair enzymes (116-118). Catalase and glutathione peroxidase, for instance, detoxify hydrogen peroxide by converting it into water, while a 11-fold higher rate of proteolysis ensures the fast removal of oxidatively damaged aggregation prone proteins (119). This combined action of various proteins enables cells to quickly restore the original redox state, the redox homeostasis, after temporary exposure to ROS. In aging cells, ROS accumulates due to increasing failure of antioxidant systems (120). Here, the redox homeostasis is not lost but shifted towards more oxidizing conditions. Such constantly elevated levels of free radicals have been shown to accompany numerous diseases such as Alzheimers disease, diabetes and cancer (121, 122).

2.4.1 Redox regulation of protein activity

While oxidative stress can cause severe damage to living cells, nature also learned to use changing redox conditions as a trigger for "bio-switches". Redox-regulated systems are able to sense ROS and, more importantly, translate those changes in ROS concentrations into cellular responses. As a result, certain processes are turned on, if their function is of advantage for the cell (31, 123), or processes are turned off, if they are needless and wasteful under conditions of oxidative stress (124). Due to their high reactivity towards ROS, cysteine residues are often involved in the redox regulation of proteins. Known redox switches comprise a variety of mechanisms including single thiol-modifications such as in OhrR and the catalytic subunit of cAPK (124, 125), intra- or intermolecular disulfide bond formation such as in Hsp33 and OxyR (31, 123) or oxidation of cofactors such as Fe-S-clusters in proteins like SoxR and FNR (115, 126). In contrast to non-specific oxidative protein damage,

these modifications are specific, reversible and most importantly they appear to influence the protein activity in a controlled manner. It appears that it is not the change of the protein's redox state itself but subsequent conformational rearrangements in the protein that trigger the changes in activity. So far, two chaperones have been found to be redox-regulated, the prokaryotic heat shock protein Hsp33 (31) and the eukaryotic oxidoreductase PDI (127-129).

Hsp33 - The cytosolic chaperone Hsp33 is inactive in the reducing environment of the cytosol (31). When ROS levels raise in cells exposed to oxidative stress, however, Hsp33 turns into a very efficient chaperone holdase with a broad substrate specificity (for review see Ref. 32, 1). A highly conserved zinc center functions as the redox-switch in Hsp33. In reduced, inactive Hsp33, the zinc ion is coordinated with very high affinity by four conserved cysteine residues that are located in the C-terminus of the protein (31, 130). Zinc not only stabilizes the C-terminus in reduced Hsp33 but it also increases the sensitivity of the chaperone to changing redox conditions. As a Lewis acid, zinc (II) lowers the pK_a values of the involved thiol groups, which stabilizes their thiolate anion status and results in increased reactivity (130). Oxidation of Hsp33 leads to zinc release and the formation of two disulfide bonds (31). Lacking the stabilizing metal cofactor, the well-structured redox-switch domain of Hsp33 unfolds (131). This is thought to expose a dimerization interface and substrate binding patches (131, 132). This is crucial for the subsequent dimerization of Hsp33, and the full activation of its chaperone activity (133).

Active Hsp33 was shown to bind with high affinity to unfolding substrate proteins, thus preventing their irreversible aggregation both *in vitro* and *in vivo* (1, 31). Bound substrate proteins are released in a very controlled manner. Only upon return to reducing conditions and in the presence of the active DnaK-system does the reduced Hsp33 dimer release its bound polypeptides (24). Transfer of the substrate proteins to the foldase DnaK ensures proper refolding of the unfolded substrates. The reduced Hsp33 dimer, in turn, dissociates into the reduced, zinc-coordinated inactive monomer (Figure 6).

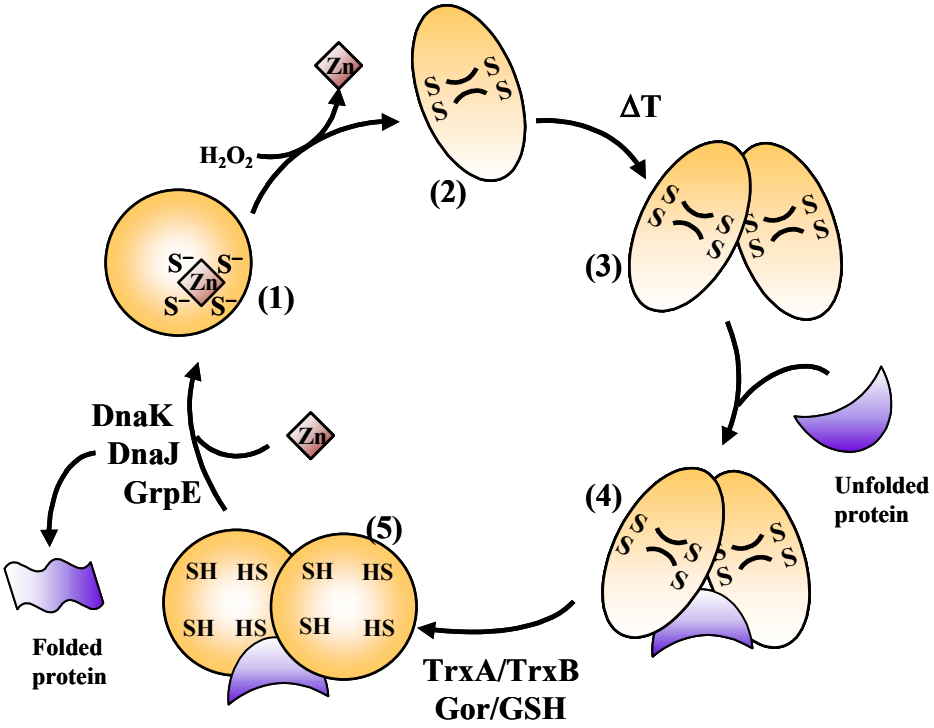

Figure 6 The redox-cycle of the molecular chaperone Hsp33 (modified from Ref. 32)

Under non-stress conditions, Hsp33 is predominantly monomeric, reduced, and inactive (1). All four conserved cysteine residues coordinate one zinc ion in a novel zinc binding motif. Oxidative stress causes the oxidation of Hsp33's cysteines. This leads to the release of zinc and the formation of two intramolecular disulfide bonds. This causes major structural rearrangements in Hsp33 (2). In a highly temperature- and concentration-dependent process, Hsp33 dimerizes and forms its high-affinity substrate-binding site (3). Active Hsp33 is now able to bind unfolding proteins and to efficiently prevent their nonspecific aggregation processes (4). Upon return to reducing conditions, Hsp33's disulfide bonds are rapidly reduced by the thioredoxin or glutharedoxin system (5) and reduced Hsp33 dimers transfer bound substrate proteins to the DnaK-system for refolding.

OxyR - The transcription factor OxyR is the H_2O_2-sensor of prokaryotic cells (134). Small amounts of hydrogen peroxide or NO activate OxyR and lead to the transcription of its target genes (107, 135, 136). Immediate up-regulation of components of the thioredoxin- and glutaredoxin-system (*gor*, *grx1*, *trxC*), of enzymes that degrade peroxides (*katG*, *ahpC*, *ahpF*) and of regulatory proteins (*fur*, *rpoS*, *flhA*) help to quickly balance the redox-state of the cell and to restore the reducing environment of the cytosol (116). To initiate transcription of the target genes, RNA polymerase forms a ternary complex with OxyR and DNA. Even though reduced and oxidized OxyR binds to DNA with the same high affinity, only oxidized OxyR is able to recruit RNA polymerase and to initiate transcription (137) (Figure 7).

The redox switch of OxyR is comprised of highly conserved cysteine residues that are able to respond to ROS with the formation of disulfide bonds, sulfenic acid, nitrosothiols or mixed disulfides with glutathione (114, 123). The nature of the introduced modification appears to be dependent on the nature of the reactive oxygen species. In the case of disulfide

bond formation, the two cysteine residues Cys199 and Cys208 are involved (123, 138). Disulfide bond formation leads to large conformational rearrangements in OxyR's C-terminal domain that allow the oxidized OxyR tetramer to bind into four major DNA groves instead of only two (139). The subsequent successful binding of RNA polymerase to the OxyR-DNA complex is thought to stabilize the structurally strained oxidized transcription factor. This structural strain in oxidized OxyR is presumably also the reason why the reduced state of OxyR is favored upon dissociation from the DNA-RNA polymerase transcription complex upon return to non-stress conditions. This allows the quick down-regulation of the oxidative stress response (138). Besides disulfide bond formation, oxidation of OxyR by various other oxidants was shown to cause distinct modifications of the absolutely conserved Cys199 (S-NO, S-OH, S-SG), which result in distinct activities of OxyR and therefore a differentiated cellular response ("micromanaging") (114).

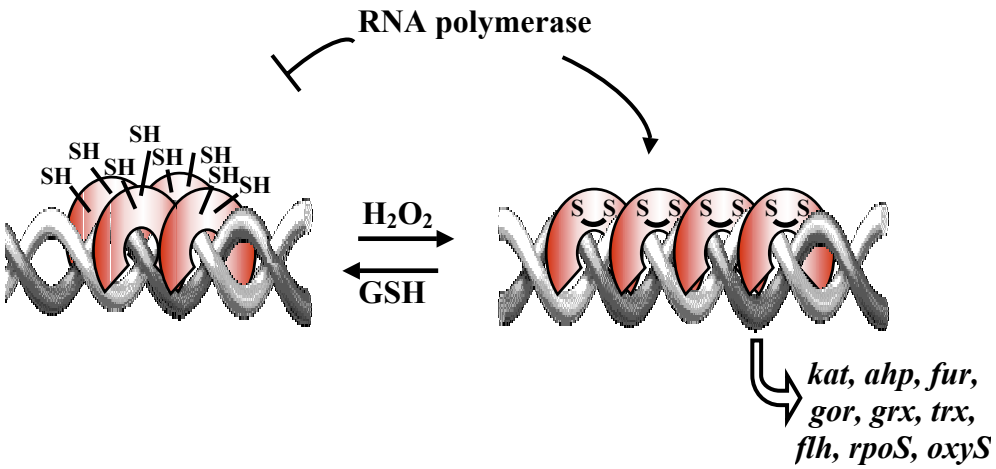

Figure 7 The redox-regulated transcription factor OxyR

Under non-stress conditions, the cysteines of the transcription factor OxyR are reduced. Although reduced OxyR is able to bind to the promoters of its target genes, it cannot interact with RNA polymerase to initiate transcription. Oxidation of OxyR by H_2O_2 causes the formation of an intramolecular disulfide bond. The concurrent structural rearrangements in the oligomer enable the transcription factor to bind to four major DNA grooves instead of only two and to successfully recruit RNA-polymerase. This triggers the transcription of genes of the oxidative stress response.

2.5 Objective

The DnaK-system, which consists of the heat shock proteins DnaK, DnaJ and GrpE, represents one of the major chaperone machineries in the cytosol of *E. coli*. It is crucial for heat stress survival by protecting thermally unfolding proteins against irreversible aggregation. Under conditions of oxidative heat stress, however, the DnaK-system appeared to fail to protect proteins against irreversible aggregation. Analysis of the protein aggregates that accumulate upon straight heat shock versus oxidative heat stress in the cell revealed a large overlap. This excludes the possibility that DnaK's inability to protect the cells can be explained by a different subset of aggregating proteins. Instead it suggests that the DnaK-system inactivates during oxidative heat stress *in vivo*.

Aim of this work was to investigate the reasons for the observed inactivation of the DnaK/DnaJ/GrpE system during oxidative heat stress conditions. In this context, the chaperone activity of DnaJ and DnaK upon exposure to oxidative heat stress treatment should be analyzed *in vitro*. Both proteins should be purified for *in vitro* studies. Chaperone activity assays should be utilized to investigate the effects of oxidative heat stress treatment (i.e. H_2O_2, 43^{o}C) on the activity of DnaK and DnaJ. To distinguish between defects in chaperone-substrate interactions and in the cooperation of the individual chaperones and co-chaperones, the chaperone activity of DnaJ and DnaK should be analyzed independently as well as dependent of the DnaK/DnaJ/GrpE refolding cycle. In case of DnaJ, the highly conserved zinc binding domain should be specifically studied during oxidative heat stress treatment. Zinc centers have been shown before to often function as redox-regulated molecular switch of protein activity (130). The thiol status of DnaJ's conserved zinc-coordinating cysteines as well as a potential zinc release by DnaJ should be monitored *in vitro* using the protein-biochemical methods. DnaK, on the other hand, contains one highly conserved cysteine. It should be investigated whether modification of this cysteine under oxidative heat stress plays a redox-regulatory role for DnaK's chaperone activity. Because DnaJ has two zinc centers, the individual roles of DnaJ's two highly conserved zinc centers should be analyzed. The recently determined NMR structure of DnaJ's zinc binding domain (83) allowed for the first time the specific mutation of either zinc center I or II. Possible *in vitro* findings about the inactivation of DnaJ or DnaK during oxidative heat stress conditions should be finally analyzed for their *in vivo* relevance.

3 Material and Methods

3.1 Material

3.1.1 Strains

name	relevant genotype	source/ reference
BB2583	W3110 pDMI.1 pUHE21-2fdΔ12(dnaJ)	M. Mayer
BB7224	MC4100 Δ*rpoH::Km zhf::*Tn*10 suhX401* Tc$_s$ *araD*$^+$	Tomoyasu et al. (171)
MG1655	wt *E. coli*	lab collection
C600	wt *E. coli*	lab collection
XL1blue	F'::Tn*10 proA*$^+$*B*$^+$ *lacIq D(lacZ)M15/recA1 endA1 gyrA96 (Nalr) thi hsdR17 (rK*$^-$*mM*$^+$*) glnV44 relA1 lac*	lab collection
JCB201	C600*dnaK7*	lab collection
PK11	MG1655 *ΔdnaJ Thr::*Tn*10*	P. Kang
KL23	PK11 pUHE21-2fdΔ12(dnaJ)	this work
TW20	PK11 pTW3 pDMI.1	T. Wolfram
TW21	PK11 pTW4 pDMI.1	T. Wolfram
TW22	PK11 pTW3	T. Wolfram
TW24	PK11 pTW4	T. Wolfram
BB7238	BB7224 pBB530 pBB353	Tomoyasu et al. (171)
AJ3	BB7224 pBB532	this work
AJ5	BB7238 pBB532	this work
JW120	JCB201 pBB353	J. Winter
JW124	MG1655 pBB353	J. Winter
JW214	KL58 pBB532 pBB530	this work
JH100	DHB4 *trxB*::Km *gor*522….mini-Tn10Tc)	J. Hoffmann
KL70	MG1655 pMOB45	this work
KL54	JCB201 pKL10	this work
KL58	BB7224 pKL10	this work
KL22	C600 *leu*$^-$ *thr*$^+$*::*Tn*10* (*dnaK756*) pWKG20	C. Georgopoulos

3.1.2 Plasmids

name	gene, resistance	source/ reference
pBB353	*dnaK dnaJ* (Spec)	Tomoyasu et al. (171)
pBB530	*grpE* (Cm)	Tomoyasu et al. (171)
pBB532	*luciferase* (Amp)	Tomoyasu et al. (171)
pDMI.1	(Kan)	M. Mayer
pKL10	pBB353 *dnaK*Cys15Ala *dnaJ* (Spec)	this work
pMOB45	*dnaK* (Cm)	Bittner et al. (192)
pTW3	pUHE21-2fdΔ12(dnaJ) *dnaJ* C161S C164S C183S C186S (Amp)	T. Wolfram
pTW4	pUHE21-2fdΔ12(dnaJ) *dnaJ* C144S C147S C197S C200S (Amp)	T. Wolfram
pUHE21-2fdΔ12(dnaJ)	*dnaJ* (Amp)	M. Mayer

PWKG20	*grpE* (Amp)	W.L. Kelley

3.1.3 Primer

All primer were purchased from Integrated DNA Technologies (http://www.idtdna.com). Listed primer are printed in forward orientation unless specified otherwise, the reverse partner comprises the complementary reversed sequence. Bases that are identical to the wild type sequence are shown in capital letters while small letters indicate new introduced bases. Base letters formatted in **bold** mark the triplet encoding the changed amino acid.

3.1.3.1 Mutagenesis Primer

name	sequence
DnaJ144S147S	CCGACTCTGGAAGAG**aGT**GACGTg**TcC**CACGGTAGCGGTGC
DnaJ161S164S	GGTACACAGCCGCAGACT**aGT**CCGACC**aGT**CATGGTTCTGG
DnaJ183S186S	CGCTGTACAGCAGACt**aGT**CCACAC**TcT**CAGGGCCGCGGTACGC
DnaJ197S200S	GCTGATCAAAGAcCCG**aGC**AACAAA**TcT**CATGGTCATGGTCG
DnaK27-63	GGGTACTACCAACTCT**gcT**GTAGCGATTATGGATGGC

3.1.3.2 Sequencing Primer

name	sequence
DnaJsequprimer reverse	GGATCTATCAACAGGAGTCCAAGC
DnaJsequprimer379 forward	GAAGCTGTACGTGGCGTGACC
DnaJsequprimer-50 forward	GAGCGGATAACAATTTCACACAG
DnaK1263-1284	GCACAGCCAGGTGTTCTCTACC
DnaK1899-1885 reverse	GACTTCTTCAAATTCAGC
DnaK3-22 forward	GGGTAAAATAATTGGTATCG
DnaK644-663	CCTTCGAAGTTCTGGCAACC

3.1.4 Proteins

Purified TrxA and TrxB were kindly provided by Dr. Charles Williams (University of Michigan) and Jörg Hoffmann (University of Michigan), respectively. All restriction enzymes were obtained from Promega (Madison, WI) or New England Biolabs.

BSA (bovine serum albumin)	Roche, Mannheim, Germany
Citrate synthase	Roche, Mannheim, Germany
Luciferase from photinus pyralis (American firefly)	Roche, Mannheim, Germany
Lysozyme	Sigma-Aldrich (Milwaukee, WI)
PfuTurbo DNA polymerase	ICN (Aurora, OH)
Rhodanese bovine liver	Stratagene, La Jolla, CA
	Sigma Chemicals Co (St. Louis, MO)

3.1.5 Antibodies, Markers, Dyes, Antibiotics and Inhibitors

α-DnaJ, polyclonal, from rabbit	StressGen (Victoria BC, Canada)
α-biotin, monoclonal, peroxidase conjugate, IgG fraction of mouse	Sigma-aldrich (Saint Souis, Missouri)
α-DnaK, polyclonal	StressGen (Victoria BC, Canada)
α-Luciferase (firefly), HRP conjugate, IgG fraction, from goat	Rockland Immunochemicals, Gilbertsville
α-mouse	Sigma (St. Louis, MO)
α-rabbit IgG, HRP conjugated, from goat	Pierce, Rockford, Illinois
1 kb DNA Ladder PR-G5711	New England Biolabs, Inc. (MD)
Ampicillin	ICN (Aurora, OH)
Bromophenolblue	ICN (Aurora, OH)
Chloramphenicol	ICN (Aurora, OH)
Complete, EDTA-free (Protease inhibitor mix)	Roche, Mannheim, Germany
Coomassie Brilliant Blue G-250	ICN (Aurora, OH)
D-Luciferin, potassium salt	Biotium (Hayward, CA)
Ethidium bromide	Gibco
Kanamycin	ICN (Aurora, OH)
Mark 12, protein molecular weight marker	Invitrogen (Carlsbad, CA)
PAR	Sigma (St. Louis, MO)
PMPS	Sigma (St. Louis, MO)
SuperSignalWest Pico	Pierce (Rockford, IL)
tetracycline	Fisher Chemical (NJ)

The following antibiotic concentrations were used:

Ampicillin	200 µg/ml
Kanamycin	20 µg/ml; 200 µg/ml
Chloramphenicol	10 µg/ml
Tetracycline	10 µg/ml
Spectinomycin	50 µg/ml

3.1.6 Chemicals

β-mercaptoethanol	ICN (Aurora, OH)
β-nicotinamide adenine dinucleotide phosphate, reduced form tetrasodium salt (NADPH)	Sigma-Aldrich (Milwaukee, WI)
[α^{32}P]ATP, 3000 Ci/mmol, 10 mCi/ml	ICN (Aurora, OH)
Acetic acid, glacial	Fisher Chemical (NJ)
Acetone	ICN (Aurora, OH)
Adenosine 5'-diphosphate sodium salt (ADP)	Sigma-Aldrich (Milwaukee, WI)
Adenosine 5'-triphosphate sodium salt (ATP)	Roche, Mannheim, Germany
Agarose	ICN (Aurora, OH)
Ammonium Sulfate	ICN (Aurora, OH)
AMS	Molecular Probes
Bacto Agar	Difco (Franklin Lakes, NJ)
Bacto Tryptone	Fisher Chemical (NJ)

Bacto Yeast extract	Fisher Chemical (NJ)
Brij58	Sigma (St. Louis, MO)
Chelex 100 Resin	BioRad
Chloroform	Fisher Chemical (NJ)
Count-off	ICN (Aurora, OH)
Diamide	ICN (Aurora, OH)
Diethylamine nitric oxide, Sodium Salt	Molecular Probes
DTNB	Sigma (St. Louis, MO)
DTT	Sigma (St. Louis, MO), Research Products International (IL)
EDTA, disodium salt	Fisher Chemical (NJ)
Ethanol	Pharmco (Brookfield, CT)
Formaldehyde (37 %)	Fisher Chemical (NJ)
Glutaraldehyde (25 %)	Fisher Chemical (NJ)
Glutathione oxidized	Sigma (St. Louis, MO)
Glutathione reduced	Sigma (St. Louis, MO)
Glycerol, ultra pure	ICN (Aurora, OH)
Glycine	ICN (Aurora, OH)
Glycylglycine	ICN (Aurora, OH)
Guanidine hydrochloride	ICN (Aurora, OH)
Hepes	ICN (Aurora, OH)
Hydrochloric acid	Fisher Chemical (NJ)
Hydrogen peroxide	Fisher Chemical (NJ)
IAM	ICN (Aurora, OH)
IPTG	Research Products International (IL)
LB Agar	Fisher Chemical (NJ)
Magnesium chloride	Fisher Chemical (NJ)
Magnesium sulfate	Fisher Chemical (NJ
Maleimide PEO_2-Biotin	PIERCE (Rockford, IL)
Methanol	Fisher Chemical (NJ)
Milk powder (fat free)	Carnation (Solon, OH)
MOPS	Teknova
Nitrogen	Cryogenics (Detroit, MI)
o-phosphoric acid	Fisher Chemical (NJ)
Phenol	ICN (Aurora, OH)
PMSF	ICN (Aurora, OH)
Potassium chloride	ICN (Aurora, OH)
Potassium hydroxide	Fisher Chemical (NJ)
Potassium phosphate, monobasic	Fisher Chemical (NJ)
SDS	Fisher Chemical (NJ)
Silver nitrate	ICN (Aurora, OH)
Sodium acetate	J.T. Baker (NJ)
Sodium azide	ICN (Aurora, OH)
Sodium carbonate anhydrous	Sigma (St. Louis, MO)
Sodium chloride	Fisher Chemical (NJ)
Sodium citrate	Sigma (St. Louis, OH)
Sodium phosphate	Fisher Chemical (NJ)
Spermidin	ICN (Aurora, OH)
Sucrose	Fisher Chemical (NJ)
TCA	ICN (Aurora, OH)

Tris-(hydroxymethyl)-aminomethan (Tris)	ICN (Aurora, OH)
Urea	ICN (Aurora, OH)
Urea, ultra pure	ICN (Aurora, OH)

All other chemicals were either purchased from Fisher, ICN, Fluka (Switzerland), Merck (Germany), Roth (Germany), Sigma or Sigma-Aldrich.

3.1.7 Buffers and Solutions

KL-buffer	Hepes-KOH, pH 8.2	30 mM
	KCl	120 mM
	NaCl	15 mM
	glycerol	4% (v/v)
LB medium	Tryptone	10 g
	Yeast Extract	5 g
	NaCl	5 g
	total volume:	1 l
Magnesium ATP (MgATP)	Tris, pH 8.5	100 mM
	$MgCl_2$	100 mM
	ATP	100 mM
	adjust pH to 7.5 with 5M NaOH	
SDS sample buffer (5x) (Laemmli)	SDS	5 g
	Glycerol	30.5 g
	1M Tris, ph 7.0	15 ml
	Bromophenol Blue	0.025 g
	ß-Mercaptoethanol	2.5 ml
	total volume:	50 ml
SDS running buffer	Glycine	288 g
	Tris	58 g
	SDS	20 g
	total volume:	20 l
SOB media	Typtone	20 g
	Yeast Extract	5 g
	NaCl	0.6 g
	KCl	0.2 g
	total volume:	1 l
TAE	Tris	242 g
	Acetic Acid	57 ml
	0.5 mM EDTA, pH 7.5	100 ml
	total volume:	10 l
TBS	NaCl	160 g
	KCl	4 g
	Tris	60 g

	total volume: adjust pH to 7.4 with HCl	1 l
TBS-T	NaCl KCl Tris Tween 20 total volume: adjust pH to 7.4 with HCl	160 g 4 g 60 g 20 ml 1 l
Western blot transfer buffer	Methanol Tris SDS Glycine total volume:	200 ml 5.8 g 0.37 g 2.93 g 1 l

3.1.8 Kits and Chromatography Material

ATP immobilized on cross-linked 4% beaded agarose, 9 atom spacer	Sigma Chemical Co (St. Louis, MO)
Blue-Sepharose HiTrap Column (5x5 ml)	Amersham Biosciences (NJ)
BrightStar BioDetection Kit	Ambion (Austin, TX)
Hydroxyapatite Bio-Gel HTP	Bio-Rad (Hercules, CA) Laboratories
Micro Bio-Spin Chromatography Columns	Bio-Rad (Hercules, CA)
NAP-5 Columns	Amersham Biosciences (NJ)
PD-10 Columns	Amersham Biosciences (NJ)
Q-Sepharose HiTrap FF (5x5 ml)	Amersham Biosciences (NJ)
QuikChange Site-directed Mutagenesis Kit	Stratagene
S-Sepharose HiTrap Columns, (5x5 ml)	Amersham Biosciences (NJ)
Superdex 75	Amersham Biosciences (NJ)
Wizard Plus SV Miniprep	Promega
Zip-Tip C4	Milipore

3.1.9 Other Material

Centricon YM-10 concentrators (Amicon Bioseparations)	Millipore (MA)
Centricon YM-30 concentrators (Amicon Bioseparations)	Millipore (MA)
Dialysis Tubing, Spectra/Por Membranes	Spectrum
Disposable plastic cuvettes, 1 ml	Fisher Lab Equipmentl (PA)
Electrode Buffer Solutions pH 4.00, 7.00, 10.00	Fisher Lab Equipmentl (PA)
Eppendorf LidBac, 2.0mL Safe-Lock tubes	Brinkmann Instruments (NY)
Greiner Tubes 50 ml	Bellco (Vineland, NJ)
Nitrocellulose Membranes (Western blotting)	Millipore (MA)
Quartz cuvettes	Hellma (Plainview, NY)
Scintillation Vials, 20 ml	Fisher Lab Equipmentl (PA)
Syringe filters, 0.45 µM, sterile	Millipore (MA)
Syringe filters, 0.8 µM, non sterile	Nalgene Nunc International (NY)
TLC plates cellulose, PEI matrix 20 cm x 20 cm	Sigma-Aldrich (Milwaukee, WI)
Tris-Glycine polyacrylamide gels (misc.)	Invitrogen (Carlsbad, CA)

Utrafiltation membrane YM10 Ø76 mm, 43mm	Millipore (MA)
Utrafiltation membrane YM30 Ø76 mm, 43mm	Millipore (MA)
Whatman Chromatography Paper	Whatman (Clifton, NJ)
X-ray film, Kodak X-OMAT AR-5 24x30	Kodak (Rochester, NY)

All other consumables were purchased from Fisher Scientific.

3.1.10 Technical Equipment

Äkta FPLC	Amersham Biosciences (NJ)
Amicon Stirred Ultrafiltration Cells	Amicon (Beverly, MA)
Autoclave 3021 Gravity	Amsco
Blotting Unit	Owl
Centrifuge J2-HS	Beckman (Fullerton, CA)
Cooling unit	Revco (Asheville, NC)
Eppendorf Centrifuge 5415R	Eppendorf (Hamburg, Germany)
Eppendorf Centrifuge 5804R	Eppendorf (Hamburg, Germany)
Eppendorf Thermoblock, 24x2mL	Eppendorf (Hamburg, Germany)
Eppendorf Thermomixer	Eppendorf (Hamburg, Germany)
Film Developer SRX-101A	Konica (Mahwah, NJ)
Fluorometer F-4500	Hitachi (Ontario, Canada)
Fraction Collector FPLC Frac-900	Amersham Biosciences (NJ)
Freezer -80 °C Ultima II	Revco (Asheville, NC)
French Pressure Cell Press	American Instrument Company
Fridge-Freezer	Whirlpool
Gel Dryer Hoefer SE 1200 Easy Breeze™	Amersham Biosciences (NJ)
Gel Electrophoresis chambers Xcell Surelock™	Invitrogen (Carlsbad, CA)
GeneAmp PCR System 9600	Perkin Elmer Cetus
Ice machine	Crystal Tips
Incubator 37 °C Model 2015	VWR Scientific (IL)
Incubator 43 °C	National, a Heinecke Company
M 555 pH/Ion Meter w/ Arm, 120V	Corning (Acton, MA)
Magnet Stirrer nuova II	Sybron / Thermolyne
Microwave	Kenmore
Pipetman, misc.	Eppendorf (Hamburg, Germany)
Power supply ECPS 3000/150	Pharmacia Fine Chemicals
Rotator for gels	Lab Line Inc.
Scale TL-2102	Denver Instrument Company
Scale, fine AB54-S	Mettler Toledo
Scanner, EPSON Expression 1680	EPSON
Shaking Water Bath	Lab-Line (Melrose Park, IL)
Spectrophotometer DU530	Beckman (Fullerton, CA)
Spectrophotometer DU640	Beckman (Fullerton, CA)
Spectrophotometer Jasco-550	Jasco (Easton, MD)
Thermoblock, metal	VWR Scientific (IL).
Thermometer, digital HH41	Omega
Vortex Mixer	VWR Scientific (IL)
Water bath M6	mgw Lauda
White Light Transilluminator FB-WLT-1417	Fisher Lab Equipmentl (PA)

3.1.11 Software

Endnote 3.1.2.	ISI Research Soft (Berkeley, CA)
EntrezPubMed	http://www3.ncbi.nlm.nih.gov/entrez/query.fcgi
FL Solutions	Hitachi (Ontario, Canada)
Microsoft Office XP Professional	Microsoft Corporation
Photoshop	Adobe
Primer Generator	http://www.med.jhu.edu/medcenter/primer/primer.cgi
ProtParam Tool	ExPasy (http://expasy.org/)
Sigma Plot 8.0 for Windows	SPSS Scientific
Spectra Manager	Jasco (Easton, MD)

3.2 Molecular-biological methods

3.2.1 Cultivation and conservation of *E. coli* strains

Strains were streaked out from permanent cultures for overnight growth at 30°C or 37°C to form single colonies on LB agar plates supplemented with the appropriate antibiotics. Plates were stored at 4°C for several days and single colonies were used to inoculate shaking liquid LB media or new agar plates. Growth in liquid cultures was followed spectroscopically by determining the optical cell density at 600 nm (OD_{600}). Permanent cell cultures were prepared from liquid cultures grown to exponentional phase by mixing 400 µl cell culture with 600 µl 20% glycerol and stored at -80°C.

3.2.2 QuikChange site-directed mutagenesis

This method introduces a specific point mutation into a target DNA sequence and is based on PRC reactions using primers that contain the desired mutation(s) and the wild type DNA as template. Primers were designed with the Primer Generator software (http://www.med.jhu.edu/medcenter/primer/primer.cgi) in a way that new restriction sites were introduced together with the amino acid exchange. With as little base pair changes as possible, primers should contain 10 to15 pairing bases up- and downstream from the mutation site, more than 50% C and G bases and a T_m higher than 78°C (according to the manufacturer). A typical PCR sample contained 1x PfuTurbo reaction buffer, 50 ng template plasmid DNA, 125 ng of the forward and reverse primer and 5 µM dNTP mix in 50 µl final volume. PfuTurbo polymerase was added during a hot start of 5 minutes at 95°C. This was followed by 18 cycles of

1. 30 sec melting at 95°C
2. 1 min annealing at 55°C

3. 10 min elongation at 68°C.

After DpnI digestion of the PCR reaction to remove all parental template DNA, the amplified PCR products were transformed into heat competent XL1 blue cells and selected for growth on LB plates with ampicillin (DnaJ) or spectinomycin (DnaK). Plasmid DNA was extracted from several transformants using the Wizard Plus SV Miniprep kit. To test for the expected restriction site, plasmid DNA was digested using buffers and protocols of the manufacturer. DNA fragments were separated by electrophoresis (30 min, 80 mV) on a 1% agarose gel supplemented with 0.01% ethidium bromide in TAE buffer. Fragment sizes were determined using the 1 kb latter as DNA standard. Finally, the plasmids were sequenced at the University of Michigan Sequencing core to verify the mutation, using primers listed in 3.1.3.2.

3.2.2.1 Construction of DnaJ zinc center mutants

Each of the two zinc ions in DnaJ's zinc binding domain are coordinated by four highly conserved cysteine residues. To analyze the individual role of zinc center I and II for DnaJ's function, mutant proteins were constructed lacking either one of the two zinc centers by exchanging the four zinc coordinating cysteine residues to serines.

Using pUH21-2fdD12(dnaJ) as parental plasmid, both cysteine residues within one cysteine rich motif were changed simultaneously using QuikChange Site-Directed Mutagenesis Kit (section 3.2.2). Once the mutation of the first cysteine motif was introduced, the second motif was changed using the partly modified plasmid as template. All used plasmids, the generated restriction sites as well as the name of the generated plasmids are listed in Table 1 and in section 3.1.3.1. The plasmids pTW3 and pTW4 were transformed into *dnaJ* deletion strain PK11 for phenotypical studies and subsequent purification.

Table 1 Construction of DnaJΔZnI and DnaJΔZnII mutants

mutated zinc center	cysteine motif with amino acid exchange	used primer	generated restriction site	plasmid
I	(1) C144S C147S (4) C197S C200S	DnaJ144S147S DnaJ197S200S	AflIII AvaI	pTW4
II	(2) C161S C164S (3) C183S C186S	DnaJ161S164S DnaJ183S186S	SpeI SpeI	pTW3

3.2.2.2 Construction of the $DnaK_{Cys15Ala}$-mutant

To investigate the role of DnaK's conserved cysteine residue Cys15 for its chaperone activity, a DnaK mutant protein was constructed, whose Cys15 was substituted with Ala (section 3.2.2). Plasmid pBB353 containing wild type DnaK was used as template and the primer DnaK27-63 was used to introduce the mutation. The constructed plasmid pKL10 was transformed into *dnaK* deletion strains for purification and phenotypic studies.

3.2.3 Preparation and transformation of heat competent cells

This procedure makes cells competent for the uptake of double stranded plasmid DNA using heat shock conditions. To prepare heat competent cells, an overnight culture of the respective *E. coli* strain was diluted 1:100 into 75 ml LB media containing 10 mM $MgSO_4$ and 10 mM $MgCl_2$ and grown until an $OD_{600\ nm}$ of 0.5 was reached. Then, the culture was incubated on ice for 20 min, the cells were pelleted (3,000 xg, 5 min, 4°C) and washed with 25 ml ice-cold 0.1 M $MgCl_2$. After a second centrifugation, the cells were resuspended in 10 ml ice-cold 0.1 M $CaCl_2$. After incubation on ice for 0.5 – 4 hours, cells were centrifuged and the pellet was resuspended in 3 ml ice cold 0.1 M $CaCl_2$, 10% v/v glycerol. The heat competent cells were aliquoted, shock frozen in dry ice/EtOH and stored at -80°C.

For transformation, 1 to 3 µl of plasmid DNA was combined with 50 µl heat competent cells. After incubation on ice for 15 min, the cells were transferred for 45 sec to a 42°C water bath followed by 2 min incubation on ice. Then, the cells were supplemented with 500 µl prewarmed SOB–media and incubated under shaking for 1 hour to express plasmid encoded antibiotic genes. Transformants were selected on LB plates containing the appropriate antibiotic and streaked out twice for single colonies.

3.3 Preparative methods

All proteins were purified after their overexpression in *E. coli* cells using typical separation methods like ammonium sulfate [$(NH_4)_2SO_4$] precipitation, affinity chromatography or ion-exchange chromatography. After harvesting the cells, each purification step was completed on ice using ice-cold solutions. To monitor the purification process, small aliquots of each fraction containing comparable protein concentrations were applied onto a 14% SDS PAGE. The protein gels were stained with Fairbanks (140).

3.3.1 Ammonium sulfate precipitation

Proteins form hydrogen bonds with water through their exposed polar and ionic groups. Addition of small ions such as ammonium sulfate [$(NH_4)_2SO_4$] removes water molecules from the protein, resulting in the precipitation of certain proteins. For the precipitation, the corresponding amount of salt was gradually added to the protein solution under slow stirring at 4°C and the protein precipitation was completed by a final 30 min incubation under the same conditions. Precipitated proteins were subsequently separated from soluble proteins by centrifugation (30 min, 4°C, 48,000xg). The protein pellet was resuspended in the appropriate buffer, followed by overnight dialysis against the same buffer to remove the excess salt.

3.3.2 Chromatography

If not mentioned otherwise, all columns were controlled via the Äkta FPLC Pharmacia. Ion-exchange chromatography columns that were used were Q-Sepharose (quaternary trimethylaminoethyl sepharose) column for anion-exchange and S-Sepharose (sulfopropyl sepharose) column for cation-exchange chromatography. Depending on the pI of the proteins as well as on the pH of the chosen buffer, DnaK or GrpE were bound to Q-Sepharose (pH>pI) while DnaJ was bound to S-Sepharose column (pH<pI). The bound proteins were eluted with gradually increasing the ionic strength. For both Q- and S-Sepharose chromatography, very efficient 5 ml HiTrap High Performance columns were used. Several columns were connected in series to achieve larger bed volumes. The used flow rate for these HiTrap columns was 5 ml/min with a maximal pressure of 0.5 MPa. To clean the columns and maintain maximal binding capacity, the ion-exchange columns were washed after each use with 5 CV 2 M NaCl, followed by 2 CV of ddH_2O. The columns were stored in 20% EtOH.

The separation principle of the hydroxyapatite (HAP) chromatography is not very well understood and the binding behavior of proteins is therefore not predictable. The $Ca_5(PO_4)_3OH$ matrix is thought to cause both ionic interactions of protein amino groups with phosphate groups and complexation of protein carboxyl groups by the calcium ions (141). Increasing phosphate concentrations compete for the protein binding and are used to elute bound proteins. For a 50 ml self poured column (30 g dry weight) a flow rate of 2 ml/min with a maximal pressure of 0.5 MPa was used. To clean the column, the HAP material was washed with 2 CV of 400 mM potassium phosphate buffer and stored in 10 mM $NaPO_4$, pH 6.0, 0.02% NaN_3.

The exact separation mechanism is also not known for the Blue Spepharose column (5 ml, HiTrap). This affinity column uses the dye Cibacron^{TM} Blue F3G-A as the stationary phase. Loading and washing procedures for this column were performed manually. The protein of interest, GrpE, was unable to bind and appeared in the flowthrough, while the majority of impurities bound to the column. For restoration, the Blue Sepharose matrix was washed with 100 ml filtered 50 mM KH_2PO_4, 1.5 M KCl, pH 7.0 and stored in 20% ethanol.

The ATPase affinity column was self-poured and contained about 10 ml 4% beaded agarose cross-linked with ATP (9 atom spacer). Only ATP binding proteins with a significant affinity for ATP bind to this column. Driven by gravity forces (flow rate of less than 0.25 ml/min), this column was used at 4^{o}C to reduce protein degradation and aggregation. Bound proteins were eluted with excess ATP in the buffer, which competed for protein binding. The column material was cleaned with ddH_2O and stored in 20% (v/v) ethanol at 4^{o}C.

Size exclusion chromatography separates molecules based on their size and shape. The column material consists of beads with a sponge like structure that allows molecules up to a certain size (exclusion size) to migrate into the material. The smaller the molecules are, the deeper they migrate into the structure and the longer it takes them to move out of the column. All molecules that are larger than the exclusion size pass the beads and elute first. The Superdex 75 gel column was equilibrated with degassed buffer, with a flow rate of 1 ml/min and a maximal pressure of 0.3 MPa. For quick buffer exchange, the disposable gel filtration columns NAP5 and PD10 were used, according to the instructions of the manufacturer.

3.3.3 Concentration and dialysis

To concentrate a protein, the solution was forced through a size exclusion ultra-filtration membrane, using pressure. The membrane was permeable for buffer and small particles but retained bigger molecules. The selected pore size depended on the molecular mass and shape of the protein of interest. To concentrate a solution, an amicon pressure cell was used, which allowed slow stirring of the protein solution and controlled application of N_2 pressure. After the desired volume was reached, the membranes were washed with 5% (w/v) NaCl and stored in 20% (v/v) ethanol.

Dialysis underlies a similar principle, except that not a change in volume but rather of the buffer composition is the aim. Pore size and dimensions of the dialysis membrane depended on the respective protein as well as on the sample volume. The dialysis tube was

placed in the appropriate ice-cold buffer, whose volume was at least 100x the volume of the dialysis sample and dialyzed overnight.

3.3.4 Purification of ATP-depleted DnaK

This protocol was adapted from a method described by Madeker (142). Overexpressed DnaK wild type protein or $DnaK_{Cys15Ala}$ mutant were purified from *E. coli* strain JW124 and KL54, respectively. Inoculated from a single colony, the cultures were grown in six liter LB medium (1 l each flask) supplemented with the respective antibiotic without shaking at 30°C overnight. Then, cell cultures were shaken (200 rpm) until $OD_{600\,nm}$ of 0.5-0.7 was reached. DnaK overexpression was induced by 1 mM IPTG and protein expression was continued for 4 - 6 h. Cells were pelleted by centrifugation (Sorvall, 4,000 rpm, 40 min, 4°C) and stored at -20°C.

To lyse the cells, the cell pellets were resuspended in buffer A (20 mM Tris-HCl, pH 7.2, 2 mM EDTA, 10% (w/v) sucrose, 5 mM DTT) supplemented with 30 mM spermidin and 200 mM KCl. 0.2 g/l PMSF (in isopropanol) as well as one tablet protease inhibitor mix (complete, EDTA-free, in ddH_2O) were added shortly before cell lysis. The final volume was 50 ml. Cells were lysed using two cycles French Press (11,000 psi, 4°C) and non-soluble components were subsequently separated from soluble proteins by centrifugation (20 min, 4°C, 48,000 xg).

Then, proteins were precipitated with 60% $(NH_4)_2SO_4$ (390g/l) (section 3.3.1) and the protein pellet was resuspended in <15 ml buffer B (buffer A with 2 mM DTT). To remove the excess of salt, the protein solution was dialyzed overnight against cold buffer B at 4°C.

For further purification, four HiTrap Q-Sepharose columns (section 3.3.2) were combined to yield a final column volume of 20 ml and equilibrated with 5 CV of buffer B supplemented with 50 mM KCl. The dialyzed protein solution was centrifuged (30 min, 4°C, 48,000 xg) to remove protein aggregates shortly before the clear supernatant was loaded onto the column. To remove non-specifically bound proteins, the column was washed with 200 ml buffer B supplemented with 50 ml KCl. Bound proteins including DnaK were eluted with a 200 ml gradient from 50 to 400 mM KCl in buffer B. KCl concentrations of 150 to 350 mM eluted DnaK. 4 ml fractions were collected on ice and SDS PAGE was used to analyze the protein composition of the fractions. Those fractions that contained the purest and most concentrated amount of DnaK were combined and concentrated to less than 10 ml using an ultrafiltration membrane (30 kDa exclusion volume). The concentrated DnaK solution was

dialyzed overnight against ice-cold buffer C (20 mM Hepes, pH 7.2, 10 mM $MgSO_4$, 10% (w/v) sucrose, 1 mM EDTA, 2 mM DTT) at 4°C.

The affinity of DnaK to ATP was used as final purification step. The ATP-agarose column (section 3.3.2) was equilibrated with at least 5 CV buffer C at 4°C using a flow rate of about 10 ml/hour. The dialyzed protein solution was applied onto the column and the column was washed with 2 CV buffer C, 5 CV buffer C supplemented with 0.5 M KCl and finally 5 CV buffer C. DnaK was eluted in 40 ml buffer C supplemented with 4 mM MgATP, 2 ml fractions were manually collected and the fractions were analyzed using SDS PAGE. Fractions containing pure DnaK were combined and concentrated to 15 ml. DnaK was extensively dialyzed (6 time 12 hours) against 2 liter buffer D (20 mM Tris, pH 7.2, 10% (w/v) sucrose, 100 mM NaCl, 40 mM KCl, 1 mM EDTA) first with and later without additional 4 mM EDTA to remove excess of MgATP.

To remove the remaining MgATP bound to DnaK, the solution was dialyzed against buffer F (50 mM Tris 7.2, 50 mM KCl, 2 mM DTT, 10% (w/v) sucrose) and applied onto a 50 ml HAP column equilibrated in the same buffer. MgATP was removed by washing the column with 2 CV buffer D, 2 CV buffer D supplemented with 1 M KCl and finally 2 CV buffer D. To elute DnaK, a gradient from 0 to 40 mM KH_2PO_4 in buffer D over 20 CV was applied and fractions of 13 ml were collected. The pooled fractions were concentrated and dialyzed against the final storage buffer D (section 3.3.3).

ATP has its absorption maximum at 260 nm and even though the DnaK preparation was ATP-depleted, small residues of the nucleotide might influence spectroscopic determination of DnaK's concentration. To obtain comparable DnaK concentrations, the Bradford assay with BSA as concentration standard was used (section 3.4.1). From six liter cell culture, ~40 mg DnaK (>99% pure) were purified. The protein was stored in 200 µl aliquots at –80°C.

3.3.5 Purification of DnaJ

Four liter of LB medium supplemented with 100 µg/ml ampicillin and 1 mM $ZnCl_2$ were inoculated with a single colony of *E. coli* strain BB2583, which expresses wild type DnaJ from the IPTG inducible plasmid pUHE2-12fdD12. Strains TW20 and TW21 were used to overexpress the DnaJ zinc center mutants DnaJΔZnI and DnaJΔZnII, respectively. The cells grew without shaking overnight at 30°C. After 10 h of growth, the culture was shaken. Once OD_{600nm} of 0.5 was reached, DnaJ expression was induced with the addition of 1 mM IPTG. After supplementing the media with additional ampicillin (100 µg/ml), protein

expression was continued for about 5 h at 30°C. Cells were harvested by centrifugation (Sorvall, 4,000 rpm, 40 min, 4°C).

DnaJ wild type as well as the zinc center mutants were purified as previously described (143) with slight modifications to remove all residual detergents. To lyse the cells, the pellet was resuspended in lysis buffer (50 mM Tris, pH 8.0, 5 mM DTT, 0.6 % (w/v) Brij58) to a final volume of less than 50 ml. After the addition of 0.8 mg/ml lysozyme, 1 mM PMSF (in isopropanol) and 1 tablet proteases inhibitor cocktail mix (complete, EDTA-free, in ddH_2O), cells were lysed by two cycles of French Press (11,000 psi, 4°C). Next, soluble proteins were separated by centrifugation (60 min, 27,000 xg, 4°C) and the soluble supernatant was diluted 1:2 with buffer A (50 mM $NaPO_4$, pH 7.0, 1 mM EDTA, 0.1% (w/v) Brij58, 2 mM DTT). Proteins including DnaJ were precipitated with 60% $(NH_4)_2SO_4$ (390 g/l) as described in section 3.3.1. The pellet was resuspended in a final volume of less than 15 ml buffer B (buffer A supplemented with 2 M urea) and the protein solution was dialyzed overnight against 2 l buffer B at 4°C.

Four HiTrap S-Sepharose columns were connected and equilibrated with 5 CV buffer B. The dialyzed protein solution was centrifuged to remove aggregates and loaded onto the column. After washing the column with 7.5 CV ml buffer B, bound proteins were eluted with a gradient ranging from 0 to 350 mM KCl in buffer B over 300 ml. Fractions of 5 ml were collected and analyzed on 14% SDS PAGE. DnaJ eluted between 40 – 120 mM KCl. Fractions with the highest amount of DnaJ were combined, concentrated to less than 15 ml using an ultra-filtration membrane (exclusion volume 30 kDa) and dialyzed overnight against 2 l ice-cold buffer C (50 mM Tris, pH 7.5, 2 M urea, 0.1% (w/v) Brij58, 2 mM DTT, 50 mM KCl) at 4°C.

As next purification step, the clear protein solution was loaded onto a HAP column (50 ml) equilibrated in buffer C. The column was first washed with 200 ml buffer D (50 mM Tris, pH 7.5, 2 M urea, 2 mM DTT, 50 mM KCl) supplemented with 1 M KCl, followed by a low salt wash in 100 ml buffer D. DnaJ was eluted using a 200 ml gradient from 50 to 400 mM KH_2PO_4 in buffer D and 3 ml fractions were collected. DnaJ eluted in a KH_2PO_4 concentration of 150 – 250 mM.

DnaJ containing fractions of the HAP column were combined and diluted into 200 ml buffer E (50 mM Tris, pH 9.0, 2 M urea, 2 mM DTT, 100 mM KCl). Two HiTrap Q-Sepharose columns were combined and equilibrated with 50 ml buffer E. DnaJ does not bind to this column and was collected in the flowthrough. The flowthrough was concentrated to less than 15 ml using an ultra-filtration membrane. Pure DnaJ was dialyzed against KL-buffer

(30 mM Hepes, pH 8.2, 120 mM KCl, 15 mM NaCl, 4% Glycerol) and all aggregates were removed by centrifugation (60 min, 48,000 xg, 4°C). The protein concentration of DnaJ was determined as described in section 3.4.1. From four l cell culture, ~100 mg DnaJ (>99% pure) were purified. DnaJ was stored in 200 µl aliquots at –20°C.

To prepare a homologous preparation of reduced zinc-bound DnaJ, 130 µM DnaJ were incubated with 2 mM DTT and 40 µM $ZnCl_2$ for 1 h at 37°C. Then, excess zinc and DTT were removed by size exclusion chromatography (Superdex 75, section 3.3.2).

3.3.6 Purification of GrpE

This protocol was adapted from a method by Zylicz and Deloche (unpublished). To avoid co-purification of DnaK, the *dnaK* deletion strain C600*dnaK756* was used for the overexpression of GrpE. 50 ml LB medium supplemented with 100 µg/ml ampicillin were inoculated with a single colony of KL22 and grown overnight at 37°C (200 rpm). The culture was diluted 1:100 into two flasks containing 1 liter LB Amp media and continuously shaken until $OD_{600\ nm}$ of 0.5 was reached. Then, expression of GrpE was induced by the addition of 1% (w/v) arabinose. The cultivation was continued for 5 h. Cells were harvested by centrifugation (Sorvall, 4,000 rpm, 40 min, 4°C) and the cell pellet was frozen at –20°C.

To lyse the cells, the cell pellet was resuspended in 7 ml of buffer A (50 mM EDTA, pH 8.0, 5 mM DTT) to reach an approximate volume of 25 ml and supplemented with buffer B (50 mM Tris, pH 8.0, 10% (w/v) sucrose) to a final volume of 50 ml. Shortly before the lysis, 0.8 mg/ml lysozyme and 100 µg/ml PMSF were added. The cells were disrupted by two cycles of French Press (11,000 psi, 4°C) and the soluble proteins were separated from the insoluble fraction by centrifugation (27,000 xg, 60 min, 4°C).

If necessary, the pH of the protein solution was adjusted to 8.0 and GrpE was precipitated with 60 % $(NH_4)_2SO_4$ (390 g/ l). The precipitated proteins were centrifuged (48,000 xg, 30 min, 4°C) and the resulting pellet was resuspended in 10 ml buffer C (50 mM Tris, pH 7.2, 1 mM EDTA, 10% (w/v) sucrose, 10 mM β-mercaptoethanol). Excess of salt was removed by dialyzing the protein solution against 2 l of ice-cold buffer C at 4°C overnight.

Four HiTrap Q-Sepharose columns (section 3.3.2) were connected and equilibrated with 5 CV of buffer C. The clear protein solution was applied onto the column. Nonspecifically bound proteins were washed off the column with 5 CV buffer C. Then, a 300 ml gradient from 0 to 400 mM NaCl was applied. GrpE eluted between 100 to 200 mM

NaCl. 5 ml fractions were collected. GrpE containing fractions were pooled, concentrated to less than 15 ml and dialyzed overnight against 2 l ice-cold buffer C at 4°C.

For the next purification step, a Blue Sepharose column (section 3.3.2) was used, which was equilibrated in buffer C. Aggregates were removed by centrifugation (48,000 xg, 30 min, 4°C) and the clear protein solution was applied onto the Blue Sepharose column using a 0.8 µM syringe filter. GrpE does not bind to this column and was therefore collected in the flowthrough as well as in the first wash fractions of the column. The GrpE containing solution was concentrated to less than 15 ml using an ultra-filtration membrane (10 kDa exclusion size) and dialyzed against 2 l buffer D (5 mM potassium phosphate buffer, pH 6.8) overnight at 4°C.

By using a 50 ml HAP column (section 3.3.2), all remaining impurities were removed. The HAP column was equilibrated with 5 CV buffer D and the dialyzed protein solution was loaded. After washing the column with 2 CV buffer D, a 400 ml gradient from 5 to 100 mM potassium phosphate in buffer D was applied. GrpE eluted between 10-50 mM potassium phosphate. 5 ml fractions were collected. The pooled fractions were concentrated and dialyzed overnight at 4°C against 2 l of storage buffer E (30 mM Hepes, pH 7.0, 10 mM KCl, 5% glycerol). The protein concentration of GrpE was determined spectroscopically as well as with the Bradford assay (section 3.4.1). ~100 mg GrpE (>99%) were purified from 2 l cell culture and stored in 200 µl aliquots at –20°C.

3.4 Protein-biochemical methods

3.4.1 Determination of protein concentration

The protein concentration of purified proteins was generally determined using absorption spectroscopy. This method is based on the absorption of the amino acids tryptophan, tyrosine and phenylalanine in the UV-range of 250-280 nm. Depending on the number of these residues, every protein has a defined molar extinction coefficient (ε) at 280 nm (M^{-1} cm^{-1}), which can be calculated (144). Applying the law of Lambert and Beer ($E = \varepsilon \cdot c \cdot d$), the concentration (c) of a pure protein solution can then be determined with a known extinction coefficient (ε), the measured extinction (E) and the thickness of the cuvette (d, in cm). The absorption of proteins was measured in quartz cuvettes using a spectrophotometer. The baseline for the protein containing buffer as well as the spectrum of the protein was measured between 400 nm and 240 nm, using the same cuvette. All used extinction coefficients are listed in Table 2.

The concentration of ATP-containing DnaK could not be measured spectroscopically, because the absorption maximum of the nucleotide ATP at about 260 nm influences absorption spectra to unknown extent. GrpE, on the other hand, contains no tryptophanes and only very few tyrosine and phenylalanine residues, which makes the spectroscopic protein determination not very accurate. Therefore, the concentration of GrpE and of all DnaK preparations was also determined using Bradford assay (145). This assay is based on the binding of Coomassie Brilliant Blue G-250 to the cationic charges of the amino acid arginine as well as to other positively charged or hydrophobic amino acids. As a result of this binding, the absorbance maximum of the dye shifts from 465 nm to 595 nm (146).

The concentrated Bradford assay reagent was diluted 1:5. 100 µl of several different protein dilutions in the respective storage buffer were prepared and added to 900 µl Bradford solution. Buffer instead of protein was used for the blank and a calibration curve was obtained using a BSA solution with known concentration. All samples were measured at 595 nm after 10 min incubation at room temperature.

Table 2 Extinction coefficients used in this work

protein	ε_{280nm} [M^{-1} cm^{-1}]	source
BSA	44,310	ExPasy
DnaJ	13,400	ExPasy
DnaK	14,650	ExPasy
GrpE	1,280	ExPasy
Firefly Luciferase	45,560*	Herbst et al. (153)
Bovine Rhodanase	59,840	ExPasy

*) λ = 278 nm

3.4.2 Oxidation and reduction of DnaJ

20 µM DnaJ in KL-buffer was oxidized in the presence of 2 mM H_2O_2 and 5 µM $CuCl_2$ at 25°C. The zinc release of DnaJ, determined with the PAR/PMPS assay (section 3.4.4.2) was used to monitor the progress of DnaJ's oxidation. To stop the oxidation reaction, the oxidants were either removed by gel filtration (section 3.3.2) or by diluting (at least 1:13) a small aliquot of oxidized DnaJ into a prepared chaperone assay reactions to determine its chaperone activity.

Oxidized DnaJ was reduced with DTT at 25°C in KL-buffer. The residual concentration of oxidants was determined to not influence the other components of the assay.

In the presence of residual oxidants, 5 mM DTT were necessary, while 2 mM DTT were sufficient to completely reduce a H_2O_2-free DnaJ preparation.

3.4.3 Inactivation and reactivation of DnaK *in vitro*

Incubation of ATP-depleted, purified DnaK at 43°C in the presence of oxidants resulted in the oxidation and inactivation of the chaperone. This process could be reversed by subsequent reduction with DTT. Loss and gain of DnaK's chaperone activity was determined before, during and after the incubation reaction. To measure the DnaK activity, an aliquot of oxidized or reduced DnaK was transferred into the activity assay mix containing buffer, DnaJ and GrpE (sections 3.6.1.1, 3.6.2) at 30°C. Dilution of the sample (at least 25-fold) during the oxidation process was sufficient to stop the oxidation process. The activity assay was started immediately by addition of luciferase.

3.4.3.1 Oxidation of DnaK

50 to 200 µl buffer (40 mM MOPS-KOH, pH 7.5, 50 mM KCl) was prewarmed at 43°C. Oxidants like H_2O_2 (2 mM) or GSSG (5 mM) were added and the reaction was started by adding 20 µM ATP-depleted DnaK. At indicated time points, samples were withdrawn and DnaK's activity was analyzed as described in sections 3.6.1.1 and 3.6.2.

3.4.3.2 Reduction of DnaK

After DnaK's inactivation in the presence of oxidants, 20 µM DnaK was diluted at least 25-fold into the luciferase refolding buffer (compare section 3.6.2) supplemented with 2 mM ATP and reductants (2 mM DTT, 14 mM GSH or 160 µM NADPH, 2.8 µM, TrxA 70 nM TrxB) at 30°C. At indicated time points, samples were withdrawn and DnaK's activity was analyzed described under 3.6.1.1 and 3.6.2.

3.4.4 Determination of free thiol groups in proteins

3.4.4.1 Ellman's assay

This assay was used to determine the number of free thiols in purified proteins. Ellman's reagent (DTNB) forms a yellow dye (TNB) after reacting with accessible thiol groups. TNB has an absorption maximum at 412 nm and can be determined spectroscopically.

To compare the number of exposed and buried thiol groups, Ellman's reagent was allowed to react with either the native or the denatured protein. Incubation of the protein in 6

M Gua-HCl for 10 minutes was used to unfold the respective polypeptides. A 10 mM DTNB stock solution was prepared in 100 mM Tris, pH 7.5. 1 to 10 µM native or denatured protein was mixed with 0.5 mM DTNB and 2 mM EDTA in plastic cuvettes and measured against a blank without protein at 412 nm. The amount of formed TNB, which corresponds to the number of reacted thiols, can be calculated using the extinction coefficient of TNB $\varepsilon_{412\ nm}$ of 13,700 M^{-1} cm^{-1} in Gua-HCl or 14,150 M^{-1} cm^{-1} in non-denaturing buffer.

3.4.4.2 PAR-PMPS assay

The number of zinc coordinating thiols and the number of zinc ions bound to DnaJ was determined using the PAR-PMPS assay (147). 4-(2-pyridylazo) resorcinol (PAR) forms complexes with free zinc [$Zn(PAR)_2$], which have a bright red color with an absorption maximum at 500 nm. The exact extinction coefficient ($\varepsilon_{500\ nm}$) of the complex in KL-buffer was determined using a zinc standard (72,710 M^{-1} cm^{-1}). PMPS, which forms mercaptide-thiols bonds was used to release bound zinc from DnaJ into the PAR containing solution.

To obtain accurate results, metal free buffers were used, which were generated by treating 50 ml KL-buffer with 5 g of Chelax 100 resin for 1 hour at 37°C. Then, 1 to 5 µM DnaJ was mixed with 0.1 mM PAR in 600 µl KL-buffer to measure any free or loosely bound zinc in the solution. Addition of 30 µM PMPS to the protein solution caused immediate zinc release and allowed the determination and calculation of the total amount of bound zinc per DnaJ molecule. PAR in buffer was used as blank and for measuring zinc release during DnaJ's oxidation process in H_2O_2 and $CuCl_2$, the blank contained the appropriate amount of $CuCl_2$.

PMPS titration can also be used to determine the total number of thiol groups in a protein that coordinate zinc (130). A titration mix containing 0.1 mM PAR, 0.2 mM PMPS in KL-buffer was added in 3 µl aliquots to the DnaJ-PAR mix. This caused a gradual zinc release. The PMPS concentration that is necessary to release all zinc allows furthermore conclusions about the number of thiol groups. Addition of high concentrations of PMPS (30 µM) was needed to quickly release all bound zinc. This was used to determine the amount of zinc bound to proteins.

3.4.4.3 AMS trapping of DnaJ

4-acetamido-4'-maleimidylstilbene-2,2'-disulfonic acid (AMS) trapping was used to monitor the thiol status of DnaJ's cysteine residues both *in vitro* and *in vivo*. AMS is a thiol specific probe that adds a molecular mass of 500 Da to each modified SH-group. For *in vitro*

AMS trapping, DnaJ samples were withdrawn during the oxidation reaction of DnaJ and the protein was precipitated with 10% TCA. For *in vivo* AMS trapping, cell aliquots were withdrawn before, during and after the stress treatment and immediately lysed by precipitation with 10% TCA. After 30 min incubation on ice, the precipitates were pelleted (30 min, 15,700 xg, 4°C) and washed twice with ice-cold acetone. The air-tried pellet was resuspended in AMS buffer (100 mM Tris, pH 8.0, 6 M urea, 0.5 % SDS, 10 mM EDTA, 15 mM AMS) and incubated for 1 h at 25°C in the dark. Then, samples were supplemented with 1x SDS buffer and separated on 14% SDS PAGE.

3.4.4.4 Biotinylation of DnaK

This method was established to analyze the thiol state and accessibility of DnaK's highly conserved cysteine *in vitro* and *in vivo*. N-Ethylmaleimide (NEM) binds to SH-groups that are accessible for modification in the native protein. Subsequent Gua-HCl treatment was used to unfold DnaK and to make buried thiol groups accessible. These are then modified with a biotin-labeled maleimide (maleimide PEO_2-Biotin). Only DnaK molecules with thiol groups that were originally not accessible, either due to intrinsic modification or inaccessibility in the protein, are biotin-labeled and can be detected with α-biotin antibodies.

For *in vitro* biotinylation, 2 µM non-treated (25°C), unfolded (43°C) or oxidized (2 mM H_2O_2, 43°C) DnaK was incubated with 100 mM NEM (1 M stock solution in EtOH) in 100 µl buffer (40 mM MOPS, pH 7.5, 50 mM KCl) for 5 min, maintaining the original reaction temperature. For *in vivo* trapping, wild type cells were grown to logarithmic phase in LB medium and exposed to the individual stress conditions. At the end of the stress treatment, 100 mM NEM (3.3 M stock solution in EtOH) was added directly to the cell cultures and incubation was continued for 5 min. Then, 500 µl cell culture or 100 µl of the NEM-trapped *in vitro* sample were precipitated with 15% TCA at 4°C. This stopped any further modifications. After 30 min incubation on ice, precipitates were pelleted by centrifugation (15 min, 15,700 xg, 4°C) and the protein pellet was washed with 10% TCA, followed by a 5% TCA wash. Next, the pellets were resuspended in 50 µl biotin buffer (10 mM maleimide PEO_2-Biotin, 200 mM MES, pH 6.5, 10 mM EDTA, 0.5% SDS) under rapid shaking for 30 min at 37°C. To ensure complete thiol modification, the protein pellet needed to be completely resuspended. TCA (10%) precipitation of the sample removed all non-bound maleimide PEO_2-Biotin. *In vitro* samples were resuspended in 200 µl 1x SDS buffer, followed by 1:10 dilution before analysis on non-reducing 14% SDS PAGE. *In vivo* samples were resuspended in SDS buffer adjusting for the original cell concentration (100 µl buffer for

500 µl cells with OD_{600nm} of 0.5). 10 µl samples were loaded onto a 14% SDS gel and electrophoresis was performed for 3 h (35 mAmp, max 200 mV). After western blotting, all biotinylated proteins were detected with 1:50,000 diluted α-biotin antibody (section 3.4.6).

3.4.5 SDS PAGE and Protein Staining

SDS polyacrylamide gel electrophoresis (PAGE) is an extremely useful method for separating and analyzing proteins. The binding of SDS molecules to amino acids in proteins causes the loss of protein structure and the addition of numerous negative charges to the proteins. This allows size dependent separation of proteins in an electrical field were small proteins migrate faster through the gel matrix than larger polypeptides.

14% Tris-glycine acrylamide gels (Invitrogen) were used for the most part. Proteins were supplemented with reducing or non-reducing SDS buffer and separated in an electrical field applying 100 to 200 mV and 35 mA per gel for one hour. Subsequent visualization of the proteins was obtained using a modified Coomassie Blue Staining (Table 3) (140) or the more sensitive Silver Staining (Table 4).

Table 3 Fairbanks Staining (Coomassie Blue Staining)

step	solution	incubation time
1. Staining with Fairbanks A	10 % acetic acid, 25 % isopropanol, 0,05 % Coomassie	1 min heating, 10 min shaking
2. Destaining with Fairbanks B	10 % acetic acid, 10 % isopropanol, 0,005 % Coomassie	1 min heating
3. Destaining with Fairbanks C	10 % acetic acid, 0,002 % Coomassie	1 min heating
4. Destaining with Fairbanks D	10 % acetic acid	1 min heating, shaking

Table 4 Silver Staining

step	solution	incubation time
1. Wash	ddH_2O	2 x 2 sec

2. Fixation	60 ml acetone 1.5 ml 50 % (w/v) TCA 25 µl 37 % formaldehyde	5 min
3. Wash	ddH_2O	3 x 5 sec, 5 min, 3 x 5 sec
4. Pre-treatment	60 ml 50 % (v/v) acetone	5 min
5. Sensitizing	60 ml ddH_2O 100 µl 10 % (w/v) $Na_2S_2O_3$	1 min
6. Wash	ddH_2O	3 x 5 sec
7. Staining	60 ml ddH_2O 1.6 ml 10 % (w/v) $AgNO_3$ 0.6 ml 37 % formaldehyde	8 min
8. Wash	ddH_2O	2 x 5 sec
9. Developing	60 ml ddH_2O + 1.2 g Na_2CO_3 + 25 µl formaldehyde + 25 µl $Na_2S_2O_3$	as appropriate
10. Stopping	1 % (v/v) acetic acid	➢ 30 sec

3.4.6 Immunoblotting (western blotting)

Western blotting, also called immunoblotting, was used to detect proteins with high specificity and selectivity. After size-dependent separation of proteins by SDS PAGE, proteins were transferred from the acrylamide gel onto a nitrocellulose membrane. The latter was then exposed to an antibody that specifically interacted with the protein of interest. Enzyme-linked second antibodies subsequently allowed visualization of the first antibody and, therefore, the detection of the protein of interest via a chemiluminescence reaction on film.

Protein samples were separated on SDS PAGE as described in section 3.4.5. Using a semi-dry electro-blotting unit, SDS-charged proteins were transferred onto a nitrocellulose membrane for 1.5 h or 12 h (DnaK), applying 50 mA per blot. The membrane was subsequently incubated for 1 h in TBS buffer containing 5% milk powder to block non-specific antibody binding. Then, the membrane was incubated for 1 h with the protein-specific first antibody (dilution 1:3,000 for DnaJ, 1:2,000 for DnaK, 1:50,000 for biotin) in

TBS buffer containing 2% milk powder. The membrane was washed in TBS-T buffer (3 x 5 min). In case of α-biotin, the first antibody was already labeled with horseradish peroxidase (HRP), which could be detected immediately without additional incubation in second antibody. All other blots were treated with a second HRP-labeled antibody, which was directed against the first antibody (α-mouse for α-DnaK, α -rabbit for α-DnaJ). After 0.5 h incubation, a second wash (3 x 5 min) followed. Labeled proteins were detected by a chemiluminescence reaction using the Pierce SuperSignalWest kit according to the instructions.

3.5 Spectroscopic methods

3.5.1 Fluorescence Measurements of DnaK

DnaK contains one tryptophan residue (Trp102) in the N-terminal ATPase domain (148). The major conformational changes that accompany substrate release or binding by DnaK massively influence the tryptophan fluorescence. Monitoring the tryptophan fluorescence is, therefore, an excellent tool to follow DnaK's stimulation by substrate proteins or DnaJ (149). Moreover, fluorescence also decreases due to heat-induced unfolding of ATP-depleted DnaK (150), which was utilized to monitor DnaK's unfolding and refolding before, during and after stress treatment.

Fluorescence of DnaK was measured using the F-4500 Fluorometer (Hitachi), which was set to time scan mode with λ_{em} of 350 nm, λ_{ex} of 295 nm and slit widths of 5 nm. 0.5 μM nucleotide-depleted DnaK or $DnaK_{Cys15Ala}$ was incubated for 15 minutes under rapid stirring at 43°C in 1.4 ml buffer (40 mM MOPS, pH 7.5, 50 mM KCl) in the presence or absence of 5 mM GSSG. Then 0.5 mM pre-warmed ATP and/or 140 mM GSH were added and incubation was continued at 43°C. Fluorescence data were corrected for the quenching factor caused by GSSG and adjusted for dilution effects.

3.5.2 Circular dichroism measurements

Circular dichroism (CD) spectroscopy measures differences in the absorption of left-polarized light versus right- polarized light by proteins, which are caused by structural variation. Measurements in the far-UV-range (190-250 nm) are used to determine secondary structural elements of proteins. The chromophore is the peptide bond and absorption increases when it is located in a regular, folded environment. α-helices, β-sheets, and random coil structures therefore result in characteristic CD spectra. The CD spectrum of a protein in

the near-UV region (250-350 nm) is characteristically for its tertiary structure. The chromophores are the aromatic amino acids and disulfide bonds, and the CD signals can be considered the fingerprint of a protein.

Both methods were used to investigate the structural integrity of the DnaJ zinc center mutants. All DnaJ proteins were dialyzed overnight against 30 mM phosphate buffer, pH 8.2, 120 mM KCl, 15 mM NaCl, 4% glycerol and the protein concentrations were adjusted to 10 µM. Cuvettes with path lengths of 1 or 10 mm were used for far UV-CD or near UV-CD, respectively. CD spectra were recorded using a Jasco J810 spectropolarimeter and 20 spectra were accumulated.

3.6 Chaperone assays *in vitro*

The activity of chaperones was analyzed using their ability to prevent protein aggregation of refolding model substrates or to support reactivation of unfolded proteins. In the case of ATP-dependent chaperones such as DnaK, ATP hydrolysis is also a good measure of the chaperone activity, because it is influenced by both substrate proteins and co-chaperone interactions.

Very important for all *in vitro* chaperone assays is the choice of the substrate proteins. Besides being an actual substrate of the chaperone of interest, they should be easy to handle to obtain reproducible results. The proteins should form detectable aggregates and have an activity assay to monitor the influence of the chaperone on its inactivation and reactivation. So far, not many substrate proteins have been established for *in vitro* use of the DnaK/DnaJ/GrpE-system and the most commonly used substrate is firefly luciferase, and less often mitochondrial citrate synthase from pig (151, 152).

Several different strategies can be used to denature substrate proteins. These result in different un- or misfolded states. Thermal unfolding of proteins is often considered a rather mild way to denature proteins, because chaperones are present during the unfolding process and bind unfolding intermediates, as compared to the complete unfolding using high concentrations of chaotropic agents such as guanidinium-HCl.

3.6.1 Light scattering experiments

Light scattering takes advantage of the fact that insoluble protein complexes scatter light. This allows following the aggregation of substrate proteins *in vitro*. Progressing protein aggregation is revealed by an increase of the light scattering signal. This can be easily measured at a fluorometer using the same emission (λ_{em}) and exitation (λ_{ex}) wavelength.

3.6.1.1 Aggregation of chemically denatured luciferase

8 µM firefly luciferase was denatured in 5 M Gua-HCl, 20 mM Hepes, pH 7.5 for at least 1 h at room temperature in a glass vial. The fluorometer (Hitachi F4500) was set to time scan mode using $\lambda_{em/ex}$ of 320 nm and slit widths of 5 nM. The denatured protein was diluted 1:100 into filtered buffer (40 mM MOPS, pH 7.5, 50 mM KCl, ± 2 mM ATP) at 30°C in the absence or presence of chaperones. Light scattering was measured for 10 min under constant stirring.

3.6.1.2 Aggregation of chemically denatured citrate synthase

30 µM citrate synthase was denatured in 6 M Gua-HCl, 20 mM Hepes, pH 7.5 for 2 hours at room temperature. Aggregation was induced by diluting the unfolded protein 1:400 into filtered buffer (40 mM MOPS, pH 7.5, 50 mM KCl). Light scattering at 20°C in the absence or presence of 0.15 µM DnaJ was followed for 400 sec using a fluorometer (Hitachi F4500) set to time scan mode with $\lambda_{em/ex}$ of 500 nm and slit widths of 2.5 nm.

3.6.2 Reactivation of chemically denatured luciferase

Luciferase catalyzes the oxidation of D-luciferin to oxyluciferin in MgATP and oxygen dependent manner. This reaction is accompanied by the production of light (luminescence), which can be a direct measure of luciferase activity. Dilution of chemically unfolded luciferase into refolding buffer results in the refolding of ~10% of luciferase molecules. In the presence of DnaK/DnaJ/GrpE, more than 80% refold, making luciferase a very suitable model substrate for analyzing the activity of the DnaK-system. Luminescence can be detected using a fluorescence spectrophometer in the luminescence mode with the lamp switched off.

Luciferase was denatured as described above (section 3.6.1.1) and diluted 1:100 under rapid stirring into Eppendorf tubes containing 300 µl prewarmed buffer (40 mM MOPS, pH 7.5, 50 mM KCl, 2 mM ATP, 50 µg/ml BSA) at 30°C. If not mentioned otherwise, a molar ratio of 10:2:10 of DnaK:DnaJ:GrpE over luciferase was used. 10 µl aliquots were taken during the refolding reaction and pipetted into 290 µl luminescence assay mix (70 µM D-luciferin, 100 mM potassium phosphate, pH 7.8, 25 mM glycylglycine, 0.2 mM EDTA, 2 mM MgATP, 0.5 mg/ml BSA) in disposable plastic cuvettes. Luminescence was measured at room temperature in time scan mode with λ_{ex} of 557 nm and slit width of 20 nm. As luciferase causes a light overshoot during the initial reaction phase, the slope of the

luminescence signal was measured 1 minute after the addition for 30 sec and extrapolated to its theoretical starting value (153).

3.6.3 Reactivation of chemically denatured citrate synthase

As part of the citrate cycle, citrate synthase catalyzes the condensation of citrate from OAA and AcCoA. This releases CoA-SH, whose thiol groups can be detected with the Ellman's reagent (section 3.4.4.1).

15 µM citrate synthase was denatured in 4.5 M Gua-HCl, 50 mM Tris-HCl, pH 8.0 for 2 h at room temperature. Under rapid stirring, the unfolded substrate was diluted 1:100 into 40 mM MOPS, pH 7.5, 50 mM KCl at 25^{o}C in the absence or presence of chaperones. After the indicated reactivation times, the activity of refolded citrate synthase was determined as described (152). 20 µl aliquots of the refolding reaction were withdrawn and diluted into a total volume of 500 µl assay buffer (50 mM Tris-HCl, pH 7.5, 100 µM DTNB, 45 µM AcCoA, 50 µM OAA). The change of absorption at 412 nm over time was recorded. Relative activities of citrate synthase were obtained by determining the initial slopes of the recorded TNB production.

3.6.4 Determination of DnaK's ATPase activity

DnaK's chaperone activity is ATP-dependent and the ATPase activity is influenced by substrate proteins as well as the co-chaperones DnaJ and GrpE. ATP hydrolysis and ADP accumulation over time can be quantified after separating the radioactively labeled nucleotides by thin layer chromatography (TLC), using PEI cellulose coated plates. 2 µl aliquots were withdrawn from the hydrolysis reactions at indicated time points and spotted directly onto TLC plates. The low pH of the matrix immediately stopped further ATP hydrolysis. The TLC plates were developed in a closed glass chamber with 2 M formic acid, 0.5 LiCl until the liquid reached the upper edge and subsequently air tried. Wrapped in plastic, the TLC plates were exposed to high sensitive phosphor imager screens for 30 to 60 min and the amount of ADP and ATP was determined using the software Biorad Quantity one 4.5.0 of the phosphor imager Biorad molecular imager FX. The intensity and volume of the signal was linear to the amount of radiolabeled nucleotides. To determine the rate of ATP hydrolysis (ADP $DnaK^{-1}$ min^{-1}) the accumulation of ADP was compared to the total amount of nucleotides per sample as well as to the available ATP at the beginning of the reaction and blotted against the time.

3.6.4.1 Steady state ATPase assay

50 µl reactions containing 40 mM MOPS, pH 7.5, 50 mM KCl, 5 mM MgCl with 200 µM ATP (0.5 µCi [α^{32}P]ATP) and indicated amounts of DnaJ and GrpE were prewarmed at 25^{o}C. The reactions were started by the addition of 0.69 µM DnaK and aliquots were taken at indicated time points as described (section 3.6.4).

3.6.4.2 Single turn over ATPase assay

First, a DnaK-ATP complex was prepared (154). 10 µM DnaK was incubated with 40 µM ATP (0.1 – 0.2 µCi/ml [α^{32}P]ATP) in 40 mM MOPS, pH 7.5, 50 mM KCl, 10 mM $MgCl_2$ for 2 min on ice to allow the DnaK-[α^{32}P]ATP complex formation. Unbound ATP was separated from the complex using a micro Bio-Spin size exclusion chromatography column. DnaK-[α^{32}P]ATP was aliquoted and quickly frozen in a dry ice/ EtOH bath until further use. DnaK concentration in the complex was determined using a Bradford assay (section 3.4.1).

To measure the single turn-over rate of ATP hydrolysis by DnaK in the presence of DnaJ and non-native substrate, 30 µl reactions containing 0.16 µM DnaJ in 40 mM MOPS, pH 7.5, 50 mM KCl were prepared and incubated at 25°C. Immediately after addition of chemically denatured luciferase (as described under 3.6.2, final conc. 0.08 µM), the reaction was started with the addition of 0.8 µM DnaK-[α^{32}P]ATP complex. Aliquots were taken at indicated time points and processed as described 3.6.4.

3.7 Phenotypic assays and other *in vivo* methods

3.7.1 Growth under stress conditions

Heat shock proteins like the DnaK-system enable wild type *E. coli* cells to grow at elevated temperatures (62, 155). Functional loss of these important chaperones causes, therefore, a growth defect under heat shock conditions. To ensure comparable expression of the plasmid encoded protein of interest, the culture media was supplemented with the appropriate antibiotic and IPTG concentrations. Then, protein synthesis was allowed at a permissive temperature for a defined time. For plate assays, cells were streaked out from a single colony and incubated overnight under the appropriate stress conditions. For growth analysis in liquid culture, stress was initiated by transferring the cell culture into prewarmed

media supplemented with the oxidant or by transferring the flask to a shaking waterbath at heat shock temperatures.

3.7.2 Cell motility assay

Wild type *E. coli* cells (MG1655) possess highly structured rotating flagella on their cell surface, which enable the bacteria to swim. The DnaK-system appears to be essential for the flagella assembly (156) and failure of the chaperone function of the DnaK-system renders the cells non-motile. This property can be easily tested on semi-liquid media.

Cells from an overnight grown LB plate were carefully dot-spotted onto plates containing 3% agar and cultivated for 6 to 15 hours at 30°C or 37°C. Bacteria with functional flagella migrate away from the original location, thereby forming a visible growth circle while non-motile cells remain in the center of inoculation.

3.7.3 Phage λ replication assay

The DnaK-system was shown to be essential for DNA replication of λ phage in infected cells (64). Successful replication of λ phage results in cell lysis. If cells grow as a bacterial lawn on agar plates, lysed areas can be detected as plaques and quantified. Cells expressing inactive DnaK or DnaJ do not form plaques. The assay was used to analyze the *in vivo* chaperone activity of DnaK and DnaJ and their mutated variants.

Cells expressing the chaperone(s) of interest were pelleted from a 5 ml overnight culture and resuspended in 2.5 ml LB containing 10 mM $MgSO_4$. 200 µl cell suspension was rapidly mixed with 3 ml of hand-warm top agar supplemented with 10 mM $MgSO_4$ and pored onto the top of prewarmed LB plates. After solidification of the layer, the surface was air-tried and 10 µl of serial dilutions of high titer λ-lysate (157) were spotted onto the surface. After overnight incubation at the desired temperature, cells supporting λ-growth were lysed, forming clearly visible plaques. Each plaque corresponded to one phage. The functional activity of DnaK or DnaJ *in vivo* corresponded to the up to 10,000-fold difference in λ-replication.

3.7.4 Determination of cellular ATP level

The nucleotide ATP is as energy resource important for many cellular processes and knowledge about its precise concentration is crucial. As the nucleotide pool reacts extremely fast to environmental or cellular changes (158), the exact determination of the ATP concentration is difficult. Alterations of temperature or nutrient availability due to sampling

procedures like cell harvesting cause major shifts in ATP/ADP ratios (158). The method used in this work appears to avoid such problems, because cells are lysed by directly diluting them into hot buffer, which immediately unfolds and inactivates ATP hydrolyzing proteins (159). Disadvantage of this method is that the detected ATP concentrations are low due to the inability to concentrate cells and HPLC analysis cannot be performed to determine ATP/ADP levels. Instead, ATP concentrations in cell lysates were measured using the fast and very sensitive luciferase assay.

Cells were grown in LB medium to logarithmic phase and exposed to stress conditions as indicated. For each time point of stress treatment, the $OD_{600\ nm}$ was determined and 50 µl cell culture was withdrawn and mixed rapidly with 950 µl hot buffer (50 mM Hepes KOH, pH 7.8, 4 mM $MgSO_4$). Samples were kept shaking at 99°C for 4 minutes and were then transferred to ice until further use.

The ATP content of the samples was measured using the luciferase assay. Luminescence is linear to the amount of available ATP. 60 µl sample was mixed with 60 µl luminescence buffer (140 µM luciferin, 200 mM potassium phosphate, pH 7.8, 50 mM glycylglycine, 0.4 mM EDTA, 4 mM MgATP, 1 mg/ml BSA) and the amount of light production was measured with a luminometer. The ratio of relative luminescence units (RLU) to ATP was determined from an ATP standard. To calculate the cellular ATP level, the number of cells per sample was determined from the measured $OD_{600\ nm}$ (OD of 1 corresponds to $5.6x10^8$ cells/ml). Then the total cell volume was calculated based on the value of $1.57\ x10^{-15}$ liter per cell (160).

4 Results

4.1 Characterization of DnaJ under oxidative stress conditions

4.1.1 DnaJ – Chaperone with two zinc centers

The DnaK/DnaJ/GrpE chaperone system in *E. coli* appeared to be inactive in preventing protein aggregation under conditions of combined heat and oxidative stress (1), while it was shown to protect cells very efficiently from heat-induced protein aggregation (37, 155, 161). To investigate this finding, we first analyzed whether oxidative stress causes a change in DnaJ's activity. The Hsp40 homologue DnaJ contains two zinc ions in its cysteine rich domain (Figure 15) (76, 86). Each zinc ion is bound by four cysteine residues arranged in two highly conserved cysteine motifs Cys-X-X-Cys-X-G-X-G (83, 85). Such zinc centers are known to be often involved in redox-regulation of proteins. Oxidation of these metal coordinating thiols can result in zinc release, which causes conformational changes that can lead to the reversible loss or gain of protein function (32). Based on domain truncation studies, the zinc binding domain of DnaJ was thought to be important for the DnaK-dependent chaperone activity of DnaJ (75, 87, 151, 162). Redox-induced changes in the zinc binding domain of DnaJ could therefore dramatically alter the function of the DnaK-system both *in vitro* and *in vivo*.

4.1.2 Zinc content of DnaJ *in vitro*

To determine whether exposure of DnaJ to oxidative stress causes the loss of DnaJ's chaperone activity *in vitro*, the protein was overexpressed in *E. coli* and purified as described (section 3.3.5). For these studies, it was essential to establish conditions to obtain fully reduced and zinc-coordinated DnaJ.

To determine the oxidation state of purified DnaJ, DnaJ was denatured to expose all thiols and incubated in the presence of the thiol-specific Ellman's reagent (DTNB). Purified DnaJ revealed 9 of the expected 10 cysteines, indicating that DnaJ is reduced after its purification. To determine the zinc concentration in our DnaJ preparation, the PAR/PMPS assay was employed (147) (section 3.4.4.2). The metal chelator PAR reacts with free zinc to form a colored $PAR(Zn)_2$ complex, which can be detected spectroscopically at 500 nm (ε_{500nm}=72,710 M^{-1} cm^{-1}). To release zinc from the high affinity zinc center, a PMPS solution was used to modify the zinc-coordinating thiols of DnaJ. This gradually induced zinc release.

The released zinc then interacts with PAR in the solution and the increasing absorption at 500 nm was used to determine the number of thiol groups involved in zinc coordination. As shown in Figure 8, nearly all of the bound zinc was released by modifying ~7 cysteines in DnaJ. This agreed well with the finding that the two zinc ions are coordinated by 8 thiol groups.

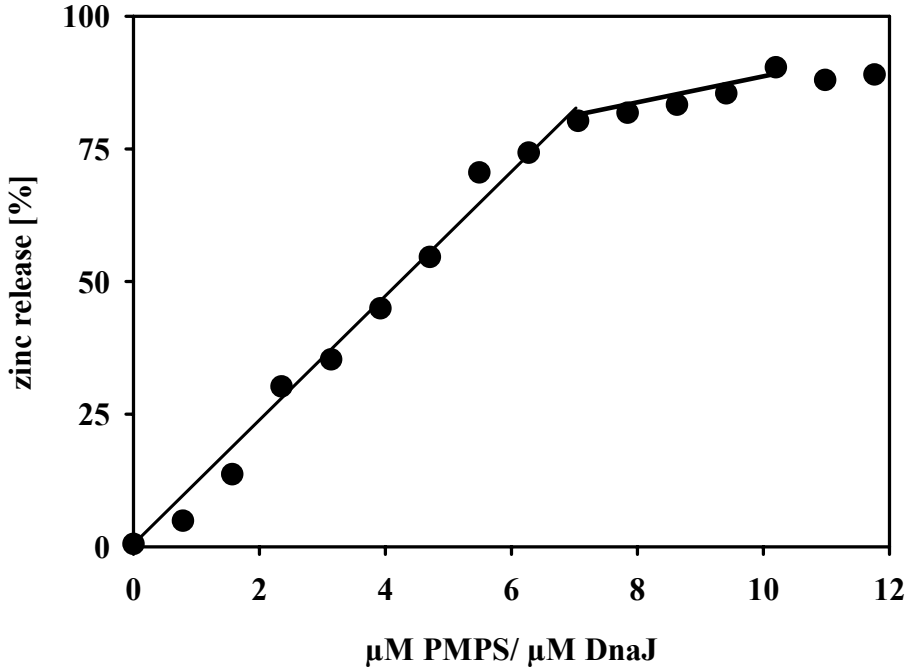

Figure 8 Thiol titration of DnaJ *in vitro*

1 µM purified DnaJ was incubated in KL-buffer in the presence of PAR. Thiol modification with PMPS caused the gradual release of bound zinc from DnaJ. The extinction of the $PAR(Zn)_2$ complex was monitored at 500 nm.

4.1.3 Oxidation of DnaJ *in vitro*

If DnaJ's zinc centers comprise a redox-regulated molecular switch, incubation of DnaJ in oxidants such as H_2O_2 should lead to zinc release, which in turn might cause a change in the activity of the chaperone. To analyze whether oxidative conditions at elevated temperatures lead indeed to zinc release, the protein was incubated at 43°C in the presence of 2 mM H_2O_2. Aliquots were withdrawn from the reaction to monitor the zinc release using the PAR/PMPS assay (section 3.4.4.2). We found that incubation in H_2O_2 caused the slow release of zinc with a T½ of 65 min. Spectroscopic analysis of oxidized DnaJ revealed, that this extended oxidation process caused the protein to partly aggregate.

To improve the conditions of DnaJ's oxidation, the oxidation reaction was performed with H_2O_2 and sub-stochiometric amounts of $CuCl_2$. Fenton reagents such as Cu^+ are known to catalyze oxidation reactions. They react with H_2O_2 to form hydroxyl radicals, which in

turn attack thiol groups of proteins. The resulting thiyl groups are very reactive and generate disulfide bonds with other thiols in the vicinity. This high reactivity allowed the oxidation process of DnaJ to proceed at 25°C. Even after 90 min of incubation in H_2O_2 and $CuCl_2$, when DnaJ had lost all its bound zinc ions with a T½ of 16.2 min (Figure 11), the measured protein spectrum suggested only negligible proteins aggregation.

4.1.4 Disulfide status of DnaJ during the oxidation process *in vitro*

Oxidation of DnaJ led to the rapid release of zinc at room temperature, presumably caused by disulfide bond formation or other modifications of DnaJ's highly conserved, zinc coordinating cysteine residues. Monitoring those thiol modifications would not only be an additional way to confirm the oxidation of DnaJ *in vitro* but would also allow the investigation of DnaJ's redox-state *in vivo*. Modification of cysteine residues by the thiol specific probe 4-acetamido-4'-maleimidylstilbene-2,2'-disulfonic acid (AMS) has been used for thiol analysis both *in vitro* and *in vivo* (31). Alkylation of thiol groups with AMS results in the addition of 500 Da per SH group, a molecular mass difference that is easily detectable on SDS PAGE. In case of fully reduced DnaJ, alkylation of all 10 cysteine residues leads to a mass difference of 5 kDa as compared to non-alkylated DnaJ (compare lane 1,2 in Figure 9). Oxidatively modified thiols, however, do not react with AMS and result in a DnaJ species with less additional mass.

DnaJ was oxidized in the presence of 2 mM H_2O_2, 5 µM $CuCl_2$ at 25°C and aliquots were withdrawn during DnaJ's oxidation at the indicated time points (Figure 9). Samples were immediately precipitated with 10% TCA to stop further oxidation, the protein pellet was washed with acetone to remove the oxidant and resuspended in AMS/urea buffer (section 3.4.4.3). The urea in the buffer caused the unfolding of DnaJ, which allowed alkylation of all free thiol groups with AMS. As shown in Figure 9 (lane 2-6), the progressing oxidation of DnaJ was nicely reflected by the gradual up-shift of the protein band over time, as fewer thiols in DnaJ remained accessible for AMS modification. DnaJ that had lost 29% of its bound zinc (Figure 9, lane 3) was still mainly AMS-modified, indicating the presence of free (reduced) thiols. Release of more than 80% zinc (lane 5), however, appeared to be the consequence of the almost complete oxidation of DnaJ's thiols, reflected by only minor molecular mass shifts that are presumably due to the modification of the two cysteine residues that are not involved in zinc binding.

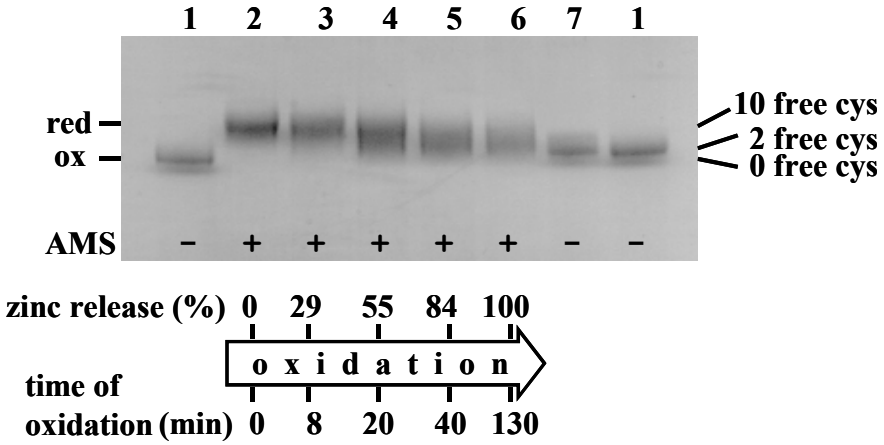

Figure 9 Disulfide status of DnaJ during the oxidation process *in vitro*

The redox status of DnaJ was analyzed by thiol trapping with AMS. Alkylation with AMS results in the addition of 500 Da per SH group. DnaJ was oxidized in the presence of 2 mM H_2O_2, 5 µM $CuCl_2$ at 25°C and the zinc release was measured immediately. Samples for the AMS trapping were taken at the same time points, precipitated with 10% TCA to remove oxidants, trapped under denaturing conditions (lane 2-6) and separated on a SDS PAGE. Lane 1 and 7 shows fully reduced and oxidized DnaJ, respectively, without AMS trapping.

4.1.5 Chaperone activity of oxidized DnaJ

4.1.5.1 Prevention of citrate synthase aggregation by DnaJ

To investigate to what extent oxidation of DnaJ affected its activity, we analyzed the chaperone activity of DnaJ *in vitro*. In addition to serve as co-chaperone for DnaK, DnaJ has also been shown to possess autonomous chaperone activity (75, 151). As a holdase, DnaJ binds tightly to non-native substrate proteins and prevents their irreversible aggregation. To analyze the chaperone activity of DnaJ, the aggregation of the model substrate citrate synthase and its prevention by DnaJ was monitored using light scattering measurements (section 3.6.1.2).

Dilution of chemically denatured citrate synthase into refolding buffer in the absence of chaperones caused rapid aggregation of the protein (Figure 10, gray line). Two-fold excess of reduced DnaJ was able to significantly prevent aggregation of citrate synthase, which was in good agreement with former studies (Figure 10, trace b). To measure the holdase activity of partially and fully oxidized DnaJ, the protein was oxidized as described (section 3.4.3.1). At several time points during the oxidation process, aliquots were withdrawn from the reaction and the progress of zinc release as well as DnaJ's activity in preventing citrate synthase aggregation was determined. DnaJ was found to start loosing its holdase activity after release of 10% of bound zinc (Figure 10, trace c). After release of 29% bound zinc, almost no chaperone activity was left (Figure 10, trace d), suggesting that not both zinc

centers had to be oxidized for this change in activity. This result suggested that DnaJ looses its activity upon oxidation by H_2O_2. Furthermore, oxidation of only one of DnaJ's two highly conserved zinc centers appeared to be sufficient for the inactivation of DnaJ.

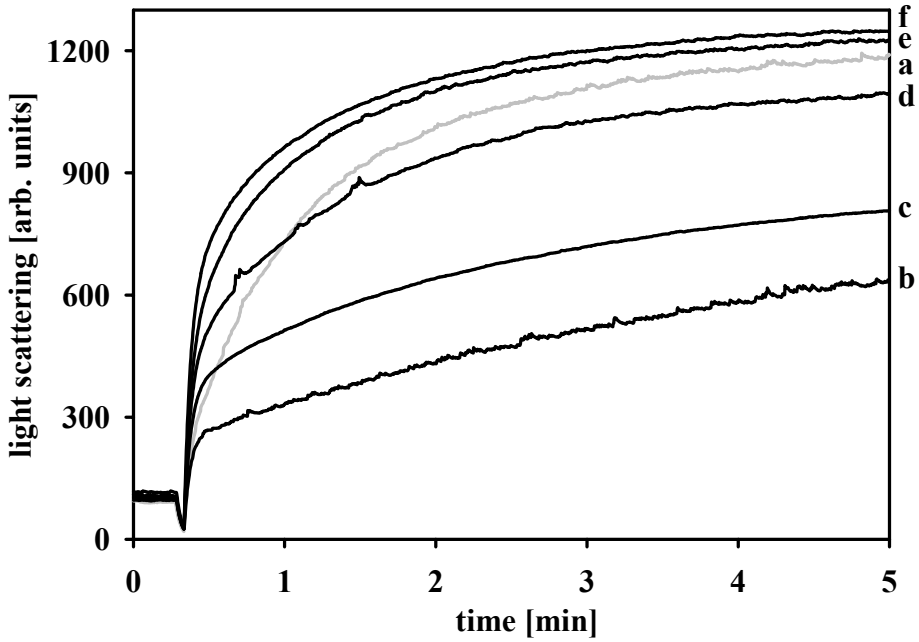

Figure 10 Aggregation of chemically denatured citrate synthase

Chemically denatured citrate synthase was diluted 1:400 (final conc. 75 nM) into refolding buffer in the absence (a, gray trace) or presence of reduced (b) or oxidized (c-f) DnaJ (150 nM). Aggregation was monitored by measuring light scattering at $\lambda_{em/ex}$ = 500 nm. 20 µM DnaJ was oxidized in the presence of 2 mM H_2O_2, 5 µM $CuCl_2$ at 25°C and its chaperone activity was determined after release of 10% zinc (c), 29% zinc (d), 55% zinc (e) and 84% zinc (f).

4.1.5.2 Prevention of spontaneous refolding of citrate synthase by DnaJ

The inhibition of protein aggregation is not the only indicator of chaperone binding. Spontaneous reactivation of non-native substrate proteins upon dilution into refolding buffer can be prevented by tight chaperone-substrate interactions. If only the reduced DnaJ species was able to interact with chemically unfolded citrate synthase, only reduced DnaJ should prevent its reactivation. Therefore, the influence of reduced and oxidized DnaJ on the reactivation of citrate synthase was analyzed as described (section 3.6.3) (152).

Citrate synthase activity was measured after 2 h of reactivation in the absence of chaperones and was set to 100%. 10-fold excess of reduced DnaJ prevented this spontaneous refolding and citrate synthase regained only 50% activity (Figure 11, time point 0, open circles). To determine the activity of oxidized DnaJ, aliquots were withdrawn from DnaJ's oxidation reaction and the zinc release as well as its chaperone activity were determined (Figure 11). Surprisingly, DnaJ did not loose its ability to prevent citrate synthase

reactivation as expected from the aggregation measurements (Figure 10). In contrast, during its oxidation reaction, DnaJ increase its ability to prevent citrate synthase reactivation with a T½ of 8.8 min and fully oxidized DnaJ prevented citrate synthase refolding to almost 100% (Figure 11, open circles).

An essential characteristic of redox-regulated proteins is that their "switch" is reversible. To investigate whether the change in DnaJ's activity was reversible, 5 mM DTT was added after 90 min of oxidation and DnaJ's chaperone activity was analyzed. Immediately after establishing reducing conditions, DnaJ resumed its original activity and allowed spontaneous citrate synthase refolding to only 50% (Figure 11). The reduction of oxidized DnaJ was much faster than the oxidation and, more importantly, it showed that the oxidation of DnaJ is fully reversible.

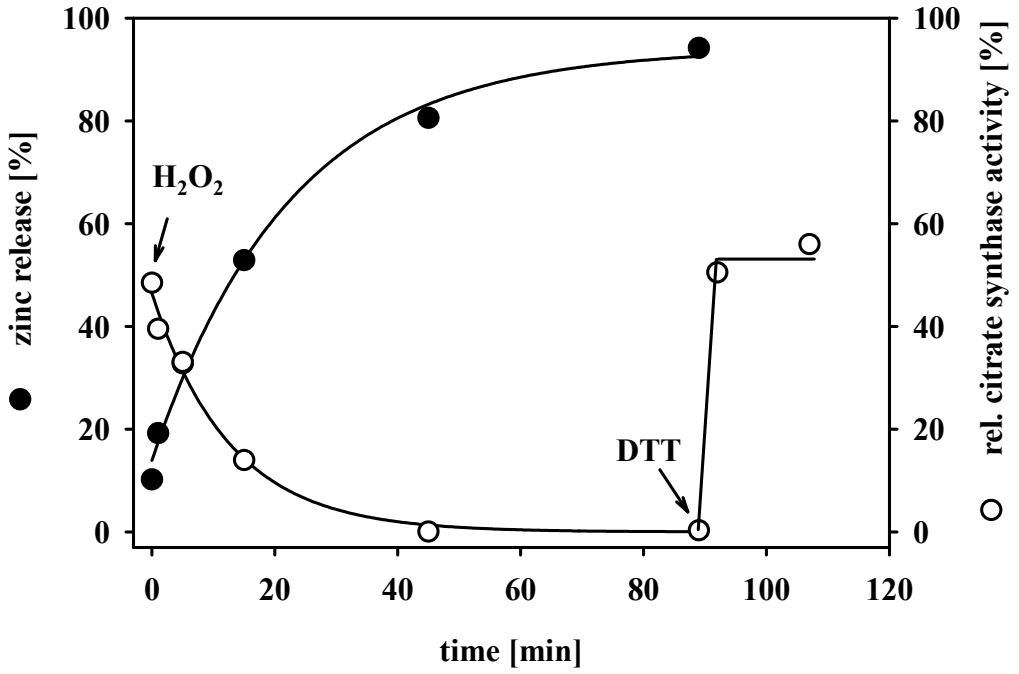

Figure 11 Zinc release and chaperone activity during the oxidation of DnaJ

DnaJ was oxidized in the presence of 2 mM H_2O_2, 5 µM $CuCl_2$ at 25°C. After 90 min of oxidation, 5 mM DTT was added to reduce DnaJ. Samples were withdrawn from the reaction at the indicated time points and the zinc content (●) as well as the chaperone activity (○) was determined immediately. Refolding of chemically unfolded citrate synthase was allowed for 2 hours. Spontaneous reactivation of citrate synthase in the absence of DnaJ was set to 100%.

While oxidized DnaJ did not prevent the aggregation of unfolded citrate synthase, it appeared to prevent its spontaneous reactivation. Two explanations could account for this, small aggregates of oxidized DnaJ might induce the irreversible aggregation of citrate

synthase that would otherwise refold, or oxidized DnaJ might form stable DnaJ-citrate synthase microaggregates that cause light scattering. Both scenarios would prevent the refolding of citrate synthase. Only in the case of microaggregates formation, however, reduction of oxidized DnaJ-substrate complexes should cause the release of the substrate protein and allow its reactivation.

4.1.5.3 Reduction of oxidized DnaJ causes substrate release

To analyze whether reduction of oxidized DnaJ caused substrate release after the potential complex formation, substrate release studies were performed. First, spontaneous reactivation of unfolded citrate synthase was completely prevented by a 10-fold molar excess of fully oxidized or reduced DnaJ. After 1 h of incubation, the samples were divided and one half was supplemented with 2 mM DTT to reduce DnaJ. Citrate synthase activity of all samples was determined during further incubation at 30°C.

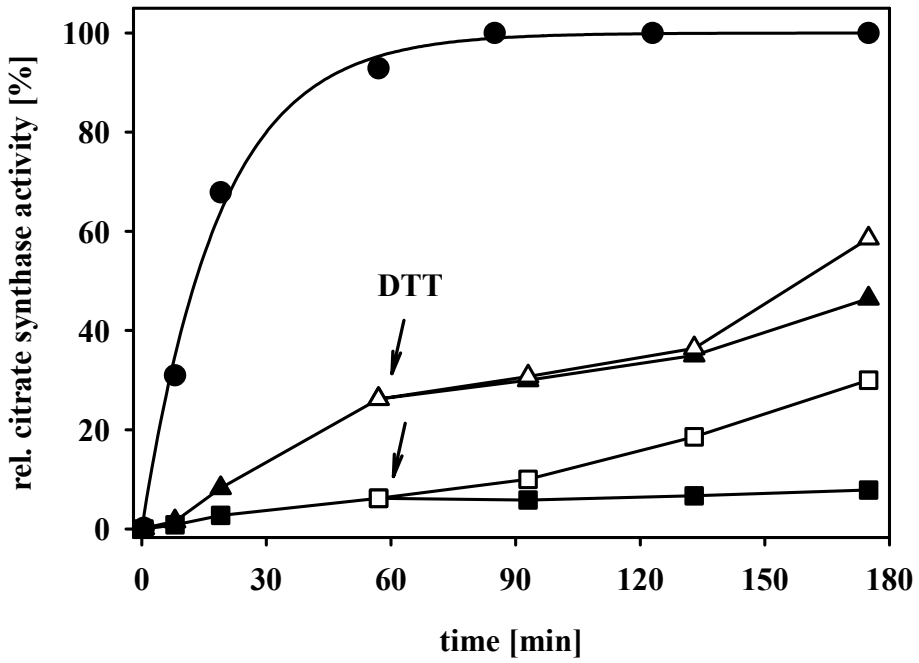

Figure 12 Substrate release from reduced and oxidized DnaJ

Chemically denatured citrate synthase was diluted 1:100 into refolding buffer in the absence (●) or presence of 10-fold excess of oxidized DnaJ (squares) or reduced DnaJ (triangles). After 60 min of incubation, the incubation reaction was split and 2 mM DTT was added to one aliquot (open symbols). Citrate synthase activity was determined at the indicated time points.

Figure 12 shows that chemically denatured citrate synthase in the absence of DnaJ refolded very fast (●), while the presence of a 10-fold excess of oxidized DnaJ (■) or reduced DnaJ (▲) prevented the reactivation to various degrees. In agreement with the earlier studies,

oxidized DnaJ almost completely prevented the refolding, while in the presence of reduced DnaJ a significant portion of citrate synthase still reactivated. Addition of DTT after 60 min of incubation resulted in the gradual release of substrate from oxidized DnaJ and the yield of citrate synthase reactivation reached ~30% after 2 h (□), suggesting that citrate synthase molecules were bound to oxidized DnaJ. The observed reactivation kinetic furthermore suggests that the substrate release is not complete after 2 h and that more citrate synthase will presumably be released after prolonged incubation.

While oxidized DnaJ started to release substrate immediately after exposure to reducing conditions, DTT addition had only minor effects on reduced DnaJ. Only after 2.5 h of incubation in the presence of DTT, a slowly increasing citrate synthase reactivation was observed. This could be caused by air oxidation of some DnaJ molecules. The results suggested that oxidized DnaJ did not induce the irreversible aggregation of citrate synthase but was able to form stable complexes with the substrate citrate synthase. Complex formation between citrate synthase and oxidized DnaJ might have caused the formation of larger oligomers, which could explain the increasing light scattering signal. The DTT-induced substrate release indicated that oxidized DnaJ bound unfolded substrate proteins in a redox-dependent manner.

4.1.5.4 DnaJ's chaperone activity in cooperation with the DnaK-system

Oxidation of DnaJ appeared to increase its holdase activity. So far it is unknown to what extent this autonomous chaperone function of DnaJ plays a role in protecting cells from heat induced aggregation *in vivo*. Its function as part of the DnaK-system, however, has been shown to be crucial for cell viability. Therefore, it was important to investigate whether the co-chaperone function of DnaJ was also influenced by its oxidation. DnaK and GrpE were purified as described (sections 3.3.4 and 3.3.6) and the influence of DnaJ's oxidation on the foldase activity of the DnaK-system was investigated. Firefly luciferase is a commonly used substrate for DnaK/DnaJ/GrpE (151). Because oxidized and reduced DnaJ prevented the aggregation as well as the spontaneous reactivation of chemically denatured luciferase to the same extent as citrate synthase (data not shown), luciferase was used for further studies.

Chemically denatured luciferase was diluted 1:100 into buffer (final concentration 0.08 μM) in the absence or presence of DnaK, GrpE and oxidized or reduced DnaJ. Aliquots were withdrawn and the luciferase activity was determined as described (section 3.6.2). While spontaneous refolding of luciferase was very low (13%), reduced DnaJ in concert with DnaK and GrpE supported luciferase refolding to 85% (Figure 13). Oxidized DnaJ was

unable to support the chaperone-induced reactivation of luciferase to the same extent. Depending on the extent of DnaJ's oxidation process, a refolding yield of only 20-60% of luciferase was observed (Figure 13, open circles). The high variability in the refolding yields is probably based on our inability to exactly monitor the oxidation state of DnaJ. In either case, it appeared that the activity of oxidized DnaJ was generally lower than the activity of reduced DnaJ. Considering the tight binding of oxidized DnaJ to unfolding substrate proteins, this reduced ability to refold luciferase together with GrpE and DnaK could be explained by a competition for substrate binding between DnaJ and DnaK. Stable DnaJ-substrate protein complexes would prevent the DnaK-assisted refolding of luciferase. In an attempt to analyze the activity of oxidized DnaJ in more detail, substrate release studies in the presence of DTT were performed (section 4.1.5.3).

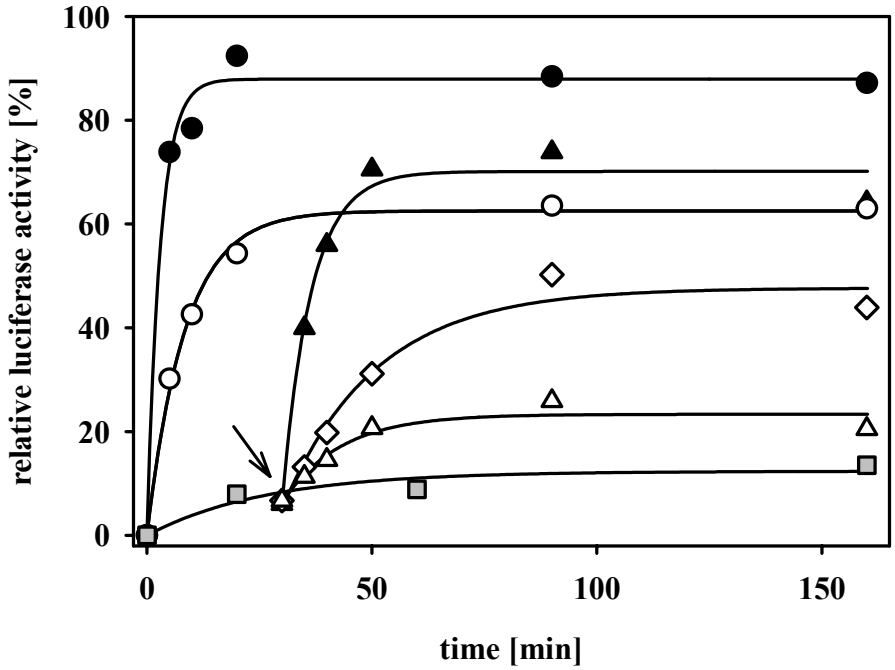

Figure 13 Substrate release from oxidized and reduced DnaJ in the presence of the DnaK-system

Chemically denatured luciferase was diluted 1:100 (final conc. 0.08 µM) into refolding buffer either in the absence of chaperones (gray squares) or in the presence of DnaK, $DnaJ_{red}$, GrpE (0.8 µM, 0.16 µM, 0.8 µM, ●) or DnaK, $DnaJ_{ox}$, GrpE (○). To analyze substrate release, complexes with reduced (filled triangles) or oxidized (open triangle) DnaJ (0.16 µM) were formed by incubation at 30°C. Then, DnaK (0.8 µM) and GrpE (0.8 µM) were added after 30 min as indicated by the arrow. To induce substrate release from oxidized DnaJ, 2 mM DTT was added together with DnaK and GrpE after 30 min (open diamonds).

Chemically denatured luciferase was incubated with oxidized or reduced DnaJ for 30 min to allow complex formation. Then, samples were supplemented with DnaK and GrpE in the absence or presence of 2 mM DTT and luciferase activity was monitored (section 3.6.2). After 30 min of complex formation with oxidized and reduced DnaJ, luciferase reactivation

was below 13%. Addition of DnaK and GrpE to complexes of unfolded luciferase and reduced DnaJ resulted in the fast release of luciferase and refolding yields of 70% (Figure 13, filled triangles). Additional presence of DTT did not influence this result (date not shown). Chaperone holdase activity of reduced DnaJ was apparently high enough to form complexes and allow refolding even after 30 min incubation at 30°C. Oxidized DnaJ, in contrast, released only little luciferase upon addition of DnaK/GrpE (Figure 13, open triangles). This release was, however, significantly increased by the subsequent addition of DTT (Figure 13, open diamonds), confirming earlier results that stable complexes are formed between oxidized DnaJ and its substrate. Independent from the activity of the various preparations of oxidized DnaJ, in no case reached oxidized DnaJ the same high degree of substrate release and refolding than reduced DnaJ.

Oxidation of DnaJ *in vitro* appeared to increase its substrate affinity, resulting in the decreased transfer of the substrate proteins to the DnaK-system. *In vivo*, the formation of such stable DnaJ-substrate complexes would prevent the premature refolding of non-native polypeptides by the DnaK-system under extended conditions of oxidative stress. So far, however, chaperone activity of oxidized DnaJ had been only analyzed *in vitro*.

4.1.6 Thiol trapping of DnaJ under oxidative stress conditions *in vivo*

Oxidation of DnaJ *in vitro* could be monitored by trapping DnaJ's zinc coordinating thiols with AMS (Figure 9). The detected shift in mobility between AMS-trapped reduced and oxidized DnaJ should be sufficient to analyze the redox-state of DnaJ *in vivo*. *E. coli* cells that lack TrxB (thioredoxin reductase) and GorA (glutathione reductase) were used for these *in vivo* studies. This strain is not able to maintain reducing conditions in the cytosol and growth is only possible in DTT containing media. Upon removal of DTT from the media, however, disulfide bond formation quickly takes place in proteins that are redox sensitive (163). Cells were grown in the presence of DTT at 37°C until an $OD_{600\ nm}$ of 0.5 was reached. Then, cells were washed to remove all DTT and to simulate oxidative stress (163, 164). This was stopped by the addition of 4 mM DTT after 15 min. At several time points before, during and after the stress, aliquots of the cell culture were withdrawn and precipitated with 10% TCA. Samples were washed, trapped with AMS as described (section 3.4.4.3) and the modification of DnaJ was analyzed using western blot (section 3.4.6).

As shown in Figure 14, DnaJ remained mainly reduced under oxidative stress *in vivo* and was able to bind to the same amount of AMS per DnaJ molecule even during extended oxidative stress (lane 6-9). Only after 15 min of oxidative stress *in vivo* a very faint oxidized

band appeared, suggesting that small amounts of DnaK became oxidized (Figure 14, lane 8). 15 min after removal of oxidative stress, DnaJ appeared to be completely reduced again (Figure 14, lane 9). This result suggested that DnaJ is not significantly sensitive to oxidative stress i*n vivo*.

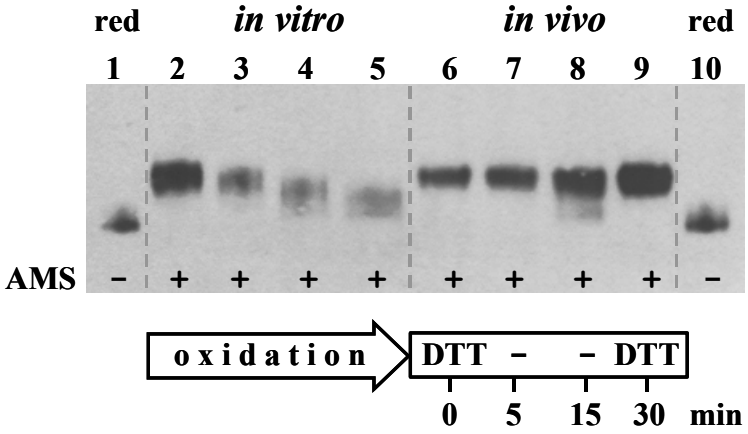

Figure 14 Thiol trapping of DnaJ *in vivo*

Cells lacking *trxB/gorA* were grown in the presence of DTT until OD_{600nm} of 0.5 was reached. Oxidative stress was started by the removal of DTT. After 15 min of stress, DTT was added to the cells. Culture samples were withdrawn at the indicated time points, precipitated with 10% TCA and trapped with AMS under denaturing conditions (lane 6-9). Proteins were separated on a SDS PAGE, transferred onto a membrane and labeled with α-DnaJ antibody. Lane 1, 10 shows fully reduced DnaJ without AMS trapping. Lanes 2-5 show AMS trapping of DnaJ during its oxidation *in vitro*.

4.2 Zinc center mutants of DnaJ

DnaJ possesses two highly conserved zinc centers, each of which is formed by two cysteine rich motifs containing the consensus sequence Cys-X-X-Cys-X-G-X-G. The zinc ions are coordinated by the four cysteine residues of two independent motifs. Chaperone activity measurements of DnaJ indicated that the oxidation-induced release of one zinc ion per DnaJ molecule was already sufficient to change its chaperone activity. If the zinc ions in DnaJ were coordinated with different affinities, oxidation would favor the release of one zinc ion over the other. Especially *in vitro*, oxidation conditions might be too harsh for this selective process and would always result in the release of both zinc ions. To better control the oxidation process of DnaJ, two zinc center mutants were constructed, which lack either one of the two zinc centers. To achieve this, all four zinc-coordinating cysteines of one zinc center were replaced by serines.

Before the structure of DnaJ's zinc binding domain was solved by NMR (83), it had been assumed that zinc center I is formed by cysteine rich motif 1 and 2, while the motifs 3

and 4 formed zinc center II. According to the NMR structure, however, cysteine motif 1 and 4 form zinc center I while motif 2 and 3 form zinc center II (Figure 15A). This means that zinc center mutants that were constructed in former studies (76) failed to investigate the role of the individual zinc centers and needed to be re-evaluated.

DnaJ's zinc center mutants were constructed by site-directed mutagenesis as described (section 3.2.2.1). All four highly conserved cysteine residues of cysteine rich motif 1 and 4 were substituted with serines to create DnaJΔZnI (C144S, C147S, C197S, C200S) while serine substitutions in cysteine motifs 2 and 3 were used to construct DnaJΔZnII (C161S, C164S, C183S, C186S). The plasmids expressing the DnaJ mutant proteins (section 3.1.2) were transformed into the *dnaJ* deletion strain (PK11) for purification and phenotypical studies.

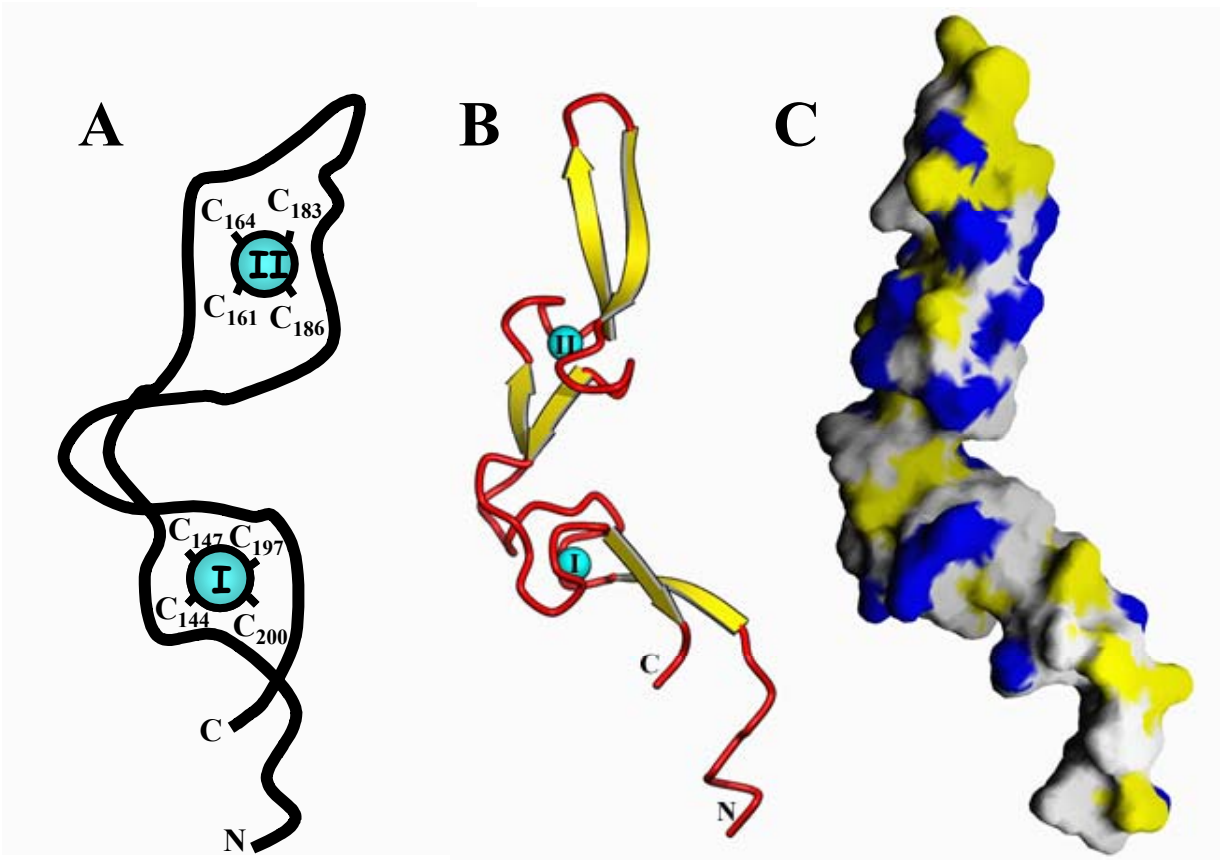

Figure 15 Cysteine-rich domain of DnaJ

A. Model of the cysteine-rich domain of wild type DnaJ according to the solution structure of the isolated cysteine rich domain (83). Zinc center I is formed by cysteine motif 1 (Cys144, Cys147) and cysteine motif 4 (Cys197, Cys200). Zinc center II is formed by cysteine motif 2 (Cys161, Cys164) and cysteine motif 3 (Cys183, Cys186). In our study, either all 4 cysteines of zinc center I were replaced by Ser residues to construct the zinc center I mutant protein DnaJΔZnI or all 4 cysteines of zinc center II were replaced by Ser residues to construct the zinc center II mutant protein DnaJΔZnII. B. Secondary structure of the cysteine-rich domain of DnaJ (PDB: 1EXK) using povscript+ (165). C. Solvent accessible surface model of the cysteine-rich domain of DnaJ using GRASP (166). Only the regions of charged side chains (blue) and of hydrophobic side chains (yellow) are depicted in color.

4.2.1 Phenotype of DnaJ zinc center mutants

The molecular chaperone DnaJ has been shown to be crucial for *E. coli* cells to grow at elevated temperatures (62). Furthermore, *dnaJ* deletion cells are immobile, because the DnaK-system is involved in flagella assembly (156), and do not support λ phage replication (64). As suggested by mutation studies, these three phenotypes appear to depend on slightly different functions of DnaJ (82), which made them an excellent tool for our initial investigations. In order to analyze the activity of the DnaJ zinc center mutants *in vivo*, *E. coli* cells were tested for these phenotypes in comparison to wild type DnaJ.

To ensure comparable protein concentrations in the respective strains, the expression of DnaJ wild type and both zinc center mutants from a plasmid was analyzed using western blot (section 3.4.6). Basal DnaJ expression without additional IPTG induction resulted in protein levels that were very similar to the levels of chromosomal DnaJ expressed from its own promoter (data not shown). Both zinc center mutants were expressed as soluble proteins, indicating that the mutations in DnaJ's zinc centers did not lead to misfolding and degradation of the proteins at 37°C. Noteworthy, the DnaJΔZnII mutant protein migrated slightly different on SDS PAGE than wild type DnaJ.

The activities of the DnaJΔZnI (strain TW24) and DnaJΔZnII (strain TW22) variant were compared to wild type DnaJ expressed from the same plasmid (strain KL23). Importantly, *dnaJ* deletion cells that expressed wild type DnaJ from the plasmid grew undistinguishable from the *E. coli* wild type strain (MG1655) at 37°C and 43°C (Figure 16). The DnaJΔZnI mutant protein enabled *dnaJ* deletion cells to grow like the wild type strain at 37°C and to form colonies after overnight growth on plates at 43°C, although with slightly smaller colonies (Figure 16). *DnaJ* deletion cells expressing DnaJΔZnII grew in smaller colonies at 37°C and completely failed to grow at 43°C (Figure 16). Absence of zinc center II appeared to render the heat shock protein DnaJ inactive in complementing this *dnaJ* phenotype.

Next, *E. coli* wild type strain and *dnaJ* deletion strains, expressing wild type or mutant DnaJ from a plasmid, were tested for their mobility on soft agar plates (section 3.7.2). Cells were spotted onto the surface of the soft agar plates and mobile cells could be easily detected after 15 hours of incubation at 37°C by a spreading circular growth around the original inoculation spot. As shown in Figure 16, the *dnaJ* deletion strain was not able to swarm.

Expression of wild type DnaJ as well as DnaJΔZnI rescued this phenotype and cells were as mobile as wild type *E. coli*. DnaJΔZnII, however, failed to substitute for active DnaJ.

Finally, all DnaJ proteins were tested for their ability to support phage λ replication. For λ replication, in contrast to growth at heat shock temperatures and flagella assembly, only the N-terminal part of DnaJ was shown to be required *in vivo* (82). All tested strains were active in this assay (Table 5). This clearly demonstrated that the lack of activity of DnaJΔZnII in the other two assays was not caused by stability and/or solubility problems of this DnaJ mutant protein *in vivo*.

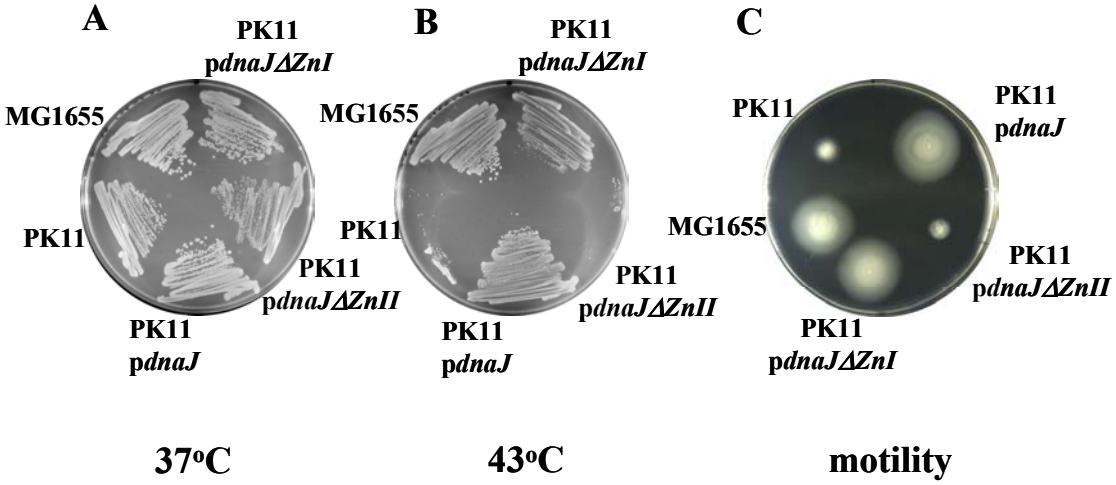

Figure 16 Zinc center II is crucial for the *in vivo* activity of DnaJ (188)

Wild type strain MG1655, *dnaJ* deletion strain PK11 as well as PK11 expressing either wild type DnaJ or the individual zinc center mutants DnaJΔZnI or DnaJΔZnII were grown on LB plates overnight at 37 °C (A) or 43°C (B). To analyze the motility of these strains at 37 °C (*C*), the *dnaJ* deletion strain PK11 as well as PK11 expressing either wild type DnaJ or the individual zinc center mutants DnaJΔZnI or DnaJΔZnII were grown on 0.3% LB agar plates for 15 h at 37°C.

In vivo analysis of the two DnaJ zinc center mutants revealed dramatic functional differences. While DnaJ lacking zinc center I was nearly as active as wild type DnaJ, DnaJ without zinc center II did not rescue the heat shock and immobility phenotype of *dnaJ* deletion cells. This suggested that the two zinc centers in DnaJ were independent units with rather distinct properties for DnaJ's function.

4.2.2 Thiol and Zinc determination of zinc center mutants *in vitro*

In vivo studies of the DnaJ zinc center mutants DnaJΔZnI and DnaJΔZnII suggested that both proteins were expressed and folded like wild type DnaJ. To exactly analyze the thiol and zinc status of both mutant proteins and to exclude even small structural changes that

might explain the changes in the *in vivo* function, the mutant proteins were overexpressed in *E. coli* and purified as described (section 3.3.5). The purification protocol did not differ from wild type DnaJ purification, which indicated that wild type and mutant proteins had very similar physical-chemical characteristics.

It was interesting to first investigate, whether each zinc center would be able to form independently from the other in the zinc center mutants DnaJΔZnI and DnaJΔZnII. Therefore, the number of free thiols as well as the amount of bound zinc was determined in both mutants using the Ellman's assay (section 3.4.4.1) and PAR/PMPS measurements (section 3.4.4.2), respectively. Wild type DnaJ contains 10 cysteine residues, 8 of which are highly conserved and are located in the zinc binding domain. In DnaJ's zinc center mutants, the four cysteine residues of two cysteine-rich motifs were replaced by serine. The Ellman's assay under denaturing conditions revealed for DnaJΔZnI the presence of 3.1 thiol groups per protein (Table 5). This corresponds to only ~50% of the expected number of thiol groups. As accessibility problems could be excluded due to the denaturing conditions, air oxidation of some thiol groups might be the reason. In the DnaJΔZnII mutant protein, 4.8 thiol groups were determined, which was close to the expected 6 thiol groups (Table 5). Analysis of the zinc content confirmed that both mutant proteins coordinated only one zinc ion per molecule. Importantly, in the absences of the thiol specific and zinc releasing agent PMPS, PAR was unable to chelate zinc, indicating that both mutant proteins bound the metal with an affinity that exceeded PAR's zinc binding constant ($K_a = 2x10^{12}\ M^{-2}$). We concluded from these results that both mutant proteins retained sufficient protein structure to bind and coordinate zinc within the respective zinc center. This clearly demonstrated that both zinc centers could form independently from each other as individual folding units.

4.2.3 Structural analysis of DnaJ zinc center mutants

DnaJ lacking zinc center II showed significant differences in its *in vivo* activity as compared to wild type DnaJ. Even though both DnaJ mutants appeared to be stable and not prone to aggregation *in vivo*, structural discrepancies might exist, especially because zinc binding modules function often as purely structural components. To exclude that the observed phenotype of PK11 expressing the DnaJΔZnII mutant protein was caused by structural changes due to the mutation, far-UV and near-UV CD spectra were recorded (section 3.5.2).

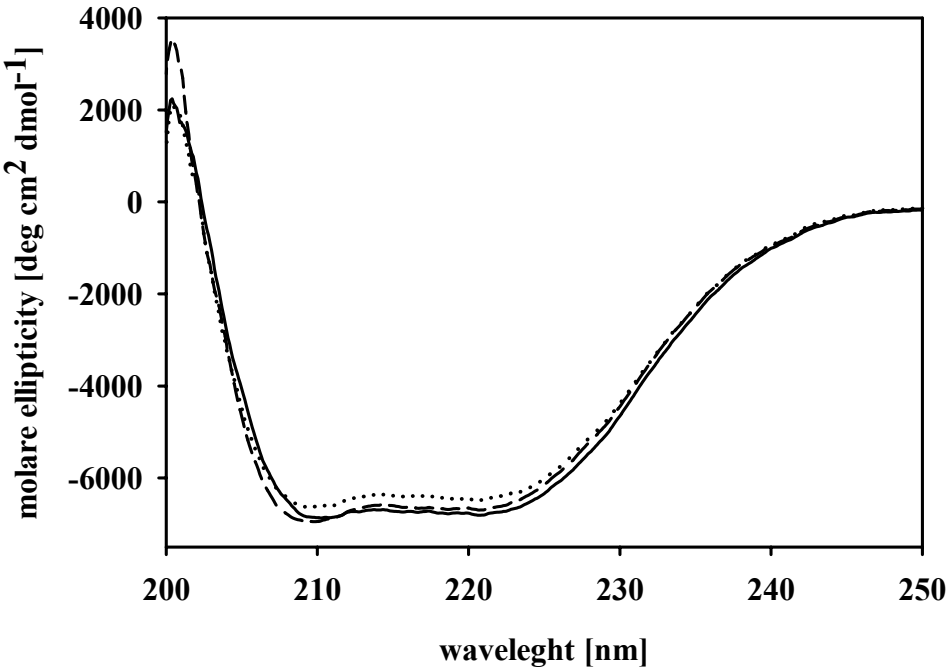

Figure 17 Far-UV CD spectra of wild type DnaJ and the DnaJ zinc center mutants (188)

Far-UV CD spectra of 10 µM wild type DnaJ (—), DnaJΔZnI (····) and DnaJΔZnII (– –) in 30 mM phosphate buffer, pH 8.2, 120 mM KCl, 15 mM NaCl, 4% glycerol. Twenty spectra were accumulated and buffer-corrected.

Figure 17 shows the far-UV CD spectra of wild type DnaJ and both DnaJ zinc center mutants. The high similarity of all three spectra indicated that the secondary structure of the DnaJ mutant proteins was not altered by the lack of either zinc center I or II.

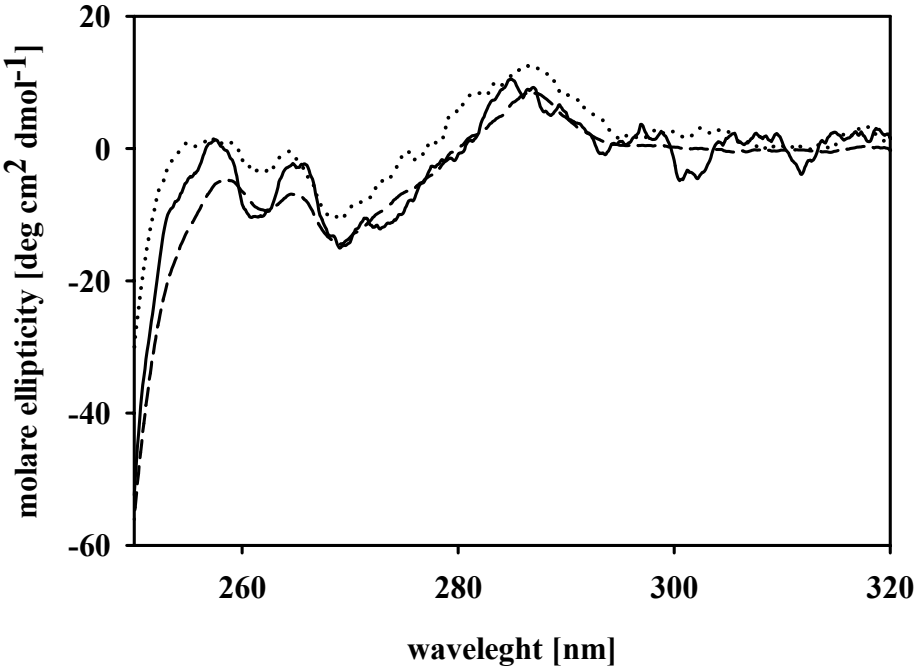

Figure 18 Near-UV CD spectra of wild type DnaJ and the DnaJ zinc center mutants (188)

Near-UV CD spectra of 10 µM wild type DnaJ (—), DnaJΔZnI (····) and DnaJΔZnII (– –) in 30 mM phosphate buffer, pH 8.2, 120 mM KCl, 15 mM NaCl, 4% glycerol.

To compare the tertiary structure of DnaJΔZnI, DnaJΔZnII and wild type DnaJ, near-UV CD spectra were recorded. Figure 18 shows that also the tertiary structure of DnaJ is not significantly influenced by the mutation of zinc center I or II. The results of far- and near-UV CD spectroscopy of DnaJ wild type and the zinc center mutants suggested that the individual zinc centers did not play a major role in the overall structure of DnaJ.

4.2.4 *In vitro* chaperone activity of DnaJ zinc center mutants

4.2.4.1 Reactivation of chemically denatured luciferase

Analysis of the reactivation of chemically denatured firefly luciferase is a well-established model assay to analyze the activity of the DnaK-system and its components *in vitro*. Only in the presence of active DnaK/DnaJ/GrpE, unfolded luciferase is able to regain more than 80% activity upon dilution into refolding buffer. Using this assay, it has been demonstrated that DnaJ lacking zinc center II due to amino acid changes C161S/C164S and C183S/C186S was inactive or 10-fold less active, respectively (76). Interestingly, not only zinc center II was reported to be important for DnaJ's co-chaperone activity. Studies with the Hsp40 yeast homologue Ydj1p showed that a mutant of this protein, lacking one cysteine residue in zinc center I, was also significantly less active in supporting luciferase refolding together with its Hsp70 partner (87).

To clearly define the roles of zinc center I and II for DnaJ's co-chaperone activity, the DnaJ mutants DnaJΔZnI and DnaJΔZnII were investigated using this assay (section 3.6.2). Luciferase was allowed to refold in the absence or presence of DnaK, GrpE and the DnaJ wild type or mutant proteins. Aliquots of the reaction were withdrawn at the indicated time points and luminescence was measured to determine luciferase activity (Figure 19). The DnaJΔZnI mutant protein was nearly as active as wild type DnaJ in refolding of luciferase. The initially slightly slower reaction did not impair the final refolding yield. In agreement with former results, the DnaJΔZnII mutant protein appeared to be nearly inactive, supporting luciferase refolding to yields that were only slightly higher than its spontaneous refolding in the absence of any chaperones (Figure 19, triangles).

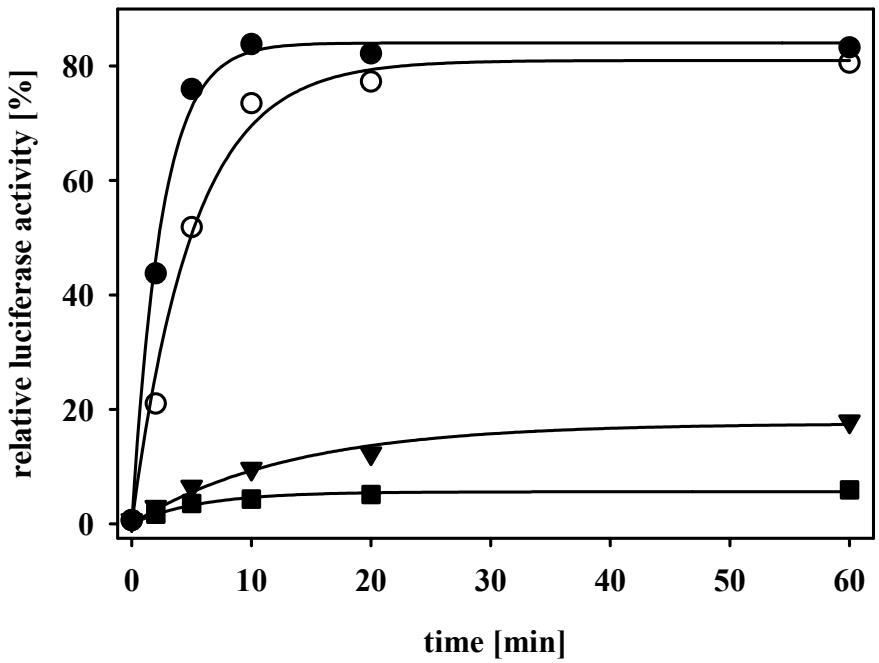

Figure 19 DnaJ lacking zinc center II does not support luciferase refolding

Gua-HCl denatured firefly luciferase was diluted 1:100 (final conc. 0.08 µM) into buffer supplemented with 0.8 µM DnaK and 0.8 µM GrpE either in the absence of DnaJ (■) or in the presence of 0.16 µM wild type DnaJ (●), DnaJΔZnI mutant protein (○), or DnaJΔZnII mutant protein (▼). The activity of luciferase was determined as described. The activity of native luciferase was set to 100%.

To better characterize the influence of zinc center I and II on DnaJ's co-chaperone activity, luciferase refolding reactions were repeated in the presence of varying DnaJ concentrations. Luciferase activity after 60 min refolding was determined as described (section 3.6.2). With wild type DnaJ, the described 2:10:10 ratio of DnaJ:DnaK:GrpE over luciferase (167) resulted in the highest luciferase refolding yield (Figure 20). Higher DnaJ concentrations decreased the amount of reactivated luciferase. The reason for this could be DnaJ's autonomous, DnaK-independent chaperone activity, which competes with DnaK for substrate binding. Increasing DnaJ concentrations reduce the substrate transfer to the foldase DnaK and therefore lower the refolding yields. Smaller amounts of DnaJ impaired the refolding activity of the DnaK-system as well. The irreversible aggregation of unfolded luciferase is a very rapid process and might be faster than the binding to DnaJ.

The refolding yields in the presence of DnaJΔZnI showed a pattern that was very similar to wild type DnaJ (Figure 20). Slightly higher concentrations of this DnaJ mutant were needed to reach the same refolding yields as wild type DnaJ, suggesting that the overall substrate affinity of this mutant is slightly lower. This might be the reason for the observed slightly smaller colony size of DnaJΔZnI-expressing *dnaJ* deletion cells after growth at heat

shock temperatures. Interestingly, increase of the DnaJΔZnI concentration to DnaJ:DnaK:GrpE ratios up to 100:10:10 did not reduce the yield of luciferase refolding (Figure 20, open circles). Apparently, DnaJΔZnI could not compete with DnaK for substrate binding, which suggested an impaired autonomous holdase activity of this DnaJ mutant protein.

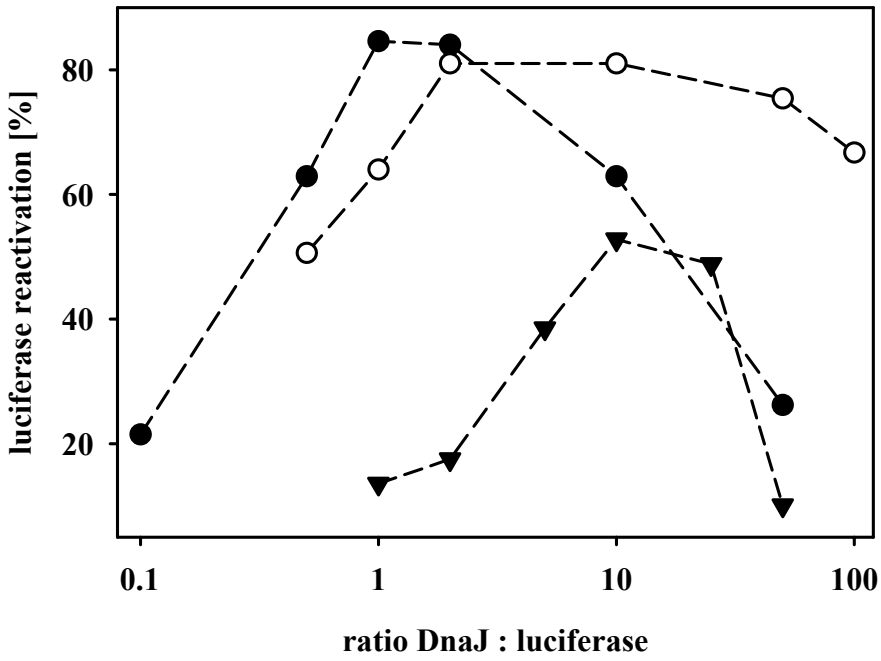

Figure 20 Luciferase refolding yields in dependence of varying DnaJ concentrations (188)

Chemically denatured luciferase (0.08 µM) was reactivated in the presence of 0.8 µM DnaK and 0.8 µM GrpE and the indicated concentrations of wild type DnaJ (●), DnaJΔZnI (○), or DnaJΔZnII (▼). The reactivation yields after 60 min of reactivation were determined and plotted against the ratio of DnaJ to luciferase.

Refolding reactions in the presence of increasing concentrations of the DnaJΔZnII mutant protein supported the luciferase refolding to a higher extent (Figure 20, triangles). Almost 60% luciferase reactivated in the presence of DnaJ:DnaK:GrpE in molar ratios of 10:10:10 over luciferase. DnaJΔZnII concentrations exceeding this limit caused decreasing refolding efficiencies. Similar to wild type DnaJ, this mutant protein appeared to compete with DnaK for substrate binding and a 50:1 excess of both DnaJ proteins over luciferase prevented substrate refolding completely. Even though zinc center II seemed to be crucial for DnaJ's co-chaperone activity, it appeared to play a significant smaller role in DnaJ's autonomous, DnaK-independent chaperone activity. Lack of zinc center I, on the other hand, impaired the ability of DnaJ to interact with unfolded substrate proteins, while it had very little influence on DnaJ's activity as co-chaperone of the DnaK folding machine. These

results differed from earlier studies and suggested that the co-chaperone activity of DnaJ did not depend on its autonomous, DnaK-independent chaperone activity (76).

Next, the luciferase refolding rates were calculated for reactions with varying DnaJ concentrations. In the absence of the DnaK-system, luciferase not only reactivated to a low final yield, but also with a slow refolding rate. DnaJ:DnaK:GrpE used in the efficient molar ratio of 2:10:10 accelerated luciferase refolding 4-fold (Figure 21, filled circles). This chaperone composition is thought to allow optimal substrate presentation by DnaJ to DnaK and to most efficiently trigger DnaK's intrinsic ATPase activity. It was, therefore, not surprising to find slower refolding rates in the presence of both higher and lower DnaJ concentrations (Figure 21, filled circles). Analyzing the refolding rates of luciferase reactions with varying DnaJΔZnI concentrations revealed that only at a 10:10:10 ratio of DnaJ:DnaK:GrpE over luciferase the same high refolding rate as with wild type DnaJ was achieved (Figure 21, open circles). This suggested that fast refolding rates were not required for maximal refolding yields and excess of DnaJΔZnI could compensate for sub-optimal refolding rates.

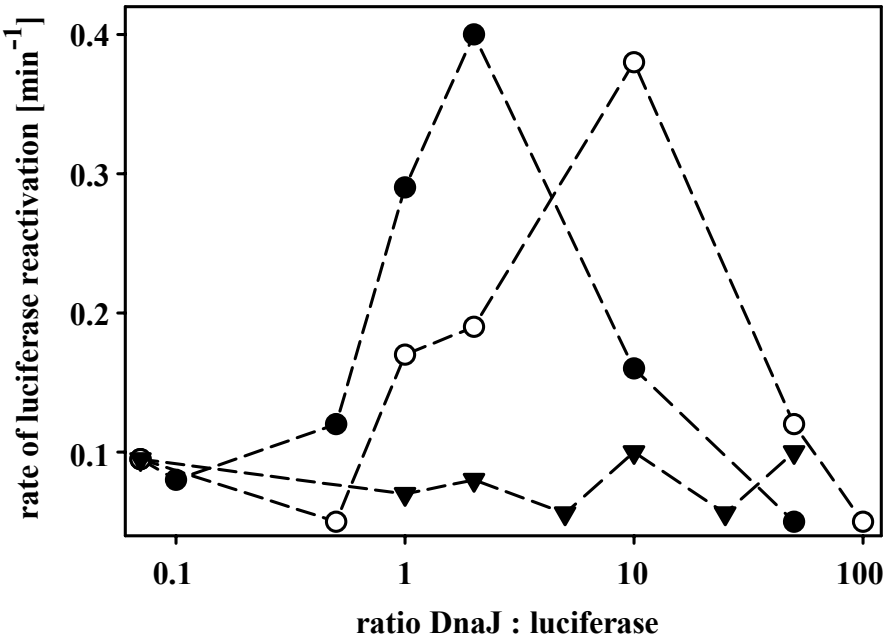

Figure 21 Luciferase refolding rates in dependence on varying DnaJ concentrations (188)

Chemically denatured luciferase (0.08 µM) was reactivated in the presence of 0.8 µM DnaK and 0.8 µM GrpE and various concentrations of wild type DnaJ (●), DnaJΔZnI (○) or DnaJΔZnII (▼). The initial reactivation rates were determined and plotted against the ratio of DnaJ to luciferase.

Luciferase refolding in the presence of the DnaJΔZnII mutant protein appeared to be slow at all concentrations. Neither low DnaJΔZnII concentrations nor excess of the

chaperone could accelerate the reaction to a faster refolding rate than spontaneous luciferase refolding in the absence of chaperones. It appeared therefore that in the presence of this DnaJ zinc center mutant the DnaK foldase machine was no longer catalytically active. Despite the low refolding rate, almost 60% of luciferase refolded at DnaJ:DnaK:GrpE ratios of 10:10:10. This suggested that increased DnaJ concentrations are able to compensate for a rate-limiting step within the refolding cycle that had been caused by the lack of zinc center II.

4.2.4.2 Autonomous, DnaK-independent chaperone activity of DnaJ zinc center mutants

Besides DnaJ's well-investigated co-chaperone activity as partner of the DnaK-system, DnaJ also possesses its own holdase activity, which is independent from DnaK. Tight binding to substrate proteins enables DnaJ to successfully prevent aggregation of unfolded polypeptides *in vitro* (75, 151). Evaluation of the luciferase refolding yields and rates in the presence of various concentrations of DnaJ wild type and the mutant proteins (Figure 20, Figure 21) suggested that absence of zinc center I impaired DnaJ's substrate binding affinity, while absence of zinc center II affected DnaJ's DnaK-dependent co-chaperone activity. To analyze the autonomous chaperone activity of DnaJ, the ability of wild type DnaJ and the zinc center mutants to prevent aggregation of unfolded substrate proteins was analyzed. Light scattering of chemically denatured luciferase was determined as described (section 3.6.1.1).

As shown in Figure 22, unfolded luciferase in the absence of chaperones quickly aggregates upon dilution into the buffer. The formation of irreversible protein aggregates is also the reason for the observed low refolding yield of luciferase (Figure 19). Wild type DnaJ has been shown to be an efficient chaperone holdase (151). In agreement with this, a DnaJ:luciferase ratio of 0.5:1 prevented the aggregation of luciferase to nearly 50% (Figure 22). The DnaJΔZnI mutant protein, on the other hand, did not reduce the aggregation of unfolded luciferase (Figure 22). This clearly indicated that the autonomous chaperone activity of this DnaJ mutant was impaired. Lack of zinc center II did not significantly influence the DnaK-independent chaperone activity of DnaJ. Like wild type DnaJ, this mutant protein could prevent nearly 50% luciferase aggregation.

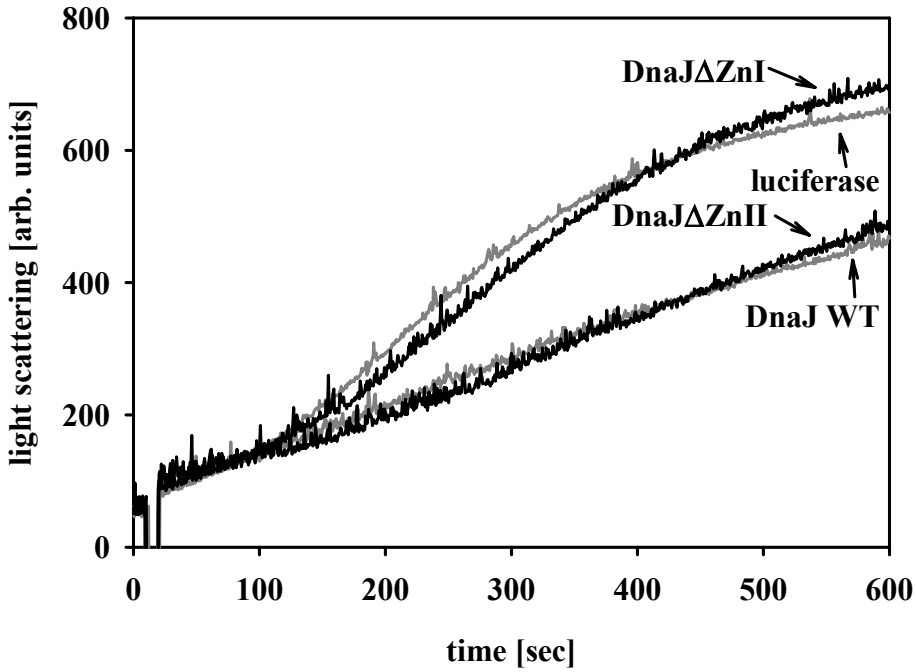

Figure 22 Zinc center I is important for DnaJ's substrate binding affinity (188)

Chemically denatured firefly luciferase was diluted 1:100 (final conc. 0.08 µM) into buffer under constant stirring at 30°C. The incubation reaction was either not supplemented with DnaJ or contained 0.04 µM wild type DnaJ, DnaJΔZnI, or DnaJΔZnII. Aggregation of luciferase was determined using light scattering measurements ($\lambda_{em/ex}$ = 320nm).

To analyze whether higher ratios of DnaJΔZnI over luciferase could compensate for the decreased substrate binding affinity of this DnaJ mutant protein, light scattering experiments with chemically denatured luciferase were repeated in the presence of higher DnaJ concentrations.

Figure 23 shows the light scattering of luciferase after 10 min luciferase aggregation in the presence of various concentrations of wild type DnaJ and the zinc center mutant proteins. Wild type DnaJ:luciferase ratios of 2:1 prevented luciferase aggregation almost completely (Figure 23, filled circles). Slightly higher concentrations of the DnaJΔZnII mutant protein were needed to observe the same effect (Figure 23, triangles). In contrast, more than 5-fold excess of DnaJΔZnI over luciferase was necessary to reduce substrate aggregation to 50% and a 10-fold excess of the DnaJ zinc center I mutant was needed to completely suppress aggregation of luciferase (Figure 23, open circles).

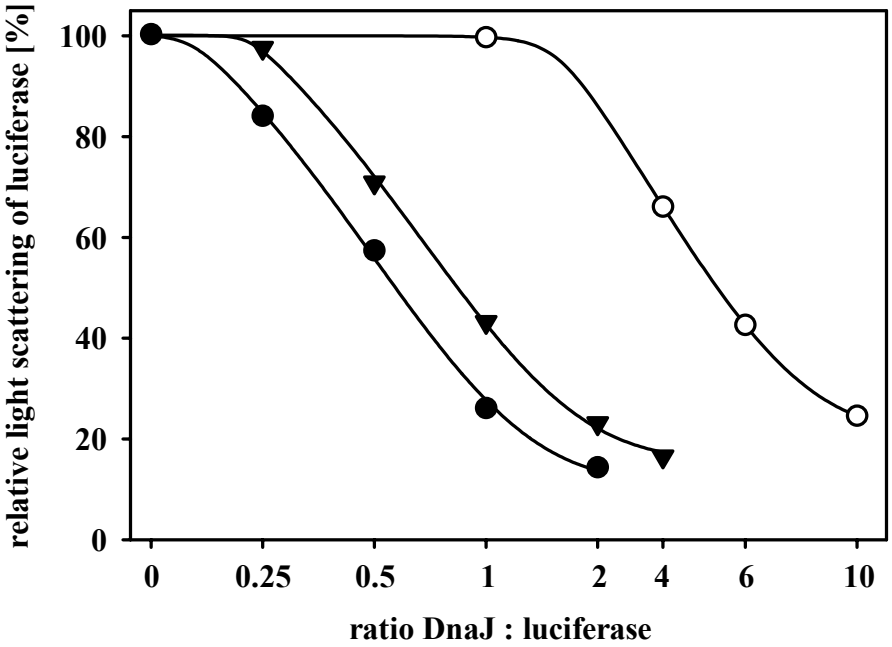

Figure 23 Autonomous chaperone activity of DnaJ lacking zinc center I is 5-fold reduced (188)

Chemically denatured firefly luciferase was diluted 1:100 (final conc. 0.08 µM) into buffer that was supplemented with various concentrations of wild type DnaJ (●), DnaJΔZnI (○), or DnaJΔZnII (▼). The light-scattering signal after 600 s was determined ($\lambda_{em/ex}$ = 320nm) and plotted against the ratio of DnaJ to luciferase. The light scattering signal in the absence of chaperones was set to 100%.

To specifically assess the interaction of the two zinc center mutant proteins with substrate proteins and DnaK, the influence of the DnaJ variants on the aggregation of chemically denatured luciferase was investigated in the presence of DnaK. The simultaneous interaction of DnaK with the substrate protein and DnaJ allows DnaJ to stimulate the ATP hydrolysis of DnaK. This is thought to cause the locking in of substrate proteins to the substrate binding site of DnaK, which in turn leads to the effective prevention of luciferase aggregation (66, 168).

In the absence of DnaJ, DnaK possesses a rather poor substrate binding affinity (Figure 24). In agreement with the literature, the presence of DnaJ appears mandatory for DnaK's transformation into its high affinity state (Figure 24) (66, 87). The DnaJΔZnI mutant protein, which had not suppressed luciferase aggregation when used with a ratio of 0.5 over luciferase (Figure 19), successfully stimulated DnaK's conversion to the high affinity state to prevent luciferase aggregation (Figure 24). Although DnaJΔZnI had failed to form stable complexes with unfolded luciferase, more transient DnaJ-substrate interactions must be sufficient to efficiently cooperate with DnaK. In contrast, DnaJ lacking zinc center II was

apparently not able to stimulate DnaK's change into its high affinity state. No further reduction of luciferase aggregation was achieved when DnaK and DnaJΔZnII were present simultaneously (Figure 24). This agreed very well with results presented earlier and explained DnaK's failure to refold luciferase in cooperation with DnaJΔZnII (Figure 19).

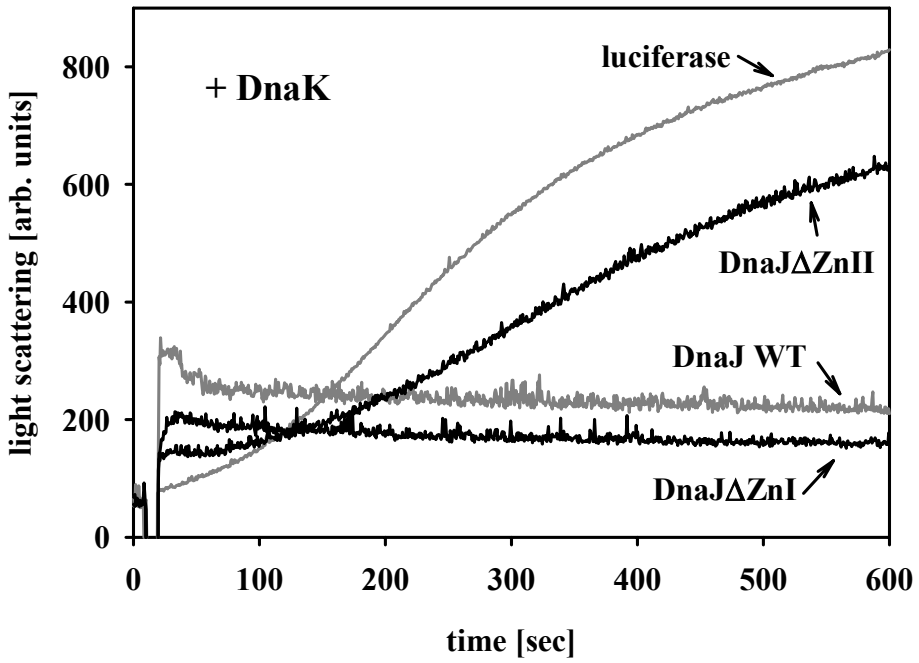

Figure 24 Co-chaperone activity of DnaJ is independent from its substrate binding affinity (188)

Chemically denatured firefly luciferase was diluted 1:100 (final conc. 0.08 µM) into buffer containing 0.8 µM DnaK and either no DnaJ or 0.04 µM wild type DnaJ, DnaJΔZnI, or DnaJΔZnII. Aggregation was determined using light scattering measurements ($\lambda_{em/ex}$ = 320nm).

To exclude that these results were substrate specific, light scattering experiments were repeated using chemically denatured rhodanese instead of luciferase. The obtained results were very similar to the results obtained with luciferase, indicating that these were not substrate specific (data not shown). These experiments clearly revealed the functional difference between both zinc center mutants. DnaJΔZnI supported with wild type activity the refolding of denatured substrates in concert with DnaK and GrpE. Its autonomous chaperone activity, however, was drastically impaired. DnaJΔZnII, on the other hand, failed to assist substrate reactivation in cooperation with the DnaK-system, whereas its DnaK independent substrate binding ability was very similar to wild type DnaJ. While zinc center I appeared to be directly involved in the formation of stable DnaJ-substrate complexes, zinc center II seemed to be crucial for DnaJ to stimulate DnaK's conformational change into the high substrate affinity state. Importantly, these functions seemed to work independently.

4.2.5 ATPase activity of DnaJ zinc center mutants

Failure of DnaJΔZnII to stimulate substrate binding and refolding by DnaK could be the consequence of several reasons. (i) binding of DnaK to substrate proteins might not be possible in the presence of DnaJΔZnII, (ii) lack of zinc center II might impair DnaJ's ability to stimulate DnaK's intrinsic ATPase activity, (iii) DnaJΔZnII might lack a second DnaK interaction site, which is necessary to induce conformational changes in DnaK that allow the chaperone to bind substrate proteins with high affinity. Such an additional interaction site had been already proposed earlier (169, 170). ATP hydrolysis of DnaK is maximally stimulated when the N-terminal J-domain of DnaJ interacts with DnaK's ATPase domain, while DnaK and DnaJ bind simultaneously to the same unfolded polypeptide chain (66, 88). As a consequence, DnaK-ADP is thought to change its conformation, which turns DnaK into its high affinity state.

The ATPase activity of DnaK was determined in single turnover experiments (section 3.6.4.2). In agreement with the literature, a 2:10 molar ratio of wild type DnaJ to DnaK stimulated ATP hydrolysis of DnaK ~50-fold (Figure 25 insert, Table 5). Addition of unfolded luciferase in a molar DnaJ:DnaK ratio of 2:10 over luciferase stimulated DnaK's ATPase rate ~600-fold (Figure 25, Table 5). Presence of DnaJΔZnII instead of wild type DnaJ stimulated DnaK's ATPase activity to a very similar extent both in the absence and presence of unfolded luciferase (Figure 25, Table 5). These results indicate that DnaJΔZnII was neither impaired in stimulating DnaK's ATPase activity nor did it hinder the additional stimulation of DnaK's ATPase activity by DnaK-substrate interactions. This suggests that a second DnaK interaction site was missing in DnaJΔZnII, which is necessary to trigger conformational changes in DnaK and allows the subsequent refolding of substrate proteins.

In the absence of unfolded luciferase, DnaJΔZnI stimulated DnaK's ATPase activity like wild type DnaJ. In the presence of unfolded luciferase, however, ATP hydrolysis of DnaK was slightly less stimulated by DnaJΔZnI than by wild type DnaJ (Figure 25, Table 5). This can be explained by the earlier observed drastically reduced substrate binding affinity of DnaJ lacking zinc center I, which decreases the chance of simultaneous DnaJ-DnaK-substrate interactions, which are necessary for maximal stimulation of DnaK's ATPase activity.

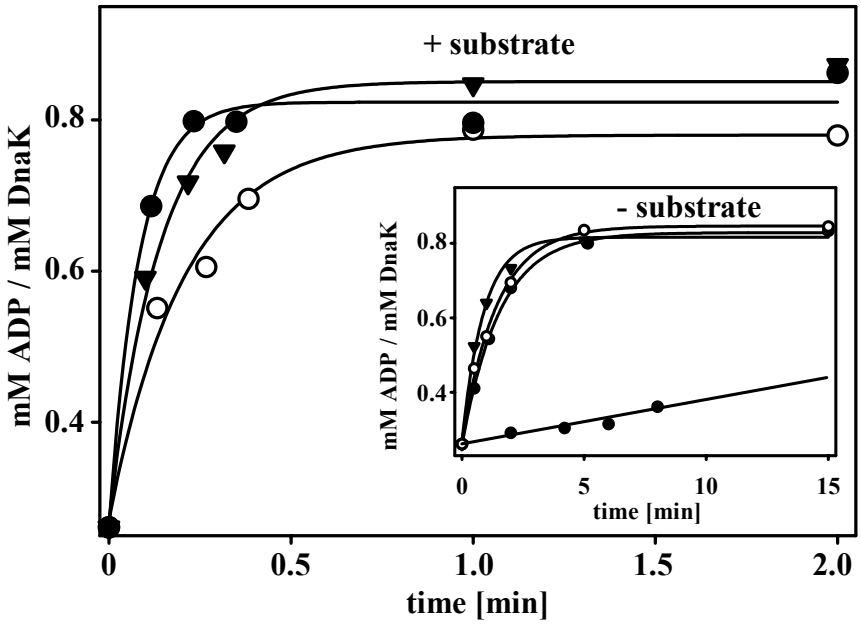

Figure 25 Influence of DnaJ zinc center mutants on the ATPase activity of DnaK (188)

Single turnover experiments using 0.8 µM DnaK were performed in the absence of unfolded substrate proteins (insert) or in the presence of 0.08µM chemically denatured luciferase. The reactions were either not supplemented with DnaJ (■) or supplemented with 0.16 µM wild type DnaJ (●), DnaJΔZnI (○) or DnaJΔZnII (▼).

Table 5 Summery of *in vitro* and *in vivo* properties of DnaJ zinc center mutants (188)

in vivo	PK11	PK11 pdnaJ	PK11 pdnaJΔZnI	PK11 pdnaJΔZnII
λ-phage replication	-	++	++	++
growth at 43°C	-	++	+	-
growth at 37°C	+	++	++	+
motility	-	++	++	-
in vitro		DnaJ WT	DnaJΔZnI	DnaJΔZnII
zinc content (µM) /DnaJ (µM)		1.4 ± 0.2	0.8 ± 0.1	0.8 ± 0.1
chaperone activity				
- DnaK independent		+++	+	+++
- DnaK dependent		+++	+++	(+)
ATPase (min^{-1}) of DnaK				
- DnaJ	0.016			
+ DnaJ		0.8 ± 0.1	0.6 ± 0.1	1.2 ± 0.2
+ DnaJ + substrate		10.1 ± 2.0	6.0 ± 1.2	10.0 ± 3.7

4.3 Characterization of DnaK under oxidative heat stress

4.3.1 DnaK's chaperone activity under oxidative heat stress *in vitro*

E. coli cells that lack the general heat shock response due to a deletion of the heat shock sigma factor σ^{32} are very sensitive to cultivation at elevated temperatures and oxidative stress (1). While in wild type strains heat shock induced molecular chaperones prevent the irreversible aggregation of polypeptides, cells lacking the σ^{32} gene suffer from damage due to the accumulation of large protein aggregates (171). Overexpression of the DnaK-system in these ΔrpoH strains rescues the heat stress phenotype by preventing aggregation of thermally unfolding proteins (1, 171). In contrast, protein aggregation was not prevented by the DnaK-system under combined heat and oxidative stress conditions. While 76% of the investigated aggregation-prone proteins were protected by DnaK/DnaJ/GrpE at heat shock temperatures (50°C), less than 2% were protected by the chaperone system under oxidative heat stress (4mM H_2O_2, 45°C). Substrate protein analysis suggested that this lack of protein function was not due to a different subset of substrate proteins that accumulated upon heat or oxidative heat stress but due to the loss of the function of the DnaK-system (1). To investigate to what extent combined heat and oxidative stress inactivates this main protein folding system, the influence of oxidative heat stress was analyzed *in vitro*.

The activity of the DnaK-system was analyzed *in vitro* by studying the influence of purified DnaK, DnaJ and GrpE on the refolding of the chemically denatured model substrate luciferase (151, 171). In the absence of chaperones, unfolded luciferase rapidly aggregated upon its dilution into refolding buffer. This allows refolding of only 3% after 30 min (Figure 26, squares). In the presence of the complete DnaK-system, however, aggregation of luciferase is prevented and more than 85% of the protein quickly reactivated (Figure 26, filled circles). This was in excellent agreement with published data (151, 171). To simulate oxidative heat stress *in vitro,* DnaK was pre-treated at 43°C with 2 mM H_2O_2. Under these conditions, no loss in DnaK's chaperone activity was observed and the activity of DnaK remained constant over an extended period of incubation (data not shown). This was presumably due to the high thermal stability of DnaK in the presence of nucleotides (150). Under nucleotide limiting conditions, however, the N-terminus of DnaK has been shown to become thermolabile and to unfold at elevated temperatures (T_m = 45°C) (150). Careful examination of the literature revealed that H_2O_2 induced oxidative stress is accompanied by a significant drop in cellular ATP levels in several organisms (172). After its purification,

however, DnaK contained a significant amount of bound ATP, which might render DnaK thermostable. Therefore, the amount of bound ATP was reduced to less than 10% (section 3.3.4) and the activity of nucleotide depleted DnaK after incubation at oxidative heat stress conditions was tested.

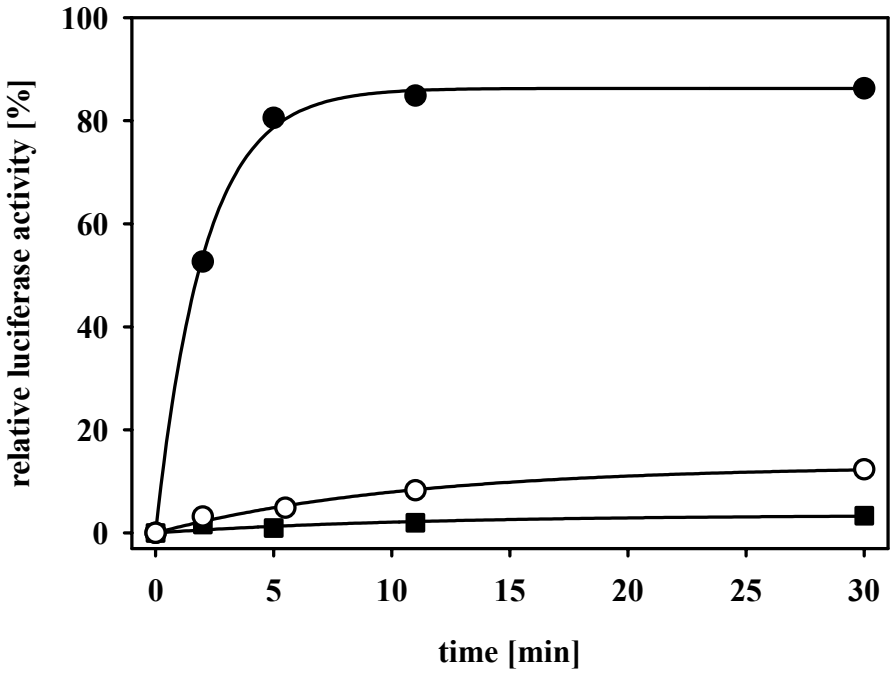

Figure 26 Oxidized DnaK is inactive in refolding chemically denatured luciferase *in vitro*.

Gua-HCl denatured firefly luciferase was diluted 1:100 (final conc. 0.08 µM) into buffer in the absence of chaperones (■) or in the presence of 0.16 µM DnaJ, 0.8 µM GrpE and either 0.8 µM non-treated DnaK (●) or 0.8 µM oxidized DnaK (○). To oxidize DnaK, 20 µM ATP-depleted DnaK was incubated at 43°C in the presence of 2 mM H_2O_2. After 15 min incubation, an aliquot was withdrawn and diluted 1:25 into the luciferase refolding reaction. The activity of luciferase was determined as described. The activity of native luciferase was set to 100%.

After 15 min incubation at oxidative heat stress treatment (43°C, 2 mM H_2O_2), DnaK was diluted into refolding buffer containing DnaJ, GrpE and ATP and the refolding assay was started immediately by the addition of unfolded luciferase (section 3.6.2). As shown in Figure 26 (open circles), oxidative heat stress treatment of ATP-depleted DnaK dramatically decreased DnaK's ability to stimulate the refolding of luciferase *in vitro*. The resulting refolding yield of luciferase was 12% and, therefore, only marginally higher than the spontaneous reactivation of luciferase. Control reactions verified that this low refolding yield was indeed caused by exposing ATP-depleted DnaK to oxidative heat stress treatment and was not due residual concentrations of H_2O_2 in the refolding reaction (results not shown). Incubation of ATP-depleted DnaK at either straight heat (43°C) or oxidative stress (30°C, 2 mM H_2O_2) revealed that it was only the exposure of DnaK to a combined heat and oxidative

stress conditions that caused the loss of DnaK's activity (data not shown). Oxidative heat stress treatment of DnaK in the presence of excess ATP or ADP did not significantly reduce DnaK's chaperone activity (Figure 27), demonstrating that the presence of nucleotides protected DnaK from this inactivation. These results showed that a combination of three conditions was necessary for DnaK's inactivation *in vitro*: low nucleotide levels, oxidative stress and elevated temperatures.

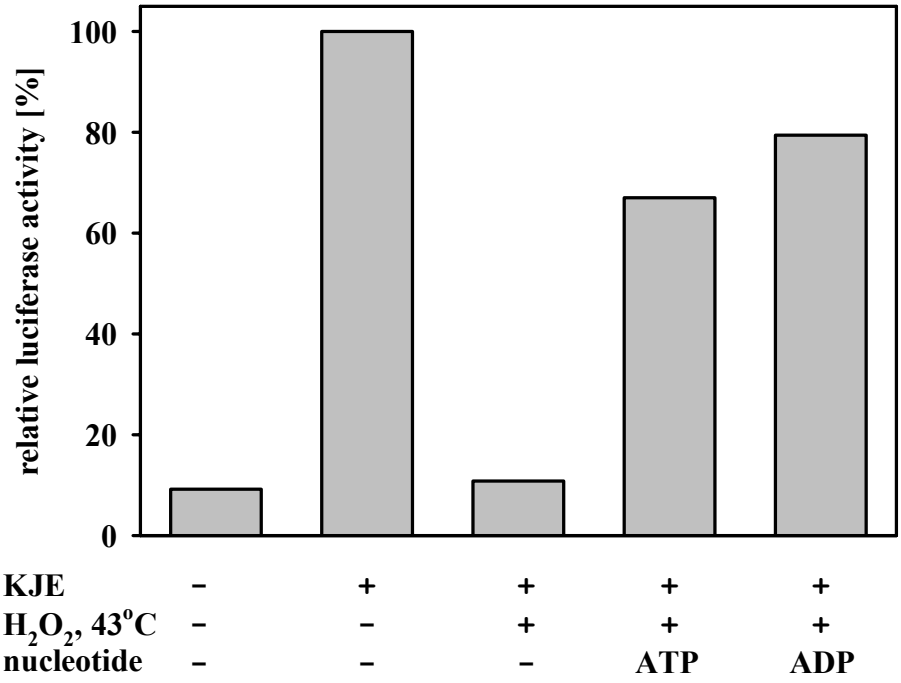

Figure 27 Nucleotides protect DnaK from inactivation at oxidative heat stress *in vitro*

Refolding of 0.8 µM chemically denatured luciferase was measured in the absence or presence of 0.8 µM DnaK, 0.16 µM DnaJ, 0.8 µM GrpE using either non-treated DnaK or ATP-depleted DnaK that had been incubated with 2 mM H_2O_2 at 43°C in the absence or presence of 2mM nucleotides for 10 min.

In order to find out, how quickly DnaK loses its activity upon exposure to oxidative heat treatment, ATP-depleted DnaK was incubated in the presence of H_2O_2 at 43°C and DnaK samples were withdrawn after 2, 5, 10 and 15 min of the stress treatment (Figure 28, filled circles). Immediately after start of oxidative heat stress treatment, DnaK started to loose its activity (T½ 6.5 min). Oxidative heat treatment of DnaK using oxidized glutathione (GSSG) instead of H_2O_2 as oxidant also inactivated DnaK, indicating that DnaK's inactivation is not specific for hydrogen peroxide (results not shown).

When cells face oxidative stress conditions, many cellular proteins are non-specifically oxidized and irreversible damaged by reactive oxygen species like H_2O_2. In these cases, oxidation renders the proteins damaged and inactive. To investigate whether DnaK's

loss of activity is due to the irreversible and non-specific oxidation of some amino acid side chains or due to the specific oxidation of cysteine residues, the reactivation of DnaK was analyzed. When, after 15 minutes of oxidative heat treatment the temperature was shifted to 30°C and reducing conditions were restored, either by the addition of micromolar concentrations of the thioredoxin system (TrxA, TrxB and NADPH) (Figure 28, closed circles) or by 14 mM GSH (data not shown), DnaK regained its full activity within minutes after the shift. The crucial component in the reactivation of DnaK *in vitro* was the presence of physiological reductants, because simply lowering the incubation temperature to 30°C did not induce any reactivation of DnaK (Figure 28, open circles). In contrast, heat-treated DnaK quickly reactivated in the absence of reductants upon lowering the temperature (data not shown). This suggested that during the oxidative heat stress treatment *in vitro*, DnaK becomes locked in an inactive conformation, which can only be reversed upon restoring a reducing environment.

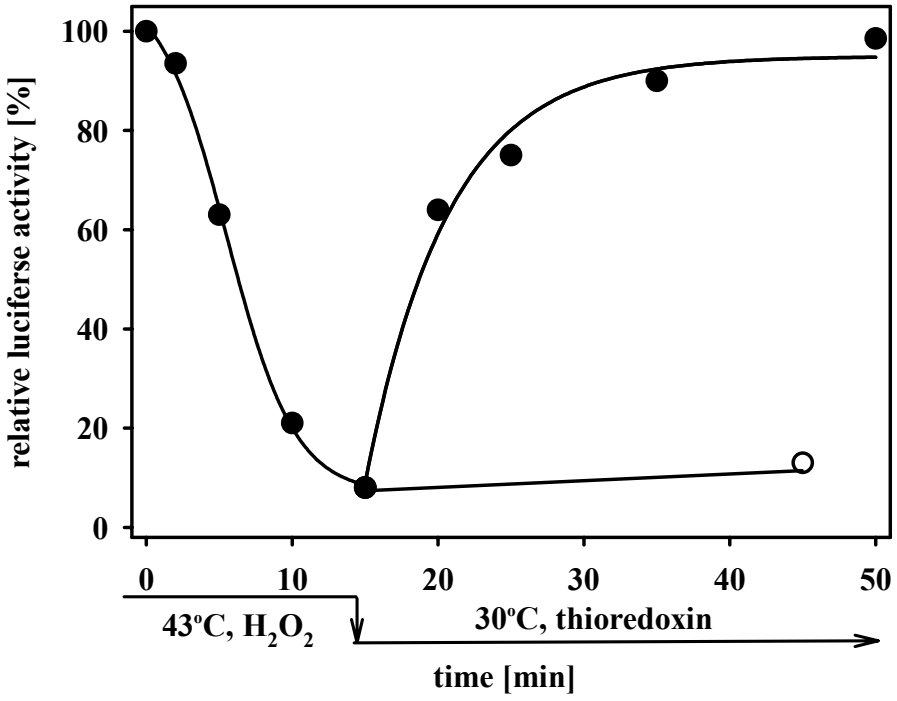

Figure 28 Reversible inactivation of nucleotide-depleted DnaK *in vitro*. (1)

20 µM nucleotide-depleted DnaK was incubated at 43°C in the presence of 2 mM H_2O_2. To monitor the activity of DnaK, the influence of DnaK on the DnaK/DnaJ/GrpE – mediated refolding of chemically denatured luciferase was tested. After 15 min of oxidative inactivation, the incubation of DnaK was continued at non-stress temperatures (30°C) in the (○) absence or in the (●) presence of reducing conditions (2.4 µM TrxA, 70 nM TrxB, 160 µM NADPH).

4.3.2 Cellular ATP level in *E. coli* under oxidative stress

The sensitivity of DnaK towards oxidative heat stress treatment *in vitro* was highly dependent on its nucleotide state (Figure 27). From the literature it was known that the cellular ATP concentration decreases in certain organism upon exposure to hydrogen peroxide (173). To analyze to what extent ATP becomes indeed limiting for DnaK *in vivo*, *E. coli* wild type strains or *rpoH* deletion cells lacking the heat shock response were exposed to H_2O_2 treatment and the cellular ATP level was determined.

As ATP levels can change extremely fast, establishing the proper nucleotide extraction method was very important (158). Rapid cell lysis together with immediate inactivation of all ATP producing and consuming proteins was crucial. After testing several different approaches, it became obvious that harvesting the cells by centrifugation and lysis resulted in significantly decreased ATP levels. Even though this sampling procedure took less than 2 min, only about 30% of the total cellular ATP concentration could be determined (data not shown). Therefore, cells were lysed by pipetting a small culture volume directly into boiling buffer (section 3.7.4) (159). Extracting ATP from a diluted cell culture rather then a concentrated cell pellet had the disadvantage that much lower concentrations of ATP were present. The sensitive luciferase activity assay had to be used to measure these low ATP concentrations instead of the qualitative and quantitative nucleotide analysis using HPLC.

Cultures of *E. coli rpoH*⁻ strains overexpressing the DnaK-system were grown to logarithmic phase at 30°C. Then, cells were exposed to H_2O_2 stress at 30°C (data not shown) or 43°C. Non-stress conditions were restored after 20 min by either lowering the temperature to 30°C or by addition of catalase to degrade H_2O_2. Samples were withdrawn during and after the stress treatment and the total cellular ATP level was determined.

In agreement with previous results, H_2O_2-induced oxidative stress caused a significant drop in the cellular ATP levels (Figure 29). Within 2 min of oxidative stress treatment at 30°C (data not shown) or 43°C (Figure 29, filled circles) the cellular ATP level dropped below 1 mM and decreased further to 0.5 mM during the incubation period. Upon restoration of non-stress by addition of catalase to the cultures, the cellular ATP level quickly recovered. After only 2 min, the ATP levels reached concentrations similar to the control culture without H_2O_2. These changes in ATP levels are not caused by changes in the energy pool of the cell due to different growth phases, because when cell growth was stopped prior to the stress treatment by the addition of the protein synthesis inhibitors tetracycline (50 µg/ml) or streptinomycin (100 µg/ml) the same result was observed. Noteworthy, very similar changes

in the cellular ATP levels were observed when *E. coli* wild type cells (MC4100) were cultivated under oxidative heat shock conditions (data not shown). Given the many ATP-binding systems that can compete for ATP binding with DnaK *in vivo*, as well as the high cellular concentration of DnaK under heat shock conditions (>50 µM at 42°C in wild type cells, >100 µM in Δ*rpoH* strains overexpressing the DnaK-system) (155), this more than 10-fold drop of cellular ATP levels should be more than sufficient to render DnaK nucleotide deprived under oxidative heat stress conditions *in vivo*.

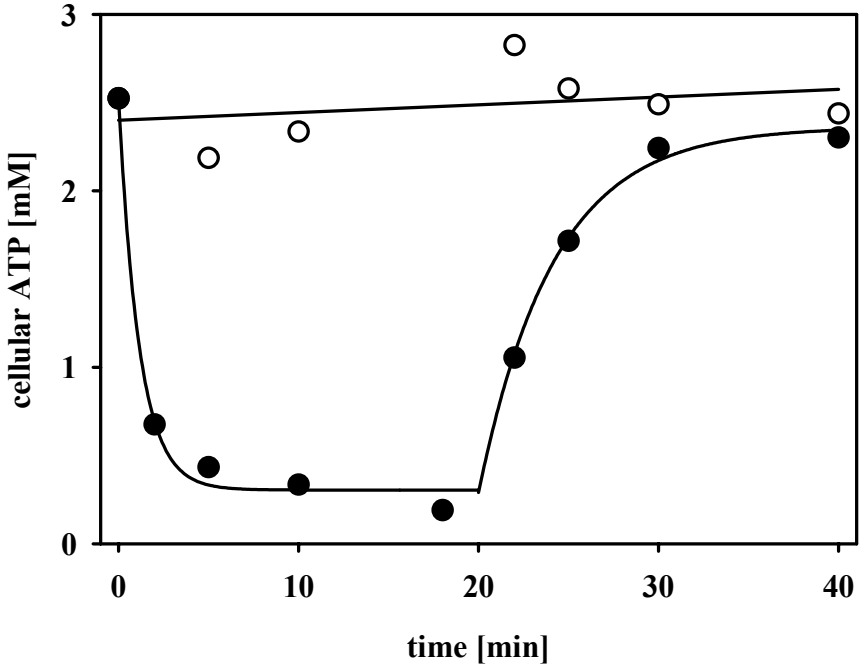

Figure 29 Decrease of intracellular ATP levels upon oxidative stress conditions (1)

Δ*rpoH* strains overexpressing DnaK/DnaJ/GrpE were grown at 30°C until exponential phase was reached. Then, the culture was diluted 1:2 into prewarmed media at 43°C in the (○) absence or (●) presence of 4 mM H_2O_2. After 20 min stress, catalase was added to quickly degrade H_2O_2 and cultures were shifted to 30°C. At defined time points, aliquots of the cell cultures were taken and the total amount of ATP was determined.

4.3.3 Thermal unfolding of DnaK

Analysis of DnaK's thermal stability revealed that DnaK's unfolding proceeds over three states with transition temperatures (T_m) at 45°C, 58°C and 73°C (150). It was shown that the low transition point at 45°C corresponds to the partial unfolding of DnaK's N-terminal domain. Structural rearrangements in the C-terminus were assigned to 58°C while at 73°C unfolding of both domains contributes to the transition (150). *In vitro,* conformational changes in DnaK can be monitored by following the intrinsic fluorescence of a single tryptophan residue, which is located close to the ATP binding site (149). Depending on

DnaK's conformations, Trp102 is masked to varying degrees, which influences its fluorescence signal (174).

To monitor the thermal unfolding of ATP-depleted DnaK upon heat stress treatment, the intrinsic fluorescence of DnaK was measured during its incubation at various temperatures in the absence or the presence of ATP (section 3.5.1). The fluorescence signal of ATP-depleted DnaK already slowly decreased at a non-stress temperature (37°C) (Figure 30), indicating small conformational changes. When the temperature was increased to heat shock temperatures (43°C) (Figure 30), however, the fluorescence signal quickly dropped. In agreement with published data, elevated temperatures apparently induced the thermal unfolding of DnaK's N-terminal ATPase domain. The small temperature increase from 43°C to 45°C further accelerated this unfolding (Figure 30). In the presence of excess ATP, however, fluorescence measurements of DnaK at 45°C did not reveal any conformational changes (Figure 30). In agreement with published data, the presence of ATP rendered DnaK thermostable at 45°C, while nucleotide-depleted DnaK unfolded significantly at this temperature.

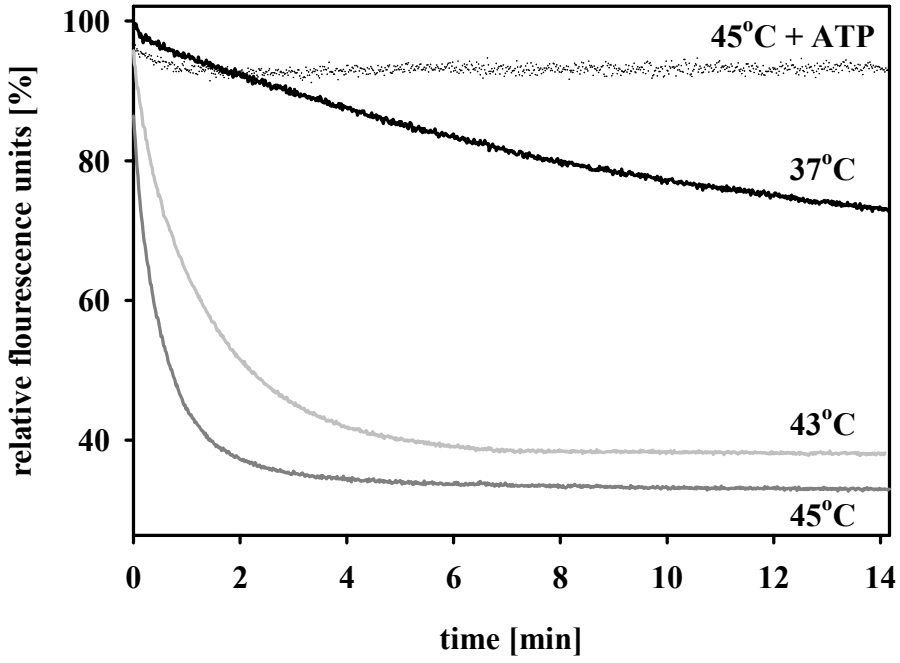

Figure 30 DnaK partially unfolds at heat shock temperatures

0.5 µM ATP-depleted DnaK was incubated at 37°C (black), 43°C (light gray) or 45°C (dark gray) and unfolding of its N-terminus was monitored measuring intrinsic tryptophane fluorescence (λ_{em}=350 nm, λ_{ex} = 295 nm). As a control, fluorescence of 0.5 µM DnaK in the presence of 0.5 mM ATP was determined at 45°C (dotted line). The fluorescence of fully folded DnaK was set to 100%.

4.3.4 Oxidation looks DnaK in unfolded conformation

The partial unfolding of DnaK's N-terminus appeared to be fully reversible, as lowering the temperature caused a slow increase in DnaK's intrinsic tryptophan fluorescence (150). More importantly, addition of ATP to unfolded DnaK triggered a much faster refolding. Presence of ATP apparently caused the refolding of DnaK by binding to DnaK and stabilizing its N-terminus (Figure 31, trace a). After thermal unfolding of DnaK in the presence of the oxidant GSSG, however, ATP was no longer capable of initiating the refolding of DnaK's N-terminal domain (Figure 31, trace b). The fluorescence signal stayed low, indicating that the protein was locked in an unfolded conformation. DnaK's loss of activity in supporting luciferase refolding after oxidative heat stress treatment *in vitro* could be completely rescued by reduction (Figure 28). Similarly, addition of reduced glutathione and ATP to GSSG-oxidized and unfolded DnaK quickly triggered the refolding of DnaK (Figure 31, trace c) with the same fast kinetic and to the same extent than non-treated DnaK.

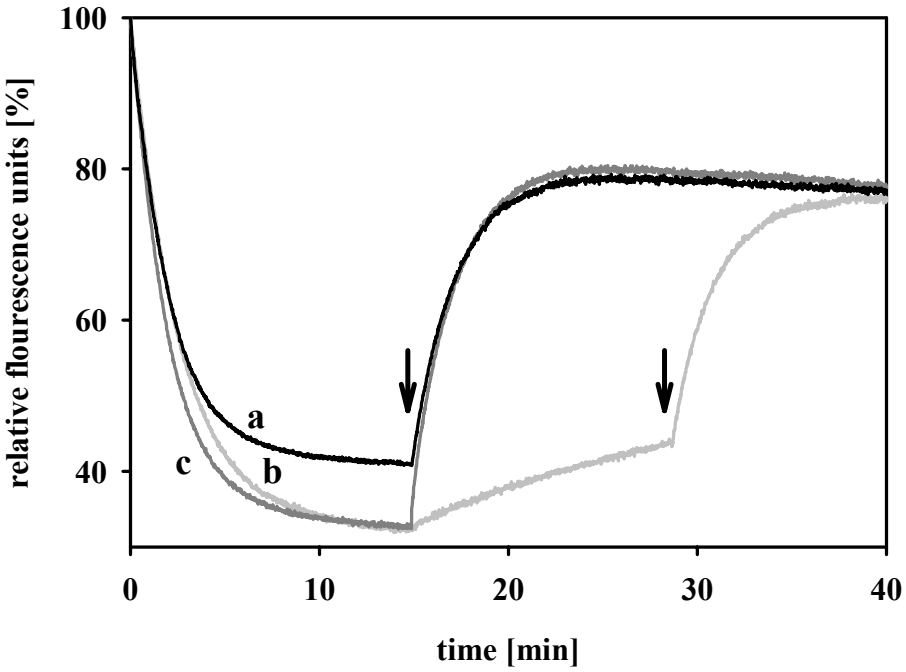

Figure 31 Oxidation of DnaK *in vitro* locks the N-terminus of DnaK in an unfolded state (1)

0.5 µM ATP-depleted DnaK was unfolded at 43°C in the absence (a) or presence (b, c) of 5 mM GSSG. As indicated by the arrow, after 15 minutes of incubation, the refolding of DnaK was initiated by the addition of a mix of 0.5 mM ATP and 14 mM GSH to (a) and (c) or only 0.5 mM ATP to (b). After further 15 min of incubation, 14 mM GSH was added to (b).

These results suggested that heat induced unfolding of the N-terminus of DnaK under nucleotide limiting conditions might expose a cysteine residue, which can be modified by oxidants *in vitro*. This modification could lock DnaK in an unfolded, inactive conformation

and prevent its refolding and reactivation until reducing conditions are restored. The small increase in the fluorescence signal of oxidized DnaK upon addition of ATP (Figure 31, trace b) suggested that not all DnaK molecules had been modified by GSSG within this 15 min incubation at 43°C. Noteworthy, thermal unfolding of DnaK in the presence of oxidized glutathione resulted overall in a lower fluorescence signal than unfolding without oxidants, suggesting that either the N-terminal unfolding is altered in oxidized DnaK or the extent of the unfolding is different. Alternatively, mixed disulfide bonds between DnaK's cysteine and GSSG could quench fluorescence, as seen for disulfide bond formation in DsbA (175). Because all samples refolded with the same kinetic, independently of the presence of GSSG/GSH in the sample, reduction of DnaK appeared not to be rate limiting for this process.

Fluorescence data of thermally unfolded, oxidized DnaK suggested that the partial unfolding of DnaK might expose a cysteine residue. Sequence alignments of DnaK revealed that chaperones of the Hsp70 family possess one conserved cysteine residue. In *E. coli* DnaK, this cysteine residue is located at position 15 and its conservation index CI among 40 other Hsp70 homologues from pro- and eukaryotes was calculated to be ≥ 0.4 (176). It is located in the N-terminal ATPase domain of DnaK and structural data reveal that bound nucleotides shield the cysteine (69).

To analyze the possibility that this conserved cysteine becomes accessible for thiol modification in certain DnaK conformations and is otherwise protected from environmental influences, the accessibility of Cys15 was measured with the Ellman's assay (section 3.4.4.1). Under denaturating conditions, the number of detected thiol groups in DnaK corresponded to the expected one cysteine per DnaK molecule. In native, ATP-bound DnaK, less than 0.2 thiol groups were determined, suggesting that Cys15 is only partly accessible in native DnaK. Further investigations with the thiol-specific reagent NBD-chloride confirmed these results and showed that Cys15 is buried in native DnaK and becomes readily accessible upon unfolding. Importantly, incubation of nucleotide depleted DnaK at elevated temperatures (20 min, 45°C) in the presence of NBD-chloride also allowed thiol modification. Similar to unfolding in high Gua-HCl concentrations caused heat conformational changes that made the cysteine residue accessible.

From these results was concluded that incubation of nucleotide-depleted DnaK at elevated temperatures causes the partial unfolding of its N-terminus. This exposes a conserved cysteine residue (Cys15), which can be oxidized and prevent DnaK's refolding. Only upon addition of reducing agents, the cysteine modification was reduced and refolding

occurred. This agreed well with our inactivation studies of DnaK that revealed that oxidatively inactivated DnaK was quickly reactivated by the addition of reducing agents.
In the presence of ATP, DnaK was rendered thermostable. The N-terminal ATPase domain did not unfold and DnaK remained active. Because the cellular ATP level dropped dramatically when cells were exposed to oxidative stress, DnaK is likely to become thermally unstable *in vivo* and unfold. This would explain its observed loss of function *in vivo*.

4.3.5 Thiol modification of DnaK's highly conserved cysteine

Oxidative thiol modifications in polypeptides can vary greatly depending on the thiol-reactivity, the number of thiol groups involved and the oxidant. Some redox-regulated proteins like Hsp33 or OxyR have been shown to form intramolecular disulfide bonds upon oxidation. In the case of DnaK, which possesses only one single cysteine residue, intermolecular disulfide bond formation can be possible if Cys15 is able to react with the cysteine of a second DnaK molecule to form a disulfide-linked dimer. Other modifications involving only one cysteine are sulfenic, sulfinic and sulfonic acid formation. In contrast to sulfenic and sulfinic acid, however, formation of sulfonic acid is irreversible and could therefore be excluded.

To investigate the nature of DnaK's thiol modification, samples of H_2O_2-oxidized and non-treated DnaK were separated with reducing and non-reducing SDS PAGE. While a disulfide-linked dimer would fall apart under reducing conditions, it should be easily detectable on non-reducing gels. As shown in Figure 32, about 50% of DnaK was disulfide-linked. The dimeric DnaK was only detected in non-reducing samples. It was not detected in samples exposed to straight heat stress, oxidative stress at 30°C or oxidative heat stress in the presence of ATP. This clearly shows that DnaK's cysteine became only accessible upon thermal unfolding of nucleotide depleted-DnaK and was able to form a disulfide-linked dimer upon inactivation due to oxidative heat stress *in vitro*. Not all DnaK molecules were associated in disulfide-linked dimers, even though the chaperone had completely lost its activity in luciferase refolding. This either indicated that the remaining monomeric DnaK molecules were active but not sufficient to support luciferase refolding or that beside the dimer also other oxidation products existed.

The existence of a disulfide-linked dimer *in vivo* would not only explain DnaK's inactivation under combined heat and oxidative stress but would also serve as proof that DnaK becomes thermally instable *in vivo* under ATP limiting conditions. However, despite numerous approaches using various conditions, we were unable to detect a disulfide-linked

dimer *in vivo* (data not shown). From this result, we concluded that the observed H_2O_2-induced dimerization of DnaK *in vitro* was presumably due to high DnaK concentrations that were used and which favored the formation of disulfide-linked dimers. The *in vivo* thiol modifications of DnaK, if present, could stop at the level of sulfenic acid formation, which is a stable modification unless a second cysteine is in close proximity.

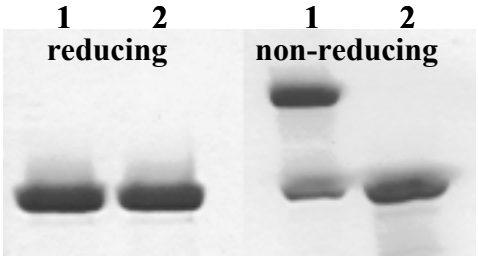

Figure 32 Oxidation of DnaK causes dimerization *in vitro*

20 µM nucleotide-depleted DnaK was incubated in the presence (lane 1) or in the absence (lane 2) of 2 mM H_2O_2 for 20 min at 45°C and analyzed by SDS PAGE under reducing or under non-reducing conditions.

To analyze whether DnaK's single cysteine becomes indeed modified *in vivo*, mass spectrometric analysis was performed in collaboration with J. Winter. DnaK-overexpressing cells were exposed to oxidative heat stress conditions (4 mM H_2O_2 at 45°C), heat shock (45°C) or oxidative stress at 30°C. Samples were prepared for MALDI-TOF and MALDI-TOF/TOF analysis as described (1) and the differentially oxidatively modified DnaK peptide 4-25 was analyzed. To avoid thiol oxidation during sample processing, free thiols were trapped with IAM *in vivo* and oxidants were carefully removed at the end of each stress treatment. Carbamidomethylated peptide 4-25 was only detected in DnaK preparations that were isolated from oxidative heat stressed cells. Under heat or oxidative stress alone, no modification of DnaK's conserved cysteine was observed, indicating that the nucleotide limiting conditions at elevated temperatures of oxidative heat stress are responsible for the unfolding of the N-terminal ATPase domain of DnaK *in vivo*. Furthermore, J. Winter found that within 5 min after exposure of Δ*rpoH* strains overexpressing DnaK/DnaJ/GrpE to oxidative heat treatment, part of the cellular DnaK pool underwent oxidative modification by H_2O_2. Cys15 was found to be oxidized to sulfenic acid, sulfinic acid and sulfonic acid. These modifications of Cys15 further confirmed its accessibility and the unfolding of DnaK's N-terminus under oxidative heat stress conditions *in vivo*.

4.3.6 Characterization of the DnaK$_{cys15ala}$ mutant protein

The results provided so far suggested that the oxidation of DnaK's Cys15 results in loss of its chaperone activity both *in vitro* and *in vivo*. To directly investigate the involvement of DnaK's conserved cysteine in this inactivation process, we constructed a DnaK mutant protein, which lacked that critical cysteine. If oxidation of Cys15 resulted in the inactivation of DnaK, this DnaK variant should be constitutive active and not lose its activity under oxidative heat stress *in vitro* and *in vivo*.

To find a suitable amino acid substitution for Cys15 in DnaK, the sequences of 40 different Hsp70 homologues from pro- and eukaryotes were studied (176). Interestingly, besides cysteine, only two other residues, alanine and valine, were represented at this position. One mitochondrial Hsp70 homologue in *Saccharomyces cerevisiae* revealed a alanine at position 15, which guided our decision to replace Cys15 in DnaK by alanine. The mutation was introduced by site directed mutagenesis as described (section 3.2.2.2) and the resulting IPTG-inducible plasmid was transformed into the *dnaK* deletion strain JCB201.

4.3.6.1 Activity of the DnaK$_{Cys15Ala}$ mutant *in vivo*

DnaK$_{cys15ala}$ was expressed as a soluble cytosolic protein and protein expression studies revealed that similar protein amounts of plasmid-encoded wild type DnaK and the DnaK$_{cys15ala}$ mutant protein were present in cells. This suggested that the DnaK$_{cys15ala}$ mutant protein was folded properly and not subjected to increased protein degradation. Furthermore, we established that 100 µM IPTG was sufficient to induce synthesis of both DnaK wild type and mutant protein to the level of chromosomal wild type DnaK. To study DnaK's activity *in vivo,* this IPTG concentration was used in all phenotypic assays including growth at heat shock temperatures, test for cell motility and support of phage λ replication.

While the *dnaK* deletion strain JCB201 was not able to grow on LB plates overnight at heat shock temperatures (42^{o}C), expression of plasmid-encoded wild type DnaK rescued this growth defect. Expression of the DnaK$_{cys15ala}$ mutant protein was equally able to rescue the growth defect, suggesting that it is able to operate as active chaperone in preventing lethal aggregation of thermally unfolding proteins (Figure 33). This suggested that the Cys15 amino acid substitution had no negative effect on the chaperone activity of DnaK *in vivo*.

The motility assay tests for the presence of flagella and the ability of *E. coli* cells to swim on 0.5% agar plates. The DnaK-system has been shown to be essential for flagella synthesis, presumably at the level of assembling the protein complex. As seen with the heat shock phenotype, the DnaK$_{Cys15Ala}$ variant was as capable as wild type DnaK to enable the

non-motile *dnaK* deletion strain JCB201 to swim (data not shown). Analysis of λ-replication was in agreement with the above results and showed that $DnaK_{Cys15Ala}$ is functionally equivalent to wild type DnaK *in vivo* (data not shown).

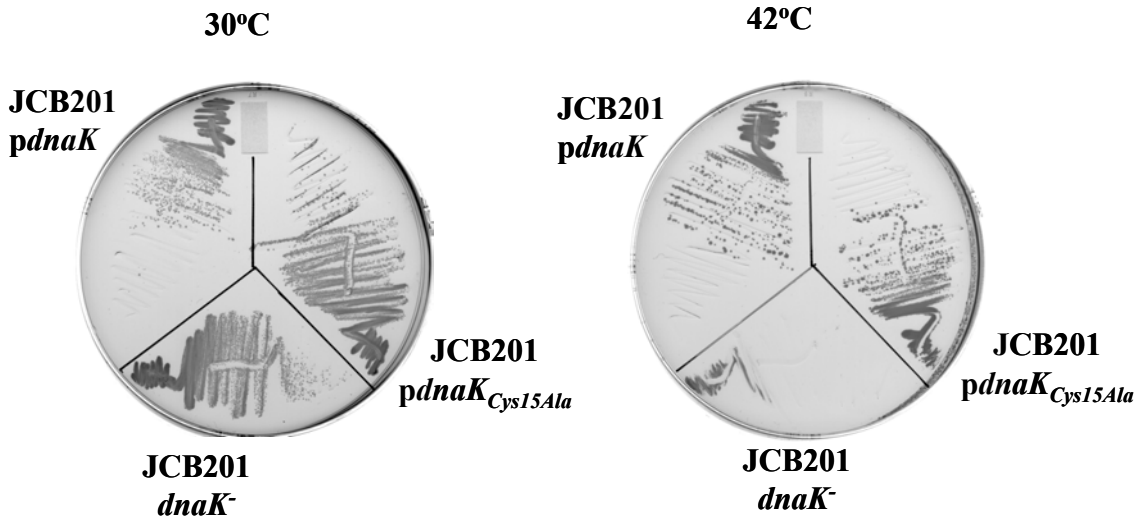

Figure 33 $DnaK_{Cys15Ala}$ mutant is active at heat shock temperatures *in vivo*

E. coli strain JCB201*dnaK7* is unable to grow on LB plates at 42°C. Expression of wild type DnaK and $DnaK_{Cys15Ala}$ from a plasmid to chromosomal level enables the strains to grow at 30°C and 42°C.

For *in vitro* analysis, the $DnaK_{Cys15Ala}$ mutant protein was overexpressed in JCB201 (*dnaK7*) and purified. Through the whole purification procedure, the $DnaK_{Cys15Ala}$ mutant protein behaved indistinguishable to wild type DnaK, which again suggested that the two proteins are very similar. Surprisingly, however, the *in vitro* activity of the purified DnaK mutant protein varied greatly from its wild type equivalent. The $DnaK_{Cys15Ala}$ mutant protein showed about 20% of the wild type activity and required different ratios of co-chaperones for the refolding of the model substrate luciferase (section 4.4.1). This prevented us from using this protein for those *in vitro* chaperone studies. Nevertheless, this $DnaK_{Cys15Ala}$ mutant protein was of big interest for *in vitro* assays that did not require chaperone activity such as fluorescence measurements to monitor DnaK's unfolding.

4.3.6.2 Thermal unfolding of the $DnaK_{Cys15Ala}$ mutant protein

ATP-depleted wild type DnaK is thermolabile. Elevated temperatures cause the unfolding of its N-terminal ATPase domain (Figure 31). Unfolding of DnaK in the presence of oxidants like H_2O_2 or GSSG appeared to block the ATP-induced refolding and rendered the chaperone inactive (Figure 31). If oxidation of Cys15 was indeed the reason of DnaK's inability to refold in the presence of ATP, the $DnaK_{Cys15Ala}$ mutant should be able to refold

even in the presence of oxidants. As described before, unfolding of DnaK was monitored by measuring its intrinsic fluorescence. Exposure of ATP-depleted $DnaK_{Cys15Ala}$ to elevated temperatures resulted in the same rapid unfolding of DnaK's N-terminal domain, as was observed in wild type DnaK (Figure 34). This indicated that DnaK's thermal instability at 42°C was not altered by the amino acid substitution. In contrast to oxidized wild type DnaK, which was unable to refold upon addition of ATP, unfolding of $DnaK_{Cys15Ala}$ in the presence of oxidants could be quickly reversed by ATP binding (Figure 34). This suggested that it is the oxidative modification of Cys15 that locks DnaK in an inactive state until reducing conditions are restored.

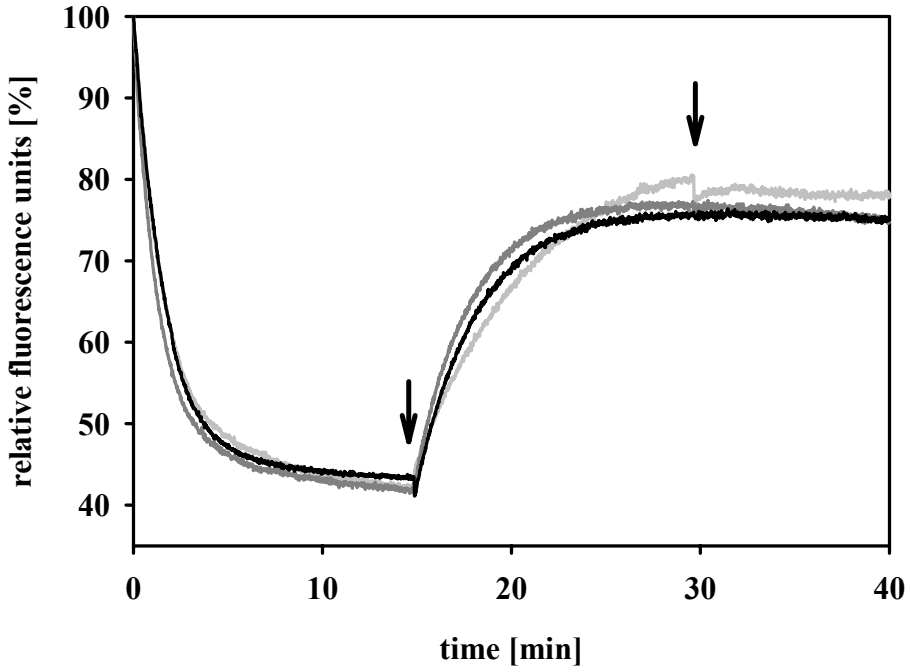

Figure 34 Oxidative inactivation of DnaK *in vitro* locks the N-terminus of $DnaK_{Cys15Ala}$ in an unfolded state

0.5 µM ATP-depleted $DnaK_{Cys15Ala}$ mutant protein was incubated at 43°C in the absence (black) or presence (gray) of 5 mM GSSG. After 15 minutes of unfolding, a mix of 0.5 mM ATP and 14 mM GSH (black, dark gray) or only 0.5 mM ATP (light gray) were added, as indicated by the arrow. After further 15 min of incubation, 14 mM GSH were added (light gray).

4.3.6.3 Role of Cys15 for DnaK's activity under oxidative heat stress *in vivo*

It has been long known that DnaK becomes up-regulated at heat shock temperatures to enable cells to survive such stress conditions. Surprising, however, was the finding that DnaK appeared to be inactive under combined heat and oxidative stress *in vivo*. My collaborator J. Winter showed that *rpoH* deletion cells overexpressing DnaK/DnaJ/GrpE accumulated large amounts of aggregating proteins under oxidative heat stress, while the

DnaK-system protected the majority of aggregation prone polypeptides under straight heat stress (1).

A *dnaK* deletion strain expressing wild type DnaK from a plasmid (JW120) is able to survive heat stress at 45°C over an extended period of time (Figure 35). To investigate the survival of this strain under combined heat and oxidative stress conditions, J. Winter treated cultures with 4 mM H_2O_2 at 45°C and withdrew samples at several time points to test for survival on plates. A few minutes after the start of stress, only 10% of the cells were still viable and after 20 minutes of oxidative heat stress treatment, the survival rate dropped to less than 0.001% (Figure 35).

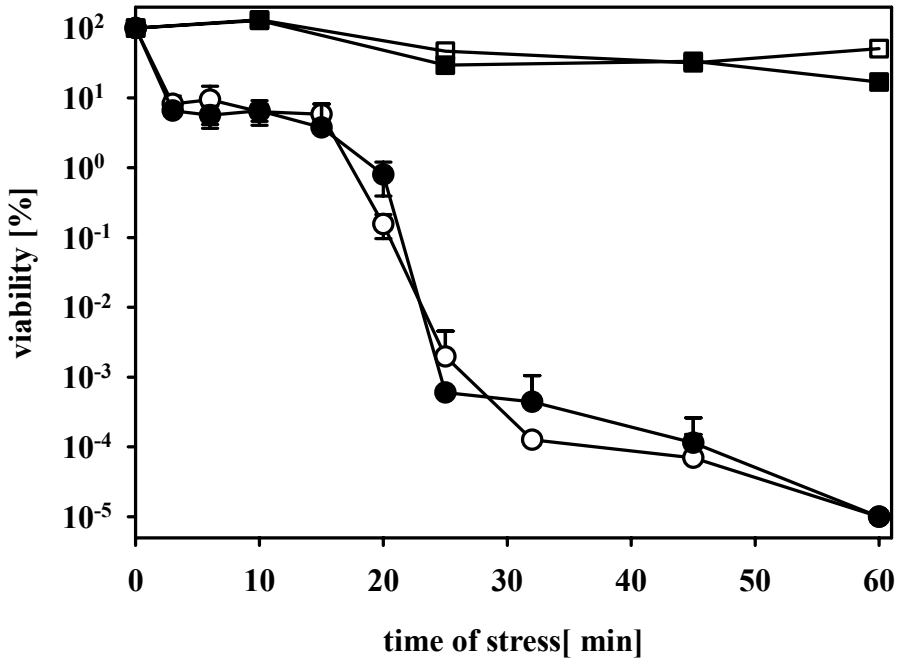

Figure 35 Cys15 does not play a redox-regulatory role in the inactivation of DnaK *in vivo* (1)

C600*dnaK7* expressing DnaK/DnaJ/GrpE (open symbols) or $DnaK_{Cys15Ala}$/DnaJ/GrpE (closed symbols) were grown at 30°C in LB medium for 4 h to express wild type levels of the DnaK-system. Then, the strains were diluted 1:20 into preheated LB medium at 45°C in the absence (squares) or presence of 4 mM H_2O_2 (circles). At the indicated time points, aliquots were removed and the viable titer was determined. The survival rates given in the graph represent the mean of two independent experiments.

Is DnaK's loss of activity under oxidative heat stress caused by the exposure and oxidation of Cys15 in thermally unfolding DnaK? If this was indeed the case, a *dnaK* deletion strain expressing the cysteine-less $DnaK_{Cys15Ala}$ mutant protein from a plasmid should be able to survive conditions of oxidative heat stress to a greater extent than cell expressing wild type DnaK. When J. Winter tested this hypothesis, however, cells expressing the mutant DnaK showed the same sensitivity to oxidative heat treatment than cells expressing wild type DnaK (Figure 35), suggesting that Cys15 had no influence on DnaK's inactivation. This

result suggested that oxidation of this conserved cysteine residue in DnaK might be a side effect of DnaK's unfolding due to low cellular ATP levels and subsequent exposure of Cys15.

4.3.7 Reactivation of inactive DnaK *in vivo*

While it appeared that the inactivation of DnaK's chaperone activity occurred independent of Cys15 modification, it was unclear to what extent oxidation of Cys15 played a role in the regulation of DnaK's reactivation upon return to non-stress conditions. Because *in vivo* thiol modifications in DnaK have been observed in oxidatively heat stressed cells (section 4.3.5), these modifications might play an important role in the reactivation process of DnaK. Oxidative stress *in vivo* causes the non-specific oxidation of many cellular polypeptides and uncontrolled reactivation of the foldase DnaK after return to non-stress conditions might lead to fruitless attempts to refold oxidatively damaged proteins. Modification of Cys15, however, would prevent the premature reactivation of DnaK after removal of the oxidants, as it locks DnaK in the unfolded conformation. Only after return to reducing conditions in the cytosol, Cys15 could be reduced and the chaperone could regain its activity. At this time, all non-specific oxidized cellular proteins might be reduced as well and the refolding activity of DnaK would be efficient.

To investigate whether Cys15 regulates the reactivation of DnaK after return to non-stress conditions, the luciferase refolding assay *in vivo* was performed as described in (1). If reduction of oxidized Cys15 was a control mechanism of DnaK's activity, it might limit the reactivation rate of DnaK, which should be detectable by a delayed luciferase refolding *in vivo*. In collaboration with J. Winter, luciferase refolding was analyzed in *rpoH* deletion cells expressing DnaJ, GrpE and either wild type DnaK or the $DnaK_{Cys15Ala}$ mutant protein. Exposure of the cells to oxidative heat stress ($43^{o}C$, 4 mM H_2O_2) caused the inactivation of the cytosolic expressed substrate luciferase. The chaperone activity of wild type DnaK and the $DnaK_{Cys15Ala}$ mutant in refolding of non-native luciferase was monitored during the recovery phase of the cells after return to non-stress conditions. The yields of luciferase refolding were low, but comparable in both strains, suggesting that inactive DnaK wild type and mutant reactivated to the same extent (data not shown). Importantly, this proofed that DnaK's oxidative inactivation *in vivo* was partly reversible. Furthermore, the rate of the $DnaK_{Cys15Ala}$-supported luciferase refolding revealed no additional lag phase than compared to the refolding by wild type DnaK (data not shown). This suggested that modification of DnaK's Cys15 played no regulatory role for the reactivation of DnaK after its inactivation

during oxidative heat stress treatment. Neither DnaK's inactivation nor its reactivation appeared to be controlled by thiol modification of Cys15.

4.3.8 Monitoring DnaK's unfolding *in vivo*

Even though oxidation of Cys15 in DnaK appeared to have no significance for the inactivation or reactivation of DnaK, it appeared to be a useful tool for analyzing the folding state of DnaK *in vivo*. Accessibility of Cys15 due to DnaK's unfolding could be a measure for its chaperone activity *in vivo*. While conformational changes of DnaK can be easily followed by fluorescence measurements *in vitro,* no method existed for analyzing the extent of DnaK's unfolding *in vivo*. Modification of DnaK's Cys15 in *E. coli* cells with thiol specific reagents such as biotin-labeled maleimide should allow conclusions about the state of DnaK's unfolding *in vivo* (section 3.4.4.4).

Cells were exposed to oxidative heat stress and in a first step all accessible thiol groups were irreversible trapped by incubating cells with the cell permeable and thiol specific probe N-Ethylmaleimide (NEM). Cells were then lysed by the addition of cold TCA and the precipitated proteins were carefully separated from the culture media by centrifugation. The proteins were resuspended in denaturing buffer and all thiol groups that became now accessible due to the denaturation were modified with a biotin-labeled malemide (Maleimide PEO_2-Biotin). Now, the proteins were separated by SDS PAGE and blotted onto a nitrocellulose membrane. Western blot analysis with α-DnaK or α -biotin antibodies was performed. If DnaK was unfolded *in vivo,* Cys15 was accessible and could be modified by NEM in the first step. This, as well as already existing oxidative modifications, excluded Cys15 from the subsequent biotinylation. The difference of the total amount of DnaK (α-DnaK labeled) and the biotinylated amount of DnaK (α -biotin labeled) corresponds therefore to *in vivo* unfolded or oxidized DnaK molecules.

The described method was first tested with purified DnaK after various stress treatments *in vitro*. While the ATP-depleted protein should remain fully folded and active at 30°C in the absence or presence of H_2O_2, elevated temperatures like 43°C are expected to trigger DnaK's unfolding in oxidant-independent manner. Therefore, only the cysteine residues of heat-treated DnaK should become NEM-labeled, while thiol groups in DnaK that had been incubated at 30°C should be biotinylated. That this was indeed the case is shown in Figure 36. Both 30°C samples ($\pm$ H_2O_2) were biotinylated to the same extent (lane 3, 4), indicating that Cys15 became accessible upon subsequent denaturation in biotin buffer. After 10 min incubation at 43°C, however, no biotinylation was detected, indicating that all DnaK

molecules were unfolded and thiol groups accessible to NEM-modification (lane 7). Thiols that had been oxidized by H_2O_2 at 43°C did not get biotinylated either (lane 8) and the result was therefore the same for both heat stress samples. In the absence of *in vitro* NEM-trapping, all thiol groups should get biotinylated after denaturation, unless they were modified by oxidation. Figure 36 clearly shows that DnaK in both 30°C samples ($\pm$ H_2O_2)(lane 1,2) as well as at 43°C (lane 5) could get biotinylated to the same extent, suggesting that these conditions did not lead to the intrinsic modification of Cys15. DnaK that had been incubated for 10 min at 43°C in the presence of H_2O_2, however, was only partially biotinylated (lane 6). This indicates that some DnaK molecules have been oxidized by H_2O_2, which prevents their biotinylation.

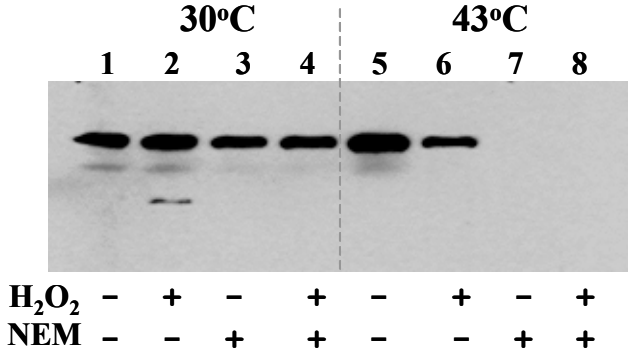

Figure 36 Cys15 of thermally unfolded DnaK gets biotinylated *in vitro*

20 µM ATP-depleted DnaK was incubated in the absence or presence of 2 mM H_2O_2 at 30°C or 43°C. After 10 min, samples were either directly precipitated with TCA or transferred for thiol trapping into prewarmed NEM (final concentration 0.1 M), incubated for 5 min at the same temperature and finally TCA precipitated. DnaK was resuspended in biotin buffer under denaturing condition and all free thiols were biotinylated during 30 min incubation at 37°C. After a second TCA precipitation, SDS PAGE was performed followed by western blot analysis using a α-biotin antibody.

To determine the extent of the unfolding of wild type DnaK or $DnaK_{Cys15Ala}$ *in vivo*, the biotinylation method was utilized to analyze *rpoH* deletion cells overexpressing the DnaK-system (section 3.4.4.4). Strains were grown to logarithmic phase and exposed to H_2O_2 treatment at 30°C or 43°C. After 10 min of stress treatment, NEM was added to the cell cultures and incubation was continued for 5 min at the same stress conditions. Then, the cells were TCA-precipitated and the non-alkylated thiol groups were biotinylated as described. In the lower part of Figure 37, the total amount of DnaK is shown, while the upper part of Figure 37 presents the biotinylated fraction of DnaK. Upon exposure of ΔrpoH cells expressing wild type DnaK to oxidative stress at 30°C, no significant unfolding takes place (lane 1, 2). In the absence and presence of H_2O_2, identical amounts of DnaK become biotinylated, indicating that these cysteines are buried under these conditions. In contrast, significantly lower

amounts of DnaK are biotinylated upon exposure of cells to oxidative stress at 43°C (lane 4). Here, the biotinylated fraction is dramatically decreased, compared to the 30°C samples (lane 1, 2) as well as to the 43°C samples in the absence of H_2O_2 (lane 3). Also at 43°C, no unfolding of DnaK occurred *in vivo*, which had been predicted from the constant cellular ATP levels under these conditions. As expected, the $DnaK_{Cys15Ala}$ mutant protein, expressed in non-stressed ΔrpoH cells (30°C), did not become biotinylated in denaturing biotin buffer (lane 6), demonstrating the high specificity of the biotin-labeled maleimide probe for thiol groups. More than 80% of DnaK was unfolded during oxidative heat stress conditions *in vivo*. Because unfolding of the chaperone leads to its inactivation, this clearly explained why the DnaK-system was no longer capable of preventing protein aggregation or supporting cell survival under oxidative heat stress conditions *in vivo* (1).

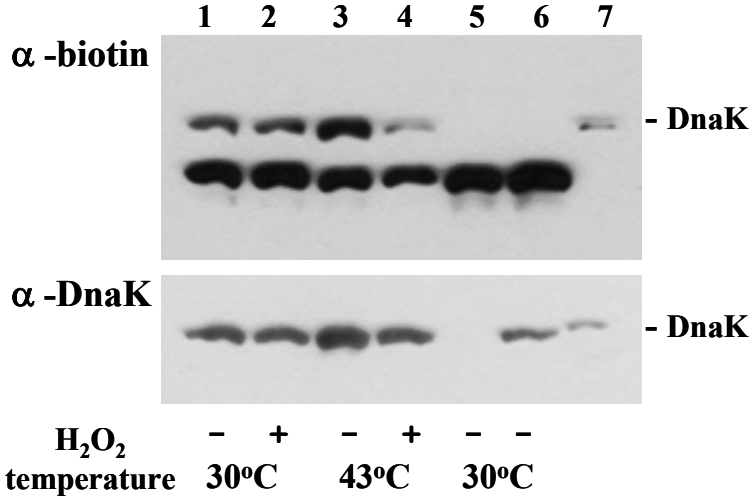

Figure 37 Oxidative heat stress causes thermal unfolding of DnaK *in vivo*

rpoH deletion cells overexpressing DnaK/DnaJ/GrpE (lane 1-4), $DnaK_{Cys15Ala}$/DnaJ/GrpE (lane 6) or no additional chaperones (lane 5) were grown at 30°C to logarithmic phase. Then, cells were split for stress treatment at 30°C or 43°C in the absence or presence of 4 mM H_2O_2 as indicated (lane 1-6). After 10 min, 0.1 M NEM was added to cultures to modify all accessible thiols. After 5 min, the cell cultures were precipitated with TCA. Free thiols were subsequently biotinylated under denaturing conditions in biotin buffer, followed by a second TCA precipitation. Proteins were separated by SDS PAGE, transferred onto a membrane and labeled with α-biotin and α-DnaK antibodies. Detected protein concentrations in both figures are not comparable, because the two antibodies possess different specificities. Lane 7 contains a DnaK standard.

4.3.9 Influence of various reactive oxygen species on cellular ATP level

Microorganisms encounter a variety of oxidants like hydrogen peroxide, hypochlrorous acid (HOCl) or nitrogen oxide (NO) during the oxidative burst of macrophages and neutrophiles. To investigate whether the inactivation of DnaK by H_2O_2 at heat shock temperatures is not specific for H_2O_2 but a general response to reactive oxygen species at

elevated temperatures, the influence of other oxidants was investigated *in vivo*. Hypochlrorous acid is a physiological relevant oxidant as it is released by neutrophiles in high concentrations in an attempt to kill bacteria. It was, therefore, of interest to determine whether HOCl treatment of cells also resulted in a decrease of cellular ATP levels and a loss of DnaK's chaperone activity. Diamide, in contrast, is known to be a non-specific thiol oxidant, which causes disulfide stress rather than oxidative stress in cells. Investigating its influence on the cellular ATP level and DnaK's activity would allow more defined conclusions about the regulation mechanism of DnaK's activity *in vivo*.

E. coli wild type cells (MC4100) were exposed to heat shock temperatures in the presence of 6 mM HOCl, 3 mM diamide or 4 mM H_2O_2 and the cellular ATP level was measured after 15 min of heat stress treatment (section 3.7.4). In agreement with former experiments, H_2O_2-induced oxidative stress caused a significant drop of the intracellular ATP concentration (Figure 38).

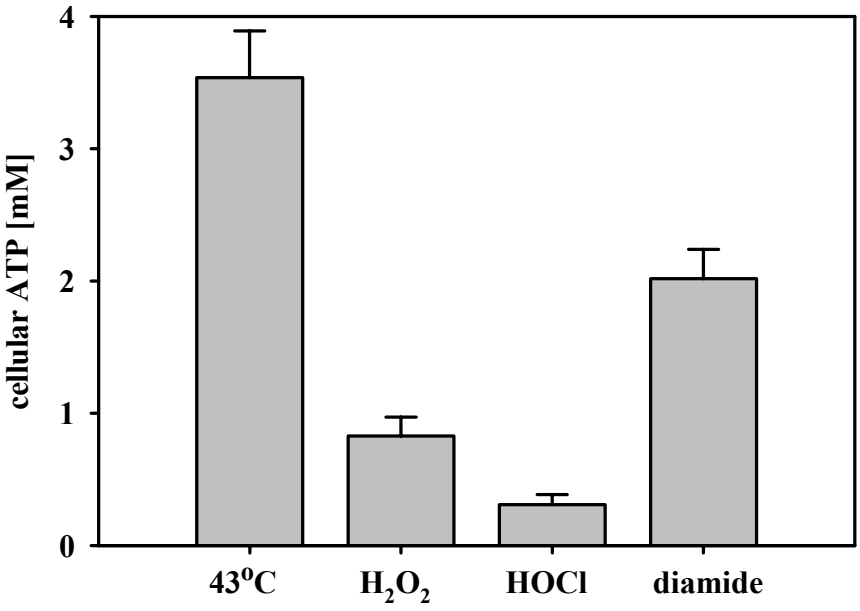

Figure 38 H_2O_2 and HOCl, but not diamide, cause drop of cellular ATP level (1)

MC4100 strains were grown at 30°C until OD_{600nm} of 0.5 was reached. Then, the culture was shifted to 43°C and 4 mM H_2O_2, 6 mM HOCl or 3 mM diamide were added. After 15 min of stress treatment, aliquots were removed and the total amount of ATP was determined as described.

Similarly, HOCl treatment appeared to trigger a dramatic decrease from 3.5 mM ATP to 0.3 mM as well. Diamide treatment, however, only caused a slight decrease of the ATP concentration to not less than 2 mM (Figure 38). The postdoc J. Winter tested the *in vivo* activity of DnaK upon exposure to these oxidants. In the presence of either H_2O_2 or HOCl, overexpression of the DnaK-system was insufficient to protect cells against oxidative heat

stress induced cell death. Upon exposure to diamide, on the other hand, overexpression of the DnaK-system significantly increased the cell viability (1). These findings significantly increase the strength of our correlation that the oxidative stress induced drop in intracellular ATP levels allows the unfolding of DnaK at elevated temperatures, causing the reversible loss of DnaK activity.

These data suggest that not only hydrogen peroxide but also other oxidative stress inducing reagents like hypochlrorous acid lead to DnaK's inactivation at elevated temperatures *in vivo*. The fundamental difference to diamide induced disulfide stress is the cellular ATP level, which appeared to decrease significantly in the presence of reactive oxygen species. Former studies demonstrated that disruption of ATP synthesis is the reason for the nucleotide deficiency. Reversible oxidative modification of GapA, a central enzyme in glycolysis, due to oxidative stress conditions has been shown to be responsible for massive reduction of cellular ATP concentrations in pro- and eukaryotes (177, 178). Disulfide stress did not cause the oxidation of GapA, which would explain why ATP levels did not decrease, rendering DnaK active *in vivo*.

4.4 *In vitro* activity of $DnaK_{Cys15Ala}$

The $DnaK_{Cys15Ala}$ mutant was constructed to analyze the role of Cys15 in DnaK's inactivation and activation process. The amino acid substitution to alanine was carefully chosen based on sequence analysis of Hsp70 homologues and was expected to create a functional DnaK mutant. While this variant behaved identically to wild type DnaK in several phenotypic studies *in vivo*, its *in vitro* activity was significantly altered. Results of those investigations are presented separately in the following chapter.

4.4.1 $DnaK_{Cys15Ala}$–supported luciferase refolding *in vitro*

Analysis of the influence of molecular chaperones on the reactivation of the chemically denatured model substrate luciferase is a commonly used activity assay for the DnaK-system (151). DnaK/DnaJ/GrpE assisted luciferase reactivation reaches a significantly higher yield than spontaneous refolding of the substrate and is a direct measure for chaperone activity. For this *in vitro* chaperone assay, a DnaK:DnaJ:GrpE ratio of 10:2:10 over luciferase had been established (167). Surprisingly, these concentrations and ratios were not optimal for the $DnaK_{Cys15Ala}$ mutant protein. When luciferase reactivation reactions were performed using identical protein concentrations of $DnaK_{Cys15Ala}$ as are established for wild type DnaK, the chaperone activity of $DnaK_{Cys15Ala}$ was significantly reduced (Figure 39, filled diamonds).

While wild type DnaK supported reactivation of more than 60% luciferase, not even 15% luciferase regained activity after $DnaK_{Cys15Ala}$-assisted refolding (Figure 39). In an attempt to investigate the reason for this impaired chaperone activity of $DnaK_{Cys15Ala}$ in more detail, luciferase refolding reactions were repeated using varying DnaK, DnaJ and GrpE ratios. 5-fold increase and decrease of the DnaJ concentration did not significantly alter the luciferase refolding yield in the presence of both wild type and mutant DnaK (data not shown). In contrast, a 2-fold increased luciferase refolding was accomplished by using the double amount of the $DnaK_{Cys15Ala}$ mutant protein (20:2:10)(Figure 39, filled triangles).

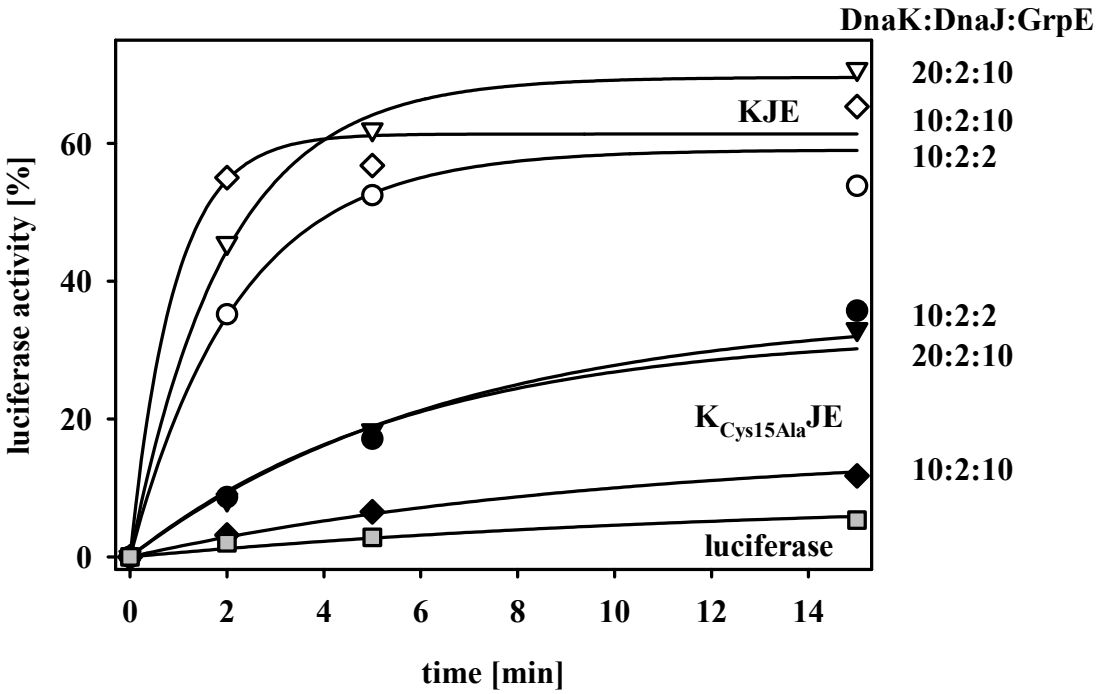

Figure 39 $DnaK_{Cys15Ala}$ is impaired in refolding chemical denatured luciferase

8 µM chemically denatured luciferase was diluted 1:100 into refolding buffer in the absence (gray squares) or presence of DnaK/DnaJ/GrpE (open symbols) or $DnaK_{Cys15Ala}$/DnaJ/GrpE (black symbols) The refolding reactions contained 0.16 µM DnaJ with either 0.8 µM DnaK, 0.8 µM GrpE (diamonds), 1.6 µM DnaK, 0.8µM GrpE (triangles) or 0.8 µM DnaK, 0.16 µM GrpE (circles). Luciferase refolding was determined at the indicated time points and activity of native luciferase was set to 100%.

Interestingly, not only a higher DnaK concentration but also a lower GrpE concentration resulted in increased luciferase refolding yields in the presence of the $DnaK_{Cys15Ala}$ mutant protein. A five times lower GrpE concentration (10:2:2) supported luciferase refolding to 35% (Figure 39, filled circles). In case of wild type DnaK, luciferase refolding yields were not significantly altered by variations in the DnaK and GrpE concentration. Just a slightly lower refolding rate was observed in the presence of a 5-fold lowered GrpE concentration (Figure 39, open circles). The adopted DnaK:DnaJ:GrpE ratio of

10:2:2 over luciferase, which significantly increased refolding yields of the $DnaK_{Cys15Ala}$-supported luciferase reactivation, is more similar to *in vivo* ratios of the DnaK-system (10:1:3)(179) than the earlier used ratio of 10:2:10. This might contribute to the observed full activity of the $DnaK_{Cys15Ala}$ mutant protein *in vivo*.

4.4.2 ATPase activity of $DnaK_{Cys15Ala}$

ATP hydrolysis of DnaK is crucial for DnaK's chaperone activity. The rate of ATP hydrolysis is influenced by the interactions of DnaK with its co-chaperones and substrate proteins. DnaJ and substrate proteins enhance DnaK's intrinsic ATPase activity and trigger substrate binding while the nucleotide exchange factor GrpE replaces ADP by ATP, which results in substrate release and facilitates a new refolding cycle. Therefore, ATPase activity assays allow conclusions about DnaK's cooperation with DnaJ and GrpE and, consequently, about DnaK's chaperone activity.

Steady state ATPase assays were performed with either wild type DnaK or the $DnaK_{Cys15Ala}$ mutant protein in the absence or presence of GrpE or DnaJ/GrpE. In contrast to single turnover experiments, ATP was not limiting and the nucleotide exchange reaction contributed to the hydrolysis rate. Initially used chaperone concentrations of 10:20:10 for DnaK:DnaJ:GrpE were based on literature data (39). The intrinsic ATPase rate of wild type DnaK was 0.022 min^{-1} and was stimulated 20-fold by DnaJ and 60-fold by DnaJ/GrpE (Table 6). Interestingly, the intrinsic ATPase rate of the $DnaK_{Cys15Ala}$ variant was with 0.087 min^{-1} about 4-fold higher than compared to wild type protein. Stimulation of the DnaK mutant by DnaJ increased its ATP hydrolysis only 6-fold, whereby approaching the ATPase rate of wild type DnaK under the same circumstances. The GrpE-induced nucleotide exchange in wild type DnaK and the $DnaK_{Cys15Ala}$ mutant protein was with of 2-fold and 2.5-fold, respectively, comparable. The presence of both co-chaperones did not enhance the ATPase rate of the mutant protein much more [Table 6, (4)]. Even though the $DnaK_{Cys15Ala}$ mutant protein possesses a 4-fold higher intrinsic ATPase activity, its ATP hydrolysis after stimulation by the whole system is almost 2-fold lower.

To find out, whether the reduced ATPase hydrolysis rate of $DnaK_{Cys15Ala}$ is the reason for its low chaperone activity *in vitro*, DnaJ concentrations were adjusted to the ones used in luciferase refolding (10:2:10 of DnaK:DnaJ:GrpE). Under these conditions, however, the $DnaK_{Cys15Ala}$ mutant protein revealed very similar rates of ATP hydrolysis than wild type DnaK (Table 6).

Table 6 Rate of ATP hydrolysis (ADP $DnaK^{-1}$ min^{-1}) by DnaK wild type and $DnaK_{Cys15Ala}$

	DnaK (1)	+ DnaJ (2)	+ GrpE (3)	+ DnaJ/GrpE (4)	+ DnaJ/GrpE (5)
DnaK wild type	0.022	0.480	0.045	1.341	0.496
$DnaK_{Cys15Ala}$	0.087	0.574	0.224	0.767	0.478

The ATPase activity of DnaK and $DnaK_{Cys15Ala}$ was determined in steady state experiments. Reactions containing buffer with 200 µM ATP (0.5 µCi [α^{32}P]ATP) and 0.69 µM DnaK or the $DnaK_{Cys15Ala}$ mutant protein in the absence (1) or presence of 1.4 µM DnaJ (2), 0.69 µM GrpE (3), 1.4 µM DnaJ, 0.69 µM GrpE (4) or 0.14 µM DnaJ, 0.69 µM GrpE (5) were prewarmed at 25°C. The assay was started by the addition of DnaK. Aliquots were withdrawn at several time points during the linear phase of each reaction and spotted onto a thin layer chromatography plate. Plates were developed and the amount of ADP and ATP were determined using a phosphorimager. Accumulated ADP was blotted against the reaction time to determine the rate of ATP hydrolysis.

4.4.3 Activity of $DnaK_{Cys15Ala}$ in preventing luciferase aggregation

To further investigate the reason for the lower chaperone activity of $DnaK_{Cys15Ala}$ *in vitro,* its substrate binding affinity was determined using the luciferase aggregation assay. While for the refolding analysis the whole DnaK-system was necessary, this assay is based on DnaK's ability to bind to unfolding proteins without stimulation by DnaJ. If $DnaK_{Cys15Ala}$ possessed a lower substrate affinity, this would explain its low luciferase refolding yields. DnaK's intrinsic substrate binding affinity is rather low and a 10-fold excess of DnaK to substrate was used. After dilution of luciferase into refolding buffer, its aggregation was monitored by light scattering (section 3.6.1.1).

Luciferase in the absence of DnaK quickly aggregated and reached its final light scattering signal after about 12 min of incubation at 30°C (Figure 40). 10-fold molar excess of wild type DnaK was able to prevent luciferase aggregation by about 30%. The same concentration of $DnaK_{Cys15Ala}$, however, did not protect luciferase from aggregation at all (Figure 40). This indicated much lower substrate binding affinities, which would also explain the lower substrate refolding yields. In the presence of sub-stochiometric amounts of DnaJ, wild type DnaK almost completely prevented aggregation of luciferase. A dramatic increase in substrate affinity in the presence of DnaJ was also observed for the $DnaK_{Cys15Ala}$ mutant protein (Figure 40). The DnaJ-supported substrate binding affinity of $DnaK_{Cys15Ala}$ is still significant lower than compared to wild type DnaK. This lower binding affinity nicely

reflected the lower refolding activity of this DnaK mutant and suggests that the lower substrate binding affinity by $DnaK_{Cys15Ala}$ is the reason for its reduced foldase activity.

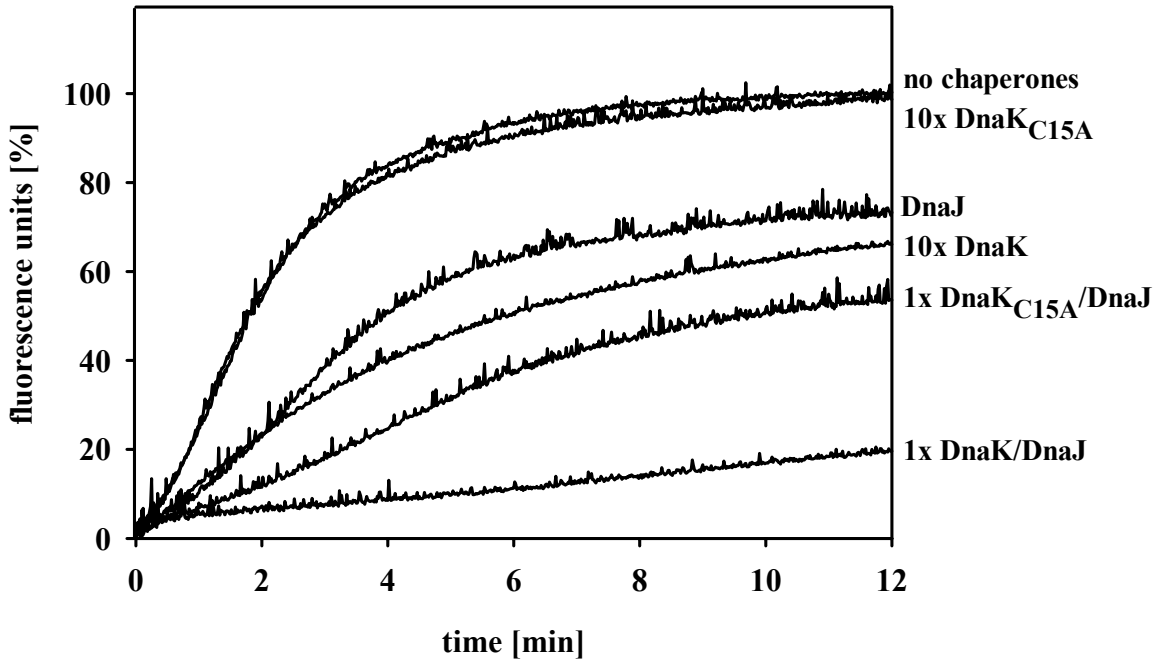

Figure 40 $DnaK_{Cys15Ala}$ is less active in preventing aggregation of chemically denatured luciferase

8 µM chemically denatured luciferase was diluted 1:100 into buffer supplemented with 1-fold (0.08 µM) or 10-fold (0.8 µM) excess of DnaK wild type or $DnaK_{Cys15Ala}$ mutant in the absence or presence of 0.02 µM DnaJ. Reactions were stirred constantly at 30°C and aggregation was monitored measuring light scattering at 320 nm ($\lambda_{ex/em}$).

5 Discussion

5.1 DnaK inactivates during oxidative heat stress

The DnaK/DnaJ/GrpE system plays a vital role in protecting proteins against heat stress induced unfolding. Surprisingly, however, under conditions of oxidative stress at elevated temperatures, the DnaK-system is no longer active (1). The foldase DnaK loses activity upon exposure of cells to reactive oxygen species such as hydrogen peroxide (H_2O_2) and hypochlorous acid (HOCl) at elevated temperatures, which is the consequence of two conditions, a dramatic drop of the cellular ATP level induced by oxidative stress and the thermolability of nucleotide-depleted DnaK. The exposure of a variety of pro- and eukaryotic cells to H_2O_2 or HOCl results in significantly degreased cellular ATP levels. Osorio and co-workers demonstrated that the ATP level in yeast dropped up to 10-fold upon treatment with 1 mM H_2O_2 (172). Comparable results were obtained in this work for *E. coli* cells that were exposed to either hydrogen peroxide or hypochlorous acid. The cellular ATP concentrations decreased within minutes after the oxidative stress treatment in a temperature independent manner. In yeast, this appears not to increase ADP levels, but the concentration of inosine (172, 180). At the same time, heat shock temperatures have been reported to increase DnaK's rate of ATP hydrolysis (181). Together with low cellular ATP levels, this presumably leads to a substantially ATP-deprived DnaK under oxidative stress at elevated temperatures. *In vitro*, ATP-deprived DnaK was shown to be thermolabile and to partially unfold at heat shock temperatures (150). This unfolding is reversible and ATP significantly accelerates the refolding of DnaK. Thermal unfolding of DnaK's ATPase domain results in the exposure of a highly conserved cysteine residue (Cys15). In the presence of oxidants, we found that this Cys15 undergoes thiol modification and renders DnaK in a partially unfolded conformation, even upon return to non-stress conditions. Chaperone activity assays demonstrated that this unfolded DnaK species is inactive in refolding non-native substrate proteins. *In vitro*, refolding and reactivation of DnaK was initiated by reductants like DTT or the thioredoxin system. Reduction of Cys15 turned DnaK back into a fully active chaperone. Investigations presented in this work revealed that oxidative stress at elevated temperatures also causes the unfolding of DnaK *in vivo*. DnaK appears to remain inactive as long as stress conditions last. Once reducing conditions in the cytosol of cells are restored, the ATP level quickly rises. Upon binding to ATP, DnaK regains its thermal stability and reactivates (1).

5.2 Modification of DnaK's cysteine does not regulate its activity

In vitro and *in vivo* analysis revealed that Cys15 in DnaK's N-terminal ATPase domain is only accessible for thiol modification after the unfolding of DnaK's N-terminus. That the modification of Cys15 is not directly involved in the inactivation process of DnaK was demonstrated by *in vivo* studies of the $DnaK_{Cys15Ala}$ mutant. Similar to wild type DnaK, the mutant protein was unable to protect cells from the stress-induced cell death caused by hydrogen peroxide combined with elevated temperatures. This suggested that DnaK's loss of activity must be a direct consequence of its partial unfolding under these stress conditions. As two out of the three detected *in vivo* modifications of Cys15 (sulfenic and sulfinic acid) were shown to be reversible (182), reduction of modified Cys15 might still play a regulatory role for the reactivation of DnaK upon return to non-stress conditions. However, *in vivo* luciferase refolding studies in the presence of either wild type DnaK or the $DnaK_{Cys15Ala}$ mutant after exposure of cells to oxidative heat stress appeared to be very similar (1). It is possible that the slower refolding kinetics of luciferase after oxidative heat stress treatment may mask other regulatory influences. Physiological reduction systems are known to be very powerful, which suggests that the reduction of Cys15 might not play a regulatory role for DnaK's activity. Nevertheless, Cys15 is an extremely useful marker to monitor the unfolding and inactivation of DnaK *in vivo*. Existence of *in vivo* thiol modifications demonstrated that DnaK unfolded in cells and will furthermore allow the investigation of the rate of DnaK's inactivation.

5.3 The chaperone activity of DnaJ is sensitive to oxidative stress

The molecular chaperone DnaJ contains two zinc centers, each of which is formed by four highly conserved cysteine residues that coordinate one zinc ion (76, 86). Because such zinc centers have been shown to often function as redox switches that regulate protein activity (130), the effect of oxidative stress on DnaJ and its chaperone activity was analyzed.

Oxidation of purified DnaJ by H_2O_2 in the presence of catalytically amounts of $CuCl_2$ resulted in the release of bound zinc with a T½ of 16.2 min. This was the consequence of the oxidative modification of DnaJ's highly conserved cysteine residues, as demonstrated by simultaneous *in vitro* thiol trapping of DnaJ. Chaperone activity assays revealed that oxidation of DnaJ increased its autonomous, DnaK-independent chaperone activity. While reduced DnaJ allowed the spontaneous reactivation of denatured citrate synthase to 50%, almost no citrate synthase reactivated in the presence of oxidized DnaJ. Noteworthy, this oxidation-induced increase of DnaJ's chaperone activity appeared to be faster (T½ 8.8 min)

than the concurrent zinc release, suggesting that oxidation of only one of DnaJ's two zinc centers might be sufficient for this change in activity. Oxidation of DnaJ was fully reversible. Upon addition of reductants such as DTT, oxidized DnaJ immediately lost its increased substrate binding affinity. Light scattering experiments of aggregating citrate synthase and luciferase suggested that oxidized DnaJ forms microaggregates with unfolded substrate proteins. Even though these complexes of oxidized DnaJ and substrate increased the light scattering signal, they appeared to allow the refolding of substrates in the presence of DTT. While reduced DnaJ, which possesses lower substrate binding affinity than oxidized DnaJ, released bound luciferase to the DnaK-system independently of DTT, oxidized DnaJ formed very stable complexes, which prevented the DnaK-supported refolding of luciferase. This is presumably due to competition for substrate binding between DnaK and oxidized DnaJ. Upon DTT addition and reduction of DnaJ, substrate was released and refolded by DnaK. DnaJ reveals autonomous, DnaK-independent chaperone activity as well as DnaK-dependent co-chaperone activity (75, 151). We found that *in vitro* oxidation of DnaJ increased its autonomous substrate binding activity and impaired its co-chaperone activity. Oxidation turned DnaJ into a very efficient chaperone holdase, which only transfers bound substrate proteins to the DnaK-system upon return to reducing conditions.

So far, no evidence was provided for DnaJ's oxidation *in vivo*. While AMS-trapping of DnaJ's zinc coordinating thiols was used to monitor DnaJ's oxidation process *in vitro*, AMS-trapping performed in *trxB gorA* deletion cells failed to show oxidized DnaJ *in vivo*. Deletion of *trxB* and *gorA* was reported to cause the accumulation of disulfide bonds in cytoplasmatic proteins in the absence of reductants in the culture media (163). Such intrinsic disulfide stress, however, might not lead to the oxidation of DnaJ. Similar to DnaJ's oxidation *in vitro*, reactive oxygen species like hydrogen peroxide might be necessary for its oxidation *in vivo*. To allow final conclusions about DnaJ's thiol status during oxidative stress *in vivo*, AMS-trapping experiments need to be repeated after exposure of wild type *E. coli* cells to H_2O_2-induced oxidative stress. Furthermore, oxidative stress can be induced by other oxidants such as hypochlorous acid or oxidative stress treatment can be intensified by increasing the cultivation temperature. Alternatively, *in vitro* oxidation studies of DnaJ using the disulfide stress inducing reagent diamide can be used to analyze the sensitivity of DnaJ's zinc centers to disulfide stress.

5.4 The redox regulated chaperone Hsp33 compensates for DnaK's inactivation

How would cells benefit from the inactivation of DnaK under oxidative stress conditions at elevated temperatures? We were able to show that the inactivation of DnaK is compensated by the activation of the redox-regulated chaperone Hsp33 (1). The very conditions of oxidative stress at elevated temperatures, which rapidly inactivate DnaK, lead to the specific activation of Hsp33. In contrast to DnaK, Hsp33 is an ATP-independent chaperone and a decrease of cellular ATP levels does not diminish its activity. Overlapping substrate specificities between the DnaK-system and Hsp33 allow complementary action, which prevents the loss of many DnaK substrate proteins (1). As efficient chaperone holdase, oxidized Hsp33 binds to a large variety of unfolding polypeptides under oxidative heat stress and keeps them in a refolding competent state (1). Return to non-stress conditions leads to the reduction of Hsp33 and the reactivation of DnaK. These are the exact conditions that prime Hsp33 to release bound substrate proteins. Hsp33 can now transfer the bound substrate proteins to the DnaK-system for refolding (Figure 41) (24).

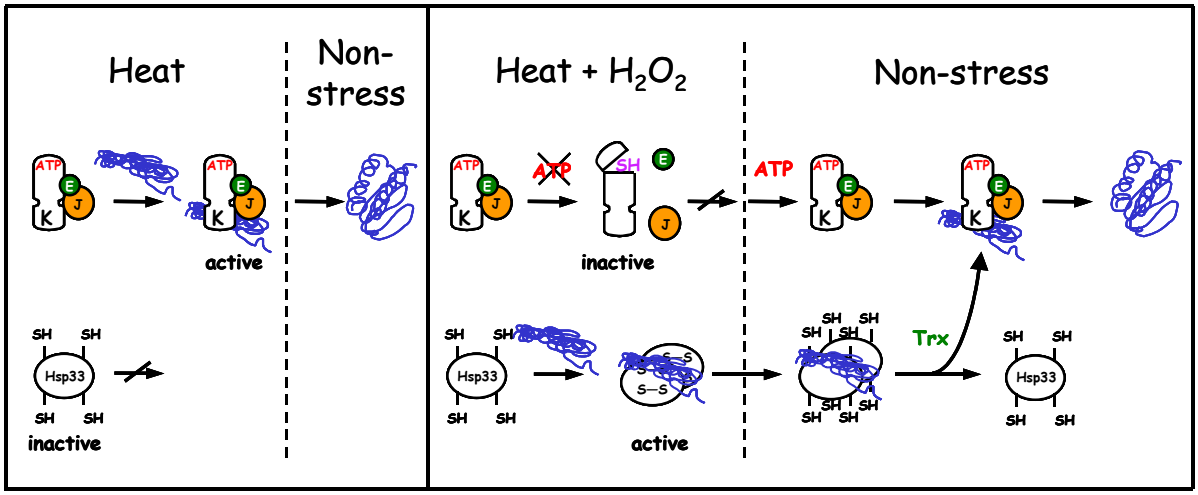

Figure 41 Model of the complementary action of DnaK and Hsp33 (1)

Under heat stress conditions, the DnaK-system binds to unfolding polypeptides to prevent their aggregation and to enable their refolding upon return to non-stress conditions. Hsp33 is inactive in the reducing environment of the cytosol. Heat stress in combination with oxidative stress results in low cellular ATP levels. ATP-deprived DnaK thermally unfolds and looses its activity. These conditions lead to Hsp33's activation by disulfide formation and dimerization. Now, active Hsp33 compensates for the lacking DnaK-system and binds to unfolded polypeptides. Upon return to non-stress conditions, cellular ATP levels rise and DnaK refolds. Reduced Hsp33 transfers bound substrate proteins to the DnaK-system for refolding.

Treatment of cells with H_2O_2 and HOCl causes a significant drop of the cellular ATP level (172) (this work). Both oxidants are produced as first line of defense by macrophages

and neutrophiles to attack invading pathogens (99). This underlines the physiological relevance of a cellular response to increasing H_2O_2 and HOCl concentrations.

Can the inactivation of DnaK during oxidative heat stress conditions be considered beneficial for cells? Substrate proteins like AcnB or GapA are known to undergo reversible oxidative modifications *in vivo* (183, 184). Premature refolding of such oxidized polypeptides by DnaK might prevent the removal of non-native modifications and hence block their successful reactivation. Cells would not only risk the irreversible loss of potential refolding competent proteins, but they would also waste ATP to drive a futile DnaK-refolding cycle. The ATP independent chaperone Hsp33, in contrast, keeps substrate proteins unfolded as long as oxidizing conditions last. Upon return to non-stress conditions, Hsp33 as well as substrate proteins get reduced. Only then is Hsp33 primed to transfer unfolded polypeptides to the DnaK-system for refolding.

5.5 Chaperone activity of $DnaK_{Cys15Ala}$

To analyze the role of Cys15 for DnaK's chaperone activity under oxidative heat stress, this cysteine residue was replaced by alanine to construct the $DnaK_{Cys15Ala}$ mutant protein. *In vivo*, this mutant protein appeared to be able to fully compensate for wild type DnaK. When expressed to wild type level in *dnaK* deletion cells, it conferred growth at heat shock temperatures, mobility on low-density media and phage λ replication. In contrast, *in vitro* investigations of the chaperone activity of purified $DnaK_{Cys15Ala}$ revealed functional differences when compared to wild type DnaK. Spectroscopic measurements, however, did not reveal any structural differences between the proteins.

In vitro, the $DnaK_{Cys15Ala}$ mutant protein was impaired in supporting the refolding of non-native luciferase in concert with DnaJ and GrpE as well as in preventing the aggregation of unfolded luciferase independent from its co-chaperones. In the absence of DnaJ and GrpE, substrate binding by DnaK-ATP only depends on its low intrinsic affinity for substrate proteins (185). The reduced activity of the $DnaK_{Cys15Ala}$ mutant protein in preventing protein aggregation suggests, therefore, that its intrinsic substrate binding affinity is reduced. As this intrinsic affinity is crucial for DnaK's foldase activity when acting in concert with DnaJ and GrpE (68, 88), reduced substrate binding by $DnaK_{Cys15Ala}$ might be the reason for the detected low yields of luciferase refolding. DnaK's substrate binding affinity was shown to depend on the hydrophobic pocket, the arch and the helical lid of DnaK's C-terminal substrate binding domain as well as the ATP-controlled mechanism of opening and closing the substrate-binding cavity (68). As Cys15 is located in DnaK's N-terminal domain, its substitution by

alanine should not directly affect DnaK's C-terminal substrate binding domain. Therefore, an ATP-mediated effect on substrate binding seems more likely.

Prevention of luciferase aggregation by the $DnaK_{Cys15Ala}$ mutant protein could be improved in the presence of DnaJ, indicating that $DnaK_{Cys15Ala}$ and DnaJ are able to cooperate. DnaJ appears to be also able to stimulate DnaK's ATPase activity and to trigger DnaK's conversion into its high affinity state. The extent of luciferase aggregation was, however, still higher in the presence of $DnaK_{Cys15Ala}$ mutant protein and DnaJ as compared to wild type DnaK and DnaJ, which might be due to fewer luciferase-$DnaK_{Cys15Ala}$-DnaJ interactions.

Interestingly, reduced ratios of the nucleotide exchange factor GrpE over DnaK significantly increased the $DnaK_{Cys15Ala}$-mediaded luciferase refolding. This supports the hypothesis that an ATP related defect of the $DnaK_{Cys15Ala}$ mutant protein caused the observed changes. Lower ratios of GrpE:DnaK should slow down the DnaK/DnaJ/GrpE refolding cycle, as nucleotide exchange was shown to be the rate-limiting step in the prokaryotic DnaK refolding machine (39). Steady state ATPase assays in the absence of substrate proteins revealed that the $DnaK_{Cys15Ala}$ mutant protein has a 4-fold increased intrinsic ATPase activity. This could be explained by an increased spontaneous nucleotide exchange in the $DnaK_{Cys15Ala}$ mutant protein. Alternatively, the purified $DnaK_{Cys15Ala}$ preparation might contain contaminations of proteins with ATPase activity. This appears unlikely, however, because the ATPase activity of the $DnaK_{Cys15Ala}$ mutant protein could be increased 2.5-fold in the presence of GrpE, similar to wild type DnaK. In contrast, stimulation of the ATPase activity of the $DnaK_{Cys15Ala}$ mutant protein by sub-stoichiometric concentrations of DnaJ did not increase the ATP hydrolysis rate as much as in case of wild type DnaK. As a consequence, ATP hydrolysis rates of wild type DnaK and the $DnaK_{Cys15Ala}$ mutant protein were identical in the presence of GrpE and low DnaJ concentrations while 2-fold excess of DnaJ over DnaK resulted in higher ATP hydrolysis rates in wild type DnaK than compared to the $DnaK_{Cys15Ala}$ mutant protein. DnaJ in such non-physiological high concentrations might mimic substrate proteins in addition to its stimulation of DnaK as co-chaperone. In case of the $DnaK_{Cys15Ala}$ mutant protein, which was shown to possess a lower affinity for substrates, this effect would be less pronounced and might explain the observed effects. Determination of the ATPase activity of both DnaK proteins in the presence of unfolded substrate proteins and DnaJ/GrpE would allow further conclusions. It appears, therefore, that the $DnaK_{Cys15Ala}$ mutant protein has an increased intrinsic ATPase activity, which could be the consequence of a faster spontaneous nucleotide exchange. This would shift $DnaK_{Cys15Ala}$ towards its ATP-bound

state, which was shown to possess a lower substrate binding affinity than the ADP-bound state (40, 186). Refolding of non-native luciferase in the presence of high GrpE concentrations might further decrease the already low substrate binding affinity of the $DnaK_{Cys15Ala}$ mutant protein by accelerating the nucleotide exchange further. This would lead to the observed low luciferase reactivation yields. Noteworthy, luciferase refolding assays in the absence of GrpE showed that the chaperone activity of the $DnaK_{Cys15Ala}$ mutant protein was not completely independent of GrpE (data not shown). Even though nucleotide exchange appears to be accelerated in the $DnaK_{Cys15Ala}$ mutant proteins, it seems to remain the rate-limiting step in the refolding cycle of this DnaK variant.

5.6 The two independent zinc centers in DnaJ

Several studies have been conducted to analyze the precise role of the individual zinc centers of class I Hsp40 homologues for their DnaK-dependent as well as their autonomous, DnaK-independent chaperone activity (76, 86, 168). Recent NMR structure data revealed, however, that most of these studies had been based on wrong conformational assumptions of the zinc binding domain (83). Other than predicted, zinc center I is not formed by cysteine motif 1 and 2, but by the two motifs that are most distant in the primary structure of DnaJ, motif 1 and 4. Cysteine motifs 2 and 3, which are adjacent in the amino acid sequence form zinc center II. Based on this new knowledge it was possible for us to specifically disrupt the individual zinc centers in DnaJ and to analyze the chaperone activity of the resulting mutant proteins *in vitro* and *in vivo*.

Using site-directed mutagenesis, all four cysteine residues of each zinc center were replaced by serines to construct DnaJΔZnI and DnaJΔZnII. Both DnaJ mutants appeared to fold into a stable conformation *in vivo*. Circular dichroism measurements of purified DnaJΔZnI and DnaJΔZnII furthermore demonstrated that their secondary and tertiary structure was very comparable to wild type DnaJ. This indicated that the two zinc centers fold independently of each other within the full length protein. This agreed with earlier observations that showed that the absence of zinc in full length DnaJ causes only minor conformational changes (187). Martinez-Yamout and co-workers demonstrated that absence of zinc leads to the unfolding of the β-hairpin structure in the isolated zinc-free cysteine-rich domain (83). When zinc is titrated back into the metal-free cysteine-rich domain, zinc center II forms first and independently of zinc center I (83). The latter appears to only coordinate zinc when the metal is present in molar ratios of Zn^{2+} to DnaJ above 1. From this result the authors concluded that the folding of DnaJ's zinc sites depends on the presence of zinc and

that one zinc site forms before the other (83). As shown in this work, both DnaJ zinc center mutants, DnaJΔZnI and DnaJΔZnII, were able to coordinate one zinc ion each, regardless of the disrupted second zinc center. The differences between our results and those obtained previously could be based on the DnaJ constructs used. While we performed our analysis with full-length protein, Martinez-Yamout and co-workers used the isolated zinc binding domain. The two zinc centers I and II, which fold into symmetric zinc binding modules, form the "wings" of a V-shaped structure (Figure 15). Two antiparallel β-strands form the outside of each zinc center. In zinc center II, the β-strands are connected by a β-hairpin loop, while in zinc center I the N-and C-terminal strands need to approach each other to form the β-strands. It is, therefore, conceivable that in the isolated cysteine-rich domain, the absence of zinc coordination in zinc center I causes the separation of the N and C termini and, therefore, the spatial separation of the two cysteine motifs of zinc center I. This would make re-coordination of the metal in zinc center I significantly more difficult than in zinc center II, where the four cysteines are relatively close in the primary sequence (188).

5.7 Zinc center I: High affinity binding site for unfolded substrate proteins

Chaperone activity studies of the DnaJΔZnI and DnaJΔZnII mutant protein revealed that zinc center I is important for the high affinity binding of DnaJ to unfolded substrate proteins. This DnaK-independent chaperone holdase activity enables DnaJ to prevent the irreversible aggregation of denatured polypeptides *in vitro* (75, 151). Martinez-Yamout and co-workers suggested that the central part of the "V-apex", which is located between both zinc binding sites of DnaJ, harbors a groove of conserved and hydrophobic residues, which might be a potential substrate-binding site (Figure 15) (83). Disruption of zinc center I in DnaJ and concomitant small local rearrangements might affect this potential substrate binding site and impair DnaJ's ability to interact with substrate proteins. The recently solved crystal structure of the yeast Hsp40 homologue Ydj1p in complex with bound peptide shows the location of the zinc binding domain in relation to the peptide-binding site (Figure 2C) (84). Other than predicted for DnaJ, the peptide binding site in Ydj1p is located outside the zinc binding domain. However, zinc center I in Ydj1p connects directly to a β-strand that is involved in peptide binding (84). It is, therefore, conceivable that mutation of zinc center I disrupts the substrate binding site of DnaJ, assuming that DnaJ possesses a similar substrate binding site as the one shown for Ydj1p. This appears likely because both Hsp40 homologues

possess the same domain organization and the structure of Ydj1p's zinc binding domain is very similar to the structure of the isolated zinc binding region of DnaJ.

Until now, DnaJ's autonomous DnaK-independent chaperone function was thought to be also essential for its DnaK-dependent co-chaperone activity. It was assumed that the high substrate affinity of DnaJ is needed for the presentation of polypeptides to DnaK. Results presented in this work, however, suggest that DnaJ's autonomous chaperone activity is largely dispensable for its interplay with DnaK. The DnaJ mutant protein lacking zinc center I is 10-fold less active than wild type DnaJ in preventing the aggregation of unfolded substrate proteins. Nevertheless, its cooperation with DnaK in preventing substrate aggregation or supporting the refolding of non-native proteins is almost identical to wild type DnaJ. This suggests that a rather transient interaction of DnaJ and substrate is sufficient for the successful cooperation with the DnaK-system. This furthermore explains, why class II Hsp40s like the yeast homologue Sis1p are fully functional as co-chaperone of DnaK, even though they lack the autonomous DnaK-independent chaperone activity (87).

DnaJ must contain an additional low-affinity substrate-binding site, which remains intact in DnaJ mutants lacking zinc center I, but appears to be affected by the disruption of zinc center II. In former studies it was shown that lack of the entire cysteine-rich domain did not impair DnaJ's affinity for substrates like σ^{32} (86). This suggests that DnaJ's low affinity substrate binding site might be located in the C-terminal domain of DnaJ, as the zinc binding domain and the C-terminal domain were both suggested to be involved in substrate binding (76, 87). In agreement with this it was shown that the first 68 amino acids of the C-terminal domain of class I homologues are crucial for the successful cooperation with DnaK (189). Furthermore, deletion of the conserved C-terminal motif G_{242}DLYV_{246} had not influence on DnaJ's autonomous chaperone activity but significantly impaired its DnaK-dependent co-chaperone function (189).

5.8 Zinc center II: A new interaction site with DnaK

Results of previous study proposed an important role of zinc center II for DnaJ's activity as co-chaperone of the DnaK-system (76). The authors explained their observed effects with the significantly reduced ability of these mutant proteins to bind to unfolded substrate proteins and to prevent their aggregation (76). Analysis of the DnaK-dependent and DnaK-independent chaperone activity of DnaJ lacking zinc center II revealed, however, that the DnaJΔZnII mutant protein binds to unfolding polypeptides with wild type activity but is unable to support the DnaK/DnaJ/GrpE-mediated refolding.

Absence of zinc center II appears to inhibit the DnaJ-mediated conversion of DnaK into its high substrate binding state. This cannot be caused by impaired DnaJ-substrate interactions, as the autonomous DnaK-independent chaperone activity of DnaJΔZnII is hardly affected. Furthermore, an increased affinity of DnaJΔZnII for unfolded polypeptides can also be excluded. In this case, DnaJ lacking zinc center II would compete with DnaK for substrate binding, especially when applied in excess. Substrate transfer to the foldase DnaK would be inhibited, resulting in even lower refolding yields. The reactivation of substrate proteins by the DnaK-system in the presence of increasing DnaJΔZnII concentrations, however, improved refolding yields.

Also the stimulation of DnaK's ATPase activity by wild type DnaJ and DnaJΔZnII was shown to be identical, leading to the maximal acceleration of hydrolysis in the presence of unfolded substrate. Only simultaneous binding of DnaK and DnaJ to the same polypeptide chain was shown to optimally stimulate ATP hydrolysis by DnaK (88). Interaction of the DnaJΔZnII mutant protein with DnaK and substrate must be therefore comparable to wild type DnaJ. This showed clearly that maximal stimulation of DnaK's ATPase activity alone is not sufficient to trigger the conformational changes in DnaK as was previously assumed (190). This would lead to the "locking in" of substrate proteins, as suggested in previous studies. Instead, an additional contact between DnaJ and DnaK appears to be necessary to convert the foldase DnaK into its high affinity substrate binding state. Zinc center II of DnaJ or structural areas close to zinc center II seem to provide such additional interaction site. In its absence, DnaJ seems unable to catalytically activate the refolding function of the DnaK-cycle. Findings of Banecki and co-workers support these findings (86). In the absence of the entire zinc binding domain, DnaJ mutants are able to bind to non-native polypeptides like wild type DnaJ and to stimulate DnaK's ATPase activity. Nevertheless, deletion of the zinc binding region rendered DnaJ incapable of stimulating DnaK's refolding function. This was very similar to our observations with the DnaJΔZnII mutant. Recently, Li and Sha constructed Ydj1p mutant proteins that lacked either zinc center II or both zinc centers. In accordance to our studies, deletion of zinc center II did not impair Ydj1p's substrate binding affinity in the refolding of substrate proteins but rendered its cooperation with Hsp70 (191).

It has long been known that DnaJ's N-terminal J-domain interacts with the ATPase domain of DnaK. Results presented in this work suggest that zinc center II comprises a second interaction site between DnaJ and its partner DnaK. This requires adjustments of the current DnaK-cycle model (Figure 42). Simultaneous binding of DnaK and DnaJ to the same

polypeptide chain brings the chaperone partners in close proximity to each other. This enhances the chance for DnaJ-DnaK interactions. Only when DnaJ gets in contact with DnaK via both interaction sites, the J-domain and zinc center II, the DnaK/DnaJ/GrpE refolding machine becomes catalytically active. Such additional interactions between DnaJ and DnaK have been proposed earlier in DnaK suppressor studies, which showed that DnaJ binds to at least two sites in DnaK (170). The authors suggested at that time that this second site of DnaJ might interact with the C-terminal substrate-binding domain of DnaK (170). It appears that we have succeeded in identifying that this required additional interaction site in class I DnaJ homologues is mediated by the highly conserved zinc center II (188).

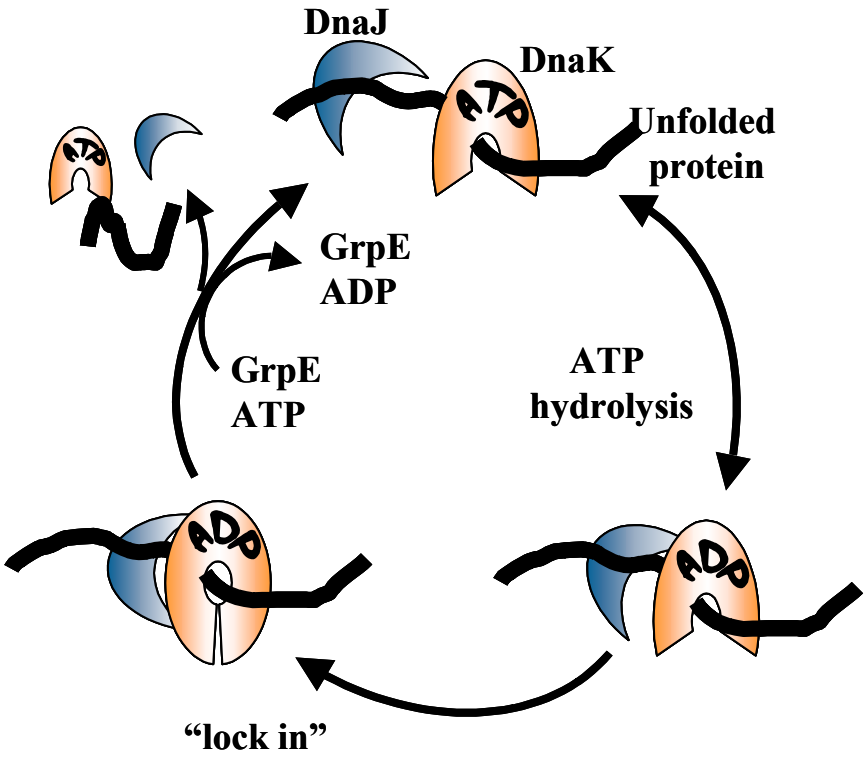

Figure 42 Model of the refolding cycle of DnaK/DnaJ/GrpE (188)

DnaK-ATP shows low affinity for unfolded polypeptides. Substrate binding is transient and characterized by high on/off rates (68). Simultaneous binding of DnaJ to a distinct site of the unfolded polypeptide chain promotes the interaction of DnaJ and DnaK (68, 88). Interaction between the J-domain of DnaJ and the N-terminal ATPase domain of DnaK stimulates ATP hydrolysis. This leads to conformational rearrangements in DnaK. For DnaK's conversion into its high substrate affinity state ("lock-in"), a second interaction with DnaJ, which is mediated by zinc center II, appears to be required. Only then is the DnaK/DnaJ/GrpE foldase machine catalytically active. The nucleotide exchange factor GrpE then exchanges ADP for ATP and unlocks DnaK.

6 Abbreviations

ε	molar extinction coefficient
λ	wave length
2D	two dimensional
A	ampere(s)
aa	amino acic
ADP	adenosine 5’-diphosphate
Amp	ampicillin
AMS	4-acetamido-4’-maleimidylstilbene-2,2’-disulfonic acid
appr.	approximately
ATP	adenosine 5’-triphosphate
BSA	bovine serum albumin
BSE	bovine spongiform encephalopathy (mad cow disease)
Ci	Curie
CoA-SH	coenzyme A
CS	citrate synthase
CV	column volume
Cys	cysteine
Da, kDa	Dalton, kilo Dalton
ddH_2O	double distilled water
diamide	diazenedicarboxylic acid bis(N,N’- dimethylamide)
DNA	deoxyribonucleic acid
DTNB	5,5'-dithio bis(2-nitrobenzoic acid) (Ellman’s reagent)
DTT	1,4 - dithiothreitol
E. coli	*Escherichia coli*
EDTA	ethylenediaminetetraacetic acid
FPLC	fast protein liquid chromatography
g	gravitational force
GSH	glutathione (reduced form)
GSSG	glutathione disulfide (oxidized form of glutathione)
Gua-HCl	guanidinium hydrochloride
h	hour(s)
HCl	hydrochloric acid
HEPES	[4-(2-Hydroxyethyl)-piperazino]-ethanesulfonic acid
HRP	horseradish peroxidase
i.e.	“id est”, that is
IAM	iodoacetamide
IPTG	isopropylthiogalactoside
K_D	dissociation constant

KOH	potassium hydroxide
LB	Luria Bertani
Luci	luciferase
M, mM, µM	molar, millimolar, micromolar
mA	milli ampere
MgATP	magnesium ATP
min	minute(s)
mRNA	messenger RNA
MW	molecular weight
$NADP^+$	β-nicotinamide adenine dinucleotide phosphate, oxidized form
NADPH	β-nicotinamide adenine dinucleotide phosphate, reduced form
NaOH	sodium hydroxide
o.n.	overnight
OAA	oxaloacetic acid
OD_{600}	optical density at 600 nm
ORF	open reading frame
PAGE	polyacrylamide gel electrophoresis
PAR	4-(2-pyridylazo) resorcinol
PBS	phosphate buffered saline
pI	isoelectric point
PMPS	p-hydroxymercuriphenylsulfonic acid
RNA	ribonucleic acid
RNase	ribonuclease
ROS	reactive oxygen species
rpm	rotations per minute
SDS	sodium dodecyl sulfate
TBS	tris buffered saline
TCA	tricarboxylic acid
Tris	tris(hydroxymethyl)-aminomethane
Trp	tryptophan
U	units
UV	ultraviolet
V	volt(s)
v/v	volume per volume
w/v	weight per volume
wt	wildtype

7 Literature

1. Winter, J., Linke, K., Jatzek, A., and Jakob, U., Severe stress causes inactivation of DnaK and Activation of the redox-regulated chaperone Hsp33, *Mol Cell, in press* (2005).
2. Anfinsen, C. B., Principles that govern the folding of protein chains, *Science, 181*, 223 (1973).
3. Eaton, W. A., Munoz, V., Hagen, S. J., Jas, G. S., Lapidus, L. J., Henry, E. R., and Hofrichter, J., Fast kinetics and mechanisms in protein folding, *Annu Rev Biophys Biomol Struct, 29*, 327 (2000).
4. Snow, C. D., Nguyen, H., Pande, V. S., and Gruebele, M., Absolute comparison of simulated and experimental protein-folding dynamics, *Nature, 420*, 102 (2002).
5. Dinner, A. R., Sali, A., Smith, L. J., Dobson, C. M., and Karplus, M., Understanding protein folding via free-energy surfaces from theory and experiment, *Trends Biochem Sci, 25*, 331 (2000).
6. Khan, F., Chuang, J. I., Gianni, S., and Fersht, A. R., The kinetic pathway of folding of barnase, *J Mol Biol, 333*, 169 (2003).
7. Vendruscolo, M., Paci, E., Karplus, M., and Dobson, C. M., Structures and relative free energies of partially folded states of proteins, *Proc Natl Acad Sci U S A, 100*, 14817 (2003).
8. Dill, K. A., and Chan, H. S., From Levinthal to pathways to funnels, *Nat Struct Biol, 4*, 10 (1997).
9. Wolynes, P. G., Onuchic, J. N., and Thirumalai, D., Navigating the folding routes, *Science, 267*, 1619 (1995).
10. Fersht, A. R., Transition-state structure as a unifying basis in protein-folding mechanisms: contact order, chain topology, stability, and the extended nucleus mechanism, *Proc Natl Acad Sci U S A, 97*, 1525 (2000).
11. Bukau, B., and Horwich, A. L., The Hsp70 and Hsp60 chaperone machines, *Cell, 92*, 351 (1998).
12. Hartl, F. U., and Hayer-Hartl, M., Molecular chaperones in the cytosol: from nascent chain to folded protein, *Science, 295*, 1852 (2002).
13. Ellis, R. J., Macromolecular crowding: obvious but underappreciated, *Trends Biochem Sci, 26*, 597 (2001).
14. Frydman, J., Folding of newly translated proteins in vivo: the role of molecular chaperones, *Annu Rev Biochem, 70*, 603 (2001).
15. Dobson, C. M., The structural basis of protein folding and its links with human disease, *Philos Trans R Soc Lond B Biol Sci, 356*, 133 (2001).
16. Horwich, A., Protein aggregation in disease: a role for folding intermediates forming specific multimeric interactions, *J Clin Invest, 110*, 1221 (2002).
17. Tan, S. Y., and Pepys, M. B., Amyloidosis, *Histopathology, 25*, 403 (1994).
18. Kelly, J. W., The alternative conformations of amyloidogenic proteins and their multi-step assembly pathways, *Curr Opin Struct Biol, 8*, 101 (1998).
19. Jaenicke, R., Protein folding: local structures, domains, subunits, and assemblies, *Biochemistry, 30*, 3147 (1991).
20. Creighton, T. E., Protein folding, *Biochem J, 270*, 1 (1990).
21. Agashe, V. R., Guha, S., Chang, H. C., Genevaux, P., Hayer-Hartl, M., Stemp, M., Georgopoulos, C., Hartl, F. U., and Barral, J. M., Function of trigger factor and DnaK

in multidomain protein folding: increase in yield at the expense of folding speed, *Cell, 117*, 199 (2004).
22. Buchner, J., and Kiefhaber, T., Folding pathway enigma, *Nature, 343*, 601 (1990).
23. Zylicz, M., and Wawrzynow, A., Insights into the function of Hsp70 chaperones, *IUBMB Life, 51*, 283 (2001).
24. Hoffmann, J. H., Linke, K., Graf, P. C., Lilie, H., and Jakob, U., Identification of a redox-regulated chaperone network, *Embo J, 23*, 160 (2004).
25. Gottesman, S., Wickner, S., and Maurizi, M. R., Protein quality control: triage by chaperones and proteases, *Genes Dev, 11*, 815 (1997).
26. Winter, J. a. Jakob., U., Beyond transcription - New mechanisms for the regulation of molecule chaperones, *Crit Rev Biochem Mol Biol, 39*, 297 (2004).
27. Haslbeck, M., and Buchner, J., Chaperone function of sHsps, *Prog Mol Subcell Biol, 28*, 37 (2002).
28. Narberhaus, F., Alpha-crystallin-type heat shock proteins: socializing minichaperones in the context of a multichaperone network, *Microbiol Mol Biol Rev, 66*, 64 (2002).
29. Ehrnsperger, M., Graber, S., Gaestel, M., and Buchner, J., Binding of non-native protein to Hsp25 during heat shock creates a reservoir of folding intermediates for reactivation, *Embo J, 16*, 221 (1997).
30. Mogk, A., Deuerling, E., Vorderwulbecke, S., Vierling, E., and Bukau, B., Small heat shock proteins, ClpB and the DnaK system form a functional triade in reversing protein aggregation, *Mol Microbiol, 50*, 585 (2003).
31. Jakob, U., Muse, W., Eser, M., and Bardwell, J. C., Chaperone activity with a redox switch, *Cell, 96*, 341 (1999).
32. Linke, K., and Jakob, U., Not every disulfide lasts forever: disulfide bond formation as a redox switch, *Antioxid Redox Signal, 5*, 425 (2003).
33. Braig, K., Otwinowski, Z., Hegde, R., Boisvert, D. C., Joachimiak, A., Horwich, A. L., and Sigler, P. B., The crystal structure of the bacterial chaperonin GroEL at 2.8 A, *Nature, 371*, 578 (1994).
34. Hunt, J. F., Weaver, A. J., Landry, S. J., Gierasch, L., and Deisenhofer, J., The crystal structure of the GroES co-chaperonin at 2.8 A resolution, *Nature, 379*, 37 (1996).
35. Xu, Z., Horwich, A. L., and Sigler, P. B., The crystal structure of the asymmetric GroEL-GroES-(ADP)7 chaperonin complex, *Nature, 388*, 741 (1997).
36. Rye, H. S., Burston, S. G., Fenton, W. A., Beechem, J. M., Xu, Z., Sigler, P. B., and Horwich, A. L., Distinct actions of cis and trans ATP within the double ring of the chaperonin GroEL, *Nature, 388*, 792 (1997).
37. Mayer, M. P., Brehmer, D., Gassler, C. S., and Bukau, B., Hsp70 chaperone machines, *Adv Protein Chem, 59*, 1 (2001).
38. Szabo, A., Langer, T., Schroder, H., Flanagan, J., Bukau, B., and Hartl, F. U., The ATP hydrolysis-dependent reaction cycle of the Escherichia coli Hsp70 system DnaK, DnaJ, and GrpE, *Proc Natl Acad Sci U S A, 91*, 10345 (1994).
39. McCarty, J. S., Buchberger, A., Reinstein, J., and Bukau, B., The role of ATP in the functional cycle of the DnaK chaperone system, *J Mol Biol, 249*, 126 (1995).
40. Schmid, D., Baici, A., Gehring, H., and Christen, P., Kinetics of molecular chaperone action, *Science, 263*, 971 (1994).
41. Theyssen, H., Schuster, H. P., Packschies, L., Bukau, B., and Reinstein, J., The second step of ATP binding to DnaK induces peptide release, *J Mol Biol, 263*, 657 (1996).
42. Packschies, L., Theyssen, H., Buchberger, A., Bukau, B., Goody, R. S., and Reinstein, J., GrpE accelerates nucleotide exchange of the molecular chaperone DnaK with an associative displacement mechanism, *Biochemistry, 36*, 3417 (1997).

43. Wegele, H., Muller, L., and Buchner, J., Hsp70 and Hsp90--a relay team for protein folding, *Rev Physiol Biochem Pharmacol, 151*, 1 (2004).
44. Chadli, A., Bouhouche, I., Sullivan, W., Stensgard, B., McMahon, N., Catelli, M. G., and Toft, D. O., Dimerization and N-terminal domain proximity underlie the function of the molecular chaperone heat shock protein 90, *Proc Natl Acad Sci U S A, 97*, 12524 (2000).
45. Maruya, M., Sameshima, M., Nemoto, T., and Yahara, I., Monomer arrangement in HSP90 dimer as determined by decoration with N and C-terminal region specific antibodies, *J Mol Biol, 285*, 903 (1999).
46. Prodromou, C., Roe, S. M., O'Brien, R., Ladbury, J. E., Piper, P. W., and Pearl, L. H., Identification and structural characterization of the ATP/ADP-binding site in the Hsp90 molecular chaperone, *Cell, 90*, 65 (1997).
47. Scheibel, T., Weikl, T., and Buchner, J., Two chaperone sites in Hsp90 differing in substrate specificity and ATP dependence, *Proc Natl Acad Sci U S A, 95*, 1495 (1998).
48. Maurizi, M. R., and Xia, D., Protein binding and disruption by Clp/Hsp100 chaperones, *Structure (Camb), 12*, 175 (2004).
49. Goloubinoff, P., Mogk, A., Zvi, A. P., Tomoyasu, T., and Bukau, B., Sequential mechanism of solubilization and refolding of stable protein aggregates by a bichaperone network, *Proc Natl Acad Sci U S A, 96*, 13732 (1999).
50. Ben-Zvi, A. P., and Goloubinoff, P., Review: mechanisms of disaggregation and refolding of stable protein aggregates by molecular chaperones, *J Struct Biol, 135*, 84 (2001).
51. Gething, M. J., and Sambrook, J., Protein folding in the cell, *Nature, 355*, 33 (1992).
52. Hartl, F. U., Molecular chaperones in cellular protein folding, *Nature, 381*, 571 (1996).
53. Morimoto, R. I., Kroeger, P. E., and Cotto, J. J., The transcriptional regulation of heat shock genes: a plethora of heat shock factors and regulatory conditions, *Exs, 77*, 139 (1996).
54. Tomoyasu, T., Ogura, T., Tatsuta, T., and Bukau, B., Levels of DnaK and DnaJ provide tight control of heat shock gene expression and protein repair in Escherichia coli, *Mol Microbiol, 30*, 567 (1998).
55. Bukau, B., Regulation of the Escherichia coli heat-shock response, *Mol Microbiol, 9*, 671 (1993).
56. Yura, T., Nagai, H., and Mori, H., Regulation of the heat-shock response in bacteria, *Annu Rev Microbiol, 47*, 321 (1993).
57. Straus, D., Walter, W., and Gross, C. A., DnaK, DnaJ, and GrpE heat shock proteins negatively regulate heat shock gene expression by controlling the synthesis and stability of sigma 32, *Genes Dev, 4*, 2202 (1990).
58. Gamer, J., Bujard, H., and Bukau, B., Physical interaction between heat shock proteins DnaK, DnaJ, and GrpE and the bacterial heat shock transcription factor sigma 32, *Cell, 69*, 833 (1992).
59. Tatsuta, T., Tomoyasu, T., Bukau, B., Kitagawa, M., Mori, H., Karata, K., and Ogura, T., Heat shock regulation in the ftsH null mutant of Escherichia coli: dissection of stability and activity control mechanisms of sigma32 in vivo, *Mol Microbiol, 30*, 583 (1998).
60. Craig, E. A., and Gross, C. A., Is hsp70 the cellular thermometer?, *Trends Biochem Sci, 16*, 135 (1991).
61. Bukau, B., and Walker, G. C., Cellular defects caused by deletion of the Escherichia coli dnaK gene indicate roles for heat shock protein in normal metabolism, *J.Bacteriol., 171*, 2337 (1989).

62. Sell, S. M., Eisen, C., Ang, D., Zylicz, M., and Georgopoulos, C., Isolation and characterization of dnaJ null mutants of Escherichia coli, *J Bacteriol, 172*, 4827 (1990).
63. Paek, K. H., and Walker, G. C., Escherichia coli dnaK null mutants are inviable at high temperature, *J Bacteriol, 169*, 283 (1987).
64. Zylicz, M., Ang, D., Liberek, K., and Georgopoulos, C., Initiation of lambda DNA replication with purified host- and bacteriophage-encoded proteins: the role of the dnaK, dnaJ and grpE heat shock proteins, *Embo J, 8*, 1601 (1989).
65. Zylicz, M., LeBowitz, J. H., McMacken, R., and Georgopoulos, C., The dnaK protein of Escherichia coli possesses an ATPase and autophosphorylating activity and is essential in an in vitro DNA replication system, *Proc Natl Acad Sci U S A, 80*, 6431 (1983).
66. Laufen, T., Mayer, M. P., Beisel, C., Klostermeier, D., Mogk, A., Reinstein, J., and Bukau, B., Mechanism of regulation of hsp70 chaperones by DnaJ cochaperones, *Proc Natl Acad Sci U S A, 96*, 5452 (1999).
67. Liberek, K., Marszalek, J., Ang, D., Georgopoulos, C., and Zylicz, M., Escherichia coli DnaJ and GrpE heat shock proteins jointly stimulate ATPase activity of DnaK, *Proc Natl Acad Sci U S A, 88*, 2874 (1991).
68. Mayer, M. P., Schroder, H., Rudiger, S., Paal, K., Laufen, T., and Bukau, B., Multistep mechanism of substrate binding determines chaperone activity of Hsp70, *Nat Struct Biol, 7*, 586 (2000).
69. Flaherty, K. M., DeLuca-Flaherty, C., and McKay, D. B., Three-dimensional structure of the ATPase fragment of a 70K heat-shock cognate protein, *Nature, 346*, 623 (1990).
70. Zhu, X., Zhao, X., Burkholder, W. F., Gragerov, A., Ogata, C. M., Gottesman, M. E., and Hendrickson, W. A., Structural analysis of substrate binding by the molecular chaperone DnaK, *Science, 272*, 1606 (1996).
71. Russell, R., Jordan, R., and McMacken, R., Kinetic characterization of the ATPase cycle of the DnaK molecular chaperone, *Biochemistry, 37*, 596 (1998).
72. Ohki, M., Uchida, H., Tamura, F., Ohki, R., and Nishimura, S., The Escherichia coli dnaJ mutation affects biosynthesis of specific proteins, including those of the lac operon, *J Bacteriol, 169*, 1917 (1987).
73. Karzai, A. W., and McMacken, R., A bipartite signaling mechanism involved in DnaJ-mediated activation of the Escherichia coli DnaK protein, *J Biol Chem, 271*, 11236 (1996).
74. Pierpaoli, E. V., Sandmeier, E., Schonfeld, H. J., and Christen, P., Control of the DnaK chaperone cycle by substoichiometric concentrations of the co-chaperones DnaJ and GrpE, *J Biol Chem, 273*, 6643 (1998).
75. Langer, T., Lu, C., Echols, H., Flanagan, J., Hayer, M. K., and Hartl, F. U., Successive action of DnaK, DnaJ and GroEL along the pathway of chaperone-mediated protein folding, *Nature, 356*, 683 (1992).
76. Szabo, A., Korszun, R., Hartl, F. U., and Flanagan, J., A zinc finger-like domain of the molecular chaperone DnaJ is involved in binding to denatured protein substrates, *Embo J, 15*, 408 (1996).
77. Wall, D., Zylicz, M., and Georgopoulos, C., The conserved G/F motif of the DnaJ chaperone is necessary for the activation of the substrate binding properties of the DnaK chaperone, *J Biol Chem, 270*, 2139 (1995).
78. Hennessy, F., Cheetham, M. E., Dirr, H. W., and Blatch, G. L., Analysis of the levels of conservation of the J domain among the various types of DnaJ-like proteins, *Cell Stress Chaperones, 5*, 347 (2000).

79. Greene, M. K., Maskos, K., and Landry, S. J., Role of the J-domain in the cooperation of Hsp40 with Hsp70, *Proc Natl Acad Sci U S A, 95*, 6108 (1998).
80. Genevaux, P., Schwager, F., Georgopoulos, C., and Kelley, W. L., Scanning Mutagenesis Identifies Amino Acid Residues Essential for the in Vivo Activity of the Escherichia coli DnaJ (Hsp40) J-Domain, *Genetics, 162*, 1045 (2002).
81. Qian, Y. Q., Patel, D., Hartl, F. U., and McColl, D. J., Nuclear magnetic resonance solution structure of the human Hsp40 (HDJ- 1) J-domain, *J Mol Biol, 260*, 224 (1996).
82. Wall, D., Zylicz, M., and Georgopoulos, C., The NH2-terminal 108 amino acids of the Escherichia coli DnaJ protein stimulate the ATPase activity of DnaK and are sufficient for lambda replication, *J Biol Chem, 269*, 5446 (1994).
83. Martinez-Yamout, M., Legge, G. B., Zhang, O., Wright, P. E., and Dyson, H. J., Solution structure of the cysteine-rich domain of the Escherichia coli chaperone protein DnaJ, *J Mol Biol, 300*, 805 (2000).
84. Li, J., Qian, X., and Sha, B., The crystal structure of the yeast Hsp40 Ydj1 complexed with its peptide substrate, *Structure (Camb), 11*, 1475 (2003).
85. Bardwell, J. C., Tilly, K., Craig, E., King, J., Zylicz, M., and Georgopoulos, C., The nucleotide sequence of the Escherichia coli K12 dnaJ+ gene. A gene that encodes a heat shock protein, *J Biol Chem, 261*, 1782 (1986).
86. Banecki, B., Liberek, K., Wall, D., Wawrzynow, A., Georgopoulos, C., Bertoli, E., Tanfani, F., and Zylicz, M., Structure-function analysis of the zinc finger region of the DnaJ molecular chaperone, *J Biol Chem, 271*, 14840 (1996).
87. Lu, Z., and Cyr, D. M., Protein folding activity of Hsp70 is modified differentially by the hsp40 co-chaperones Sis1 and Ydj1, *J Biol Chem, 273*, 27824 (1998).
88. Han, W., and Christen, P., Mechanism of the targeting action of DnaJ in the DnaK molecular chaperone system, *J Biol Chem* (2003).
89. Gamer, J., Multhaup, G., Tomoyasu, T., McCarty, J. S., Rudiger, S., Schonfeld, H. J., Schirra, C., Bujard, H., and Bukau, B., A cycle of binding and release of the DnaK, DnaJ and GrpE chaperones regulates activity of the Escherichia coli heat shock transcription factor sigma32, *Embo J, 15*, 607 (1996).
90. Rudiger, S., Schneider-Mergener, J., and Bukau, B., Its substrate specificity characterizes the DnaJ co-chaperone as a scanning factor for the DnaK chaperone, *Embo J, 20*, 1042 (2001).
91. Han, W., and Christen, P., Interdomain communication in the molecular chaperone DnaK, *Biochem J, 369*, 627 (2003).
92. Han, W., and Christen, P., Mutations in the interdomain linker region of DnaK abolish the chaperone action of the DnaK/DnaJ/GrpE system, *FEBS Lett, 497*, 55 (2001).
93. Minami, Y., Hohfeld, J., Ohtsuka, K., and Hartl, F. U., Regulation of the heat-shock protein 70 reaction cycle by the mammalian DnaJ homolog, Hsp40, *J Biol Chem, 271*, 19617 (1996).
94. Ziegelhoffer, T., Lopez-Buesa, P., and Craig, E. A., The dissociation of ATP from hsp70 of Saccharomyces cerevisiae is stimulated by both Ydj1p and peptide substrates, *J Biol Chem, 270*, 10412 (1995).
95. Dekker, P. J., and Pfanner, N., Role of mitochondrial GrpE and phosphate in the ATPase cycle of matrix Hsp70, *J Mol Biol, 270*, 321 (1997).
96. Bimston, D., Song, J., Winchester, D., Takayama, S., Reed, J. C., and Morimoto, R. I., BAG-1, a negative regulator of Hsp70 chaperone activity, uncouples nucleotide hydrolysis from substrate release, *Embo J, 17*, 6871 (1998).

97. Deuerling, E., Schulze-Specking, A., Tomoyasu, T., Mogk, A., and Bukau, B., Trigger factor and DnaK cooperate in folding of newly synthesized proteins, *Nature, 400*, 693 (1999).
98. Teter, S. A., Houry, W. A., Ang, D., Tradler, T., Rockabrand, D., Fischer, G., Blum, P., Georgopoulos, C., and Hartl, F. U., Polypeptide flux through bacterial Hsp70: DnaK cooperates with trigger factor in chaperoning nascent chains, *Cell, 97*, 755 (1999).
99. Storz, G., and Imlay, J. A., Oxidative stress, *Curr Opin Microbiol, 2*, 188 (1999).
100. Sutton, H. C., and Winterbourn, C. C., On the participation of higher oxidation states of iron and copper in Fenton reactions, *Free Radic Biol Med, 6*, 53 (1989).
101. Berlett, B. S., and Stadtman, E. R., Protein oxidation in aging, disease, and oxidative stress, *J Biol Chem, 272*, 20313 (1997).
102. Droge, W., Free radicals in the physiological control of cell function, *Physiol Rev, 82*, 47 (2002).
103. Claiborne, A., Yeh, J. I., Mallett, T. C., Luba, J., Crane, E. J., 3rd, Charrier, V., and Parsonage, D., Protein-sulfenic acids: diverse roles for an unlikely player in enzyme catalysis and redox regulation, *Biochemistry, 38*, 15407 (1999).
104. Aslund, F., and Beckwith, J., Bridge over troubled waters: sensing stress by disulfide bond formation, *Cell, 96*, 751 (1999).
105. Ritz, D., and Beckwith, J., Roles of thiol-redox pathways in bacteria, *Annu Rev Microbiol, 55*, 21 (2001).
106. Holmgren, A., Glutaredoxin from Escherichia coli and calf thymus, *Methods Enzymol, 113*, 525 (1985).
107. Aslund, F., Zheng, M., Beckwith, J., and Storz, G., Regulation of the OxyR transcription factor by hydrogen peroxide and the cellular thiol-disulfide status, *Proc Natl Acad Sci U S A, 96*, 6161 (1999).
108. Gilbert, H. F., Molecular and cellular aspects of thiol-disulfide exchange, *Adv Enzymol Relat Areas Mol Biol, 63*, 69 (1990).
109. Bushweller, J. H., Aslund, F., Wuthrich, K., and Holmgren, A., Structural and functional characterization of the mutant Escherichia coli glutaredoxin (C14----S) and its mixed disulfide with glutathione, *Biochemistry, 31*, 9288 (1992).
110. Sies, H., Role of reactive oxygen species in biological processes, *Klin Wochenschr, 69*, 965 (1991).
111. Miller, R., and Britigan, B., Role of oxidants in microbial pathophysiology, *Clin. Microbiol. Rev., 10*, 1 (1997).
112. Hampton, M. B., Kettle, A. J., and Winterbourn, C. C., Inside the neutrophil phagosome: oxidants, myeloperoxidase, and bacterial killing, *Blood, 92*, 3007 (1998).
113. Schoonbroodt, S., Legrand-Poels, S., Best-Belpomme, M., and Piette, J., Activation of the NF-kappaB transcription factor in a T-lymphocytic cell line by hypochlorous acid, *Biochem J, 321*, 777 (1997).
114. Kim, S. O., Merchant, K., Nudelman, R., Beyer, W. F. J., Keng, T., DeAngelo, J., Hausladen, A., and Stamler, J. S., OxyR: a molecular code for redox-related signaling, *Cell, 109*, 383 (2002).
115. Pomposiello, P. J., and Demple, B., Redox-operated genetic switches: the SoxR and OxyR transcription factors, *Trends Biotechnol, 19*, 109 (2001).
116. Zheng, M., Wang, X., Templeton, L. J., Smulski, D. R., LaRossa, R. A., and Storz, G., DNA microarray-mediated transcriptional profiling of the Escherichia coli response to hydrogen peroxide, *J Bacteriol, 183*, 4562 (2001).
117. Martindale, J. L., and Holbrook, N. J., Cellular response to oxidative stress: signaling for suicide and survival, *J Cell Physiol, 192*, 1 (2002).

118. Gasch, A. P., Spellman, P. T., Kao, C. M., Carmel-Harel, O., Eisen, M. B., Storz, G., Botstein, D., and Brown, P. O., Genomic expression programs in the response of yeast cells to environmental changes, *Mol Biol Cell, 11*, 4241 (2000).
119. Davies, K. J., Lin, S. W., and Pacifici, R. E., Protein damage and degradation by oxygen radicals. IV. Degradation of denatured protein, *J Biol Chem, 262*, 9914 (1987).
120. Finkel, T., and Holbrook, N. J., Oxidants, oxidative stress and the biology of ageing, *Nature, 408*, 239 (2000).
121. Aliev, G., Smith, M. A., Seyidov, D., Neal, M. L., Lamb, B. T., Nunomura, A., Gasimov, E. K., Vinters, H. V., Perry, G., LaManna, J. C., and Friedland, R. P., The role of oxidative stress in the pathophysiology of cerebrovascular lesions in Alzheimer's disease, *Brain Pathol, 12*, 21 (2002).
122. Kovacic, P., and Jacintho, J. D., Mechanisms of carcinogenesis: focus on oxidative stress and electron transfer, *Curr Med Chem, 8*, 773 (2001).
123. Zheng, M., Aslund, F., and Storz, G., Activation of the OxyR transcription factor by reversible disulfide bond formation, *Science, 279*, 1718 (1998).
124. Humphries, K. M., Juliano, C., and Taylor, S. S., Regulation of cAMP-dependent protein kinase activity by glutathionylation, *J Biol Chem* (2002).
125. Fuangthong, M., and Helmann, J. D., The OhrR repressor senses organic hydroperoxides by reversible formation of a cysteine-sulfenic acid derivative, *Proc Natl Acad Sci U S A, 99*, 6690 (2002).
126. Scott, C., and Green, J., Miscoordination of the iron-sulfur clusters of the anaerobic transcription factor, FNR, allows simple repression but not activation, *J Biol Chem, 277*, 1749 (2002).
127. Tsai, B., and Rapoport, T. A., Unfolded cholera toxin is transferred to the ER membrane and released from protein disulfide isomerase upon oxidation by Ero1, *J Cell Biol, 159*, 207 (2002).
128. Lumb, R. A., and Bulleid, N. J., Is protein disulfide isomerase a redox-dependent molecular chaperone?, *Embo J, 21*, 6763 (2002).
129. Tsai, B., Rodighiero, C., Lencer, W. I., and Rapoport, T. A., Protein disulfide isomerase acts as a redox-dependent chaperone to unfold cholera toxin, *Cell, 104*, 937 (2001).
130. Jakob, U., Eser, M., and Bardwell, J. C., Redox switch of hsp33 has a novel zinc-binding motif, *J Biol Chem, 275*, 38302 (2000).
131. Graf, P. C., Martinez-Yamout, M., VanHaerents, S., Lilie, H., Dyson, H. J., and Jakob, U., Activation of the redox-regulated chaperone Hsp33 by domain unfolding, *J Biol Chem, 279*, 20529 (2004).
132. Raman, B., Siva Kumar, L. V., Ramakrishna, T., and Mohan Rao, C., Redox-regulated chaperone function and conformational changes of Escherichia coli Hsp33, *FEBS Lett, 489*, 19 (2001).
133. Graumann, J., Lilie, H., Tang, X., Tucker, K. A., Hoffmann, J. H., Vijayalakshmi, J., Saper, M., Bardwell, J. C., and Jakob, U., Activation of the redox-regulated molecular chaperone Hsp33--a two-step mechanism, *Structure (Camb), 9*, 377 (2001).
134. Christman, M. F., Storz, G., and Ames, B. N., OxyR, a positive regulator of hydrogen peroxide-inducible genes in Escherichia coli and Salmonella typhimurium, is homologous to a family of bacterial regulatory proteins, *Proc Natl Acad Sci U S A, 86*, 3484 (1989).
135. Hausladen, A., Privalle, C. T., Keng, T., DeAngelo, J., and Stamler, J. S., Nitrosative stress: activation of the transcription factor OxyR, *Cell, 86*, 719 (1996).
136. Storz, G., and Tartaglia, L. A., OxyR: a regulator of antioxidant genes, *J Nutr, 122*, 627 (1992).

137. Kullik, I., Toledano, M. B., Tartaglia, L. A., and Storz, G., Mutational analysis of the redox-sensitive transcriptional regulator OxyR: regions important for oxidation and transcriptional activation, *J Bacteriol, 177*, 1275 (1995).
138. Lee, C., Lee, S. M., Mukhopadhyay, P., Kim, S. J., Lee, S. C., Ahn, W. S., Yu, M. H., Storz, G., and Ryu, S. E., Redox regulation of OxyR requires specific disulfide bond formation involving a rapid kinetic reaction path, *Nat Struct Mol Biol, 11*, 1179 (2004).
139. Toledano, M. B., Kullik, I., Trinh, F., Baird, P. T., Schneider, T. D., and Storz, G., Redox-dependent shift of OxyR-DNA contacts along an extended DNA- binding site: a mechanism for differential promoter selection, *Cell, 78*, 897 (1994).
140. Wong, C., Sridhara, S., Bardwell, J. C., and Jakob, U., Heating greatly speeds Coomassie blue staining and destaining, *Biotechniques, 28*, 426 (2000).
141. Lottspeich, F., and Zorbas, H., *Bioanalytik*, Spektrum Akademischer Verlag, Heidelberg,Berlin (1998).
142. Madeker, J., Reinigung und Charakterisierung prokaryotischer Stressproteine, in *Biophysik und physikalische Biochemie*, Universität Regensburg, Regensburg (1992).
143. Buchberger, A., Schroder, H., Buttner, M., Valencia, A., and Bukau, B., A conserved loop in the ATPase domain of the DnaK chaperone is essential for stable binding of GrpE, *Nat Struct Biol, 1*, 95 (1994).
144. Gill, S. C., and von Hippel, P. H., Calculation of protein extinction coefficients from amino acid sequence data, *Anal Biochem, 182*, 319 (1989).
145. Bradford, M. M., A rapid and sensitive method for the quantitation of microgram quantities of protein utilizing the principle of protein-dye binding., *Anal Biochem, 72*, 248 (1976).
146. Compton, S. J., and Jones, C. G., Mechanism of dye response and interference in the Bradford protein assay., *Anal Biochem, 151*, 369 (1985).
147. Hunt, J. B., Neece, S. H., and Ginsburg, A., *Anal Biochem, 146*, 150 (1985).
148. Bardwell, J. C., and Craig, E. A., Major heat shock gene of Drosophila and the Escherichia coli heat-inducible dnaK gene are homologous, *Proc Natl Acad Sci U S A, 81*, 848 (1984).
149. Palleros, D. R., Reid, K. L., McCarty, J. S., Walker, G. C., and Fink, A. L., DnaK, hsp73, and their molten globules. Two different ways heat shock proteins respond to heat, *J Biol Chem, 267*, 5279 (1992).
150. Montgomery, D., Jordan, R., McMacken, R., and Freire, E., Thermodynamic and structural analysis of the folding/unfolding transitions of the Escherichia coli molecular chaperone DnaK, *J Mol Biol, 232*, 680 (1993).
151. Schroder, H., Langer, T., Hartl, F. U., and Bukau, B., DnaK, DnaJ and GrpE form a cellular chaperone machinery capable of repairing heat-induced protein damage, *Embo J, 12*, 4137 (1993).
152. Buchner, J., Grallert, H., and Jakob, U., Analysis of chaperone function using citrate synthase as nonnative substrate protein, *Methods Enzymol, 290*, 323 (1998).
153. Herbst, R., Schafer, U., and Seckler, R., Equilibrium intermediates in the reversible unfolding of firefly (Photinus pyralis) luciferase, *J Biol Chem, 272*, 7099 (1997).
154. Mayer, M. P., Laufen, T., Paal, K., McCarty, J. S., and Bukau, B., Investigation of the interaction between DnaK and DnaJ by surface plasmon resonance spectroscopy, *J Mol Biol, 289*, 1131 (1999).
155. Mogk, A., Tomoyasu, T., Goloubinoff, P., Rudiger, S., Roder, D., Langen, H., and Bukau, B., Identification of thermolabile Escherichia coli proteins: prevention and reversion of aggregation by DnaK and ClpB, *Embo J, 18*, 6934 (1999).

156. Shi, W., Zhou, Y., Wild, J., Adler, J., and Gross, C. A., DnaK, DnaJ, and GrpE are required for flagellum synthesis in Escherichia coli, *J Bacteriol, 174*, 6256 (1992).
157. Sambrook, J., Fritsch, E. F., and Maniatis, T., *Molecular Cloning: A Laboratory Manual*, Cold Spring Harbor Lab. Press, Plainview, NY (1989).
158. Meyer, S., Noisommit-Rizzi, N., Reuss, M., and Neubauer, P., Optimized analysis of intracellular adenosine and guanosine phosphates in Escherichia coli, *Anal Biochem, 271*, 43 (1999).
159. Yang, N. C., Ho, W. M., Chen, Y. H., and Hu, M. L., A convenient one-step extraction of cellular ATP using boiling water for the luciferin-luciferase assay of ATP, *Anal Biochem, 306*, 323 (2002).
160. Korber, P., Zander, T., Herschlag, D., and Bardwell, J. C., A new heat shock protein that binds nucleic acids, *J Biol Chem, 274*, 249 (1999).
161. Diamant, S., Ben-Zvi, A. P., Bukau, B., and Goloubinoff, P., Size-dependent disaggregation of stable protein aggregates by the DnaK chaperone machinery, *J Biol Chem, 275*, 21107 (2000).
162. Banecki, B., and Zylicz, M., Real time kinetics of the DnaK/DnaJ/GrpE molecular chaperone machine action, *J Biol Chem, 271*, 6137 (1996).
163. Prinz, W. A., Aslund, F., Holmgren, A., and Beckwith, J., The role of the thioredoxin and glutaredoxin pathways in reducing protein disulfide bonds in the Escherichia coli cytoplasm, *J Biol Chem, 272*, 15661 (1997).
164. Bessette, P. H., Aslund, F., Beckwith, J., and Georgiou, G., Efficient folding of proteins with multiple disulfide bonds in the Escherichia coli cytoplasm, *Proc Natl Acad Sci U S A, 96*, 13703 (1999).
165. Fenn, T. D., Ringe, D., and Petskoa, G. A., POVScript+: a program for model and data visualization using persistence of vision ray-tracing, *J. Appl. Cryst., 36*, 944 (2003).
166. Nicholls, A., Sharp, K. A., and Honig, B., Protein folding and association: insights from the interfacial and thermodynamic properties of hydrocarbons, *Proteins, 11*, 281 (1991).
167. Buchberger, A., Gassler, C. S., Buttner, M., McMacken, R., and Bukau, B., Functional defects of the DnaK756 mutant chaperone of Escherichia coli indicate distinct roles for amino- and carboxyl-terminal residues in substrate and co-chaperone interaction and interdomain communication, *J Biol Chem, 274*, 38017 (1999).
168. Lu, Z., and Cyr, D. M., The conserved carboxyl terminus and zinc finger-like domain of the co- chaperone Ydj1 assist Hsp70 in protein folding, *J Biol Chem, 273*, 5970 (1998).
169. Suh, W. C., Lu, C. Z., and Gross, C. A., Structural features required for the interaction of the Hsp70 molecular chaperone DnaK with its cochaperone DnaJ, *J Biol Chem, 274*, 30534 (1999).
170. Suh, W. C., Burkholder, W. F., Lu, C. Z., Zhao, X., Gottesman, M. E., and Gross, C. A., Interaction of the Hsp70 molecular chaperone, DnaK, with its cochaperone DnaJ, *Proc Natl Acad Sci U S A, 95*, 15223 (1998).
171. Tomoyasu, T., Mogk, A., Langen, H., Goloubinoff, P., and Bukau, B., Genetic dissection of the roles of chaperones and proteases in protein folding and degradation in the Escherichia coli cytosol, *Mol Microbiol, 40*, 397 (2001).
172. Osorio, H., Carvalho, E., del Valle, M., Gunther Sillero, M. A., Moradas-Ferreira, P., and Sillero, A., H2O2, but not menadione, provokes a decrease in the ATP and an increase in the inosine levels in Saccharomyces cerevisiae. An experimental and theoretical approach, *Eur J Biochem, 270*, 1578 (2003).

173. Hyslop, P. A., Hinshaw, D. B., Scraufstatter, I. U., Cochrane, C. G., Kunz, S., and Vosbeck, K., Hydrogen peroxide as a potent bacteriostatic antibiotic: implications for host defense, *Free Radic Biol Med, 19*, 31 (1995).
174. Moro, F., Fernandez, V., and Muga, A., Interdomain interaction through helices A and B of DnaK peptide binding domain, *FEBS Lett, 533*, 119 (2003).
175. Wunderlich, M., and Glockshuber, R., Redox properties of protein disulfide isomerase (DsbA) from Escherichia coli, *Protein Sci, 2*, 717 (1993).
176. Karlin, S., and Brocchieri, L., Heat shock protein 70 family: multiple sequence comparisons, function, and evolution, *J Mol Evol, 47*, 565 (1998).
177. Hyslop, P. A., Hinshaw, D. B., Halsey, W. A., Jr., Schraufstatter, I. U., Sauerheber, R. D., Spragg, R. G., Jackson, J. H., and Cochrane, C. G., Mechanisms of oxidant-mediated cell injury. The glycolytic and mitochondrial pathways of ADP phosphorylation are major intracellular targets inactivated by hydrogen peroxide, *J Biol Chem, 263*, 1665 (1988).
178. Weber, H., Engelmann, S., Becher, D., and Hecker, M., Oxidative stress triggers thiol oxidation in the glyceraldehyde-3-phosphate dehydrogenase of Staphylococcus aureus, *Mol Microbiol, 52*, 133 (2004).
179. Slepenkov, S. V., and Witt, S. N., The unfolding story of the Escherichia coli Hsp70 DnaK: is DnaK a holdase or an unfoldase?, *Mol Microbiol, 45*, 1197 (2002).
180. Danshina, P. V., Schmalhausen, E. V., Avetisyan, A. V., and Muronetz, V. I., Mildly oxidized glyceraldehyde-3-phosphate dehydrogenase as a possible regulator of glycolysis, *IUBMB Life, 51*, 309 (2001).
181. Grimshaw, J. P., Jelesarov, I., Schonfeld, H. J., and Christen, P., Reversible thermal transition in GrpE, the nucleotide exchange factor of the DnaK heat-shock system, *J Biol Chem, 276*, 6098 (2001).
182. Woo, H. A., Chae, H. Z., Hwang, S. C., Yang, K. S., Kang, S. W., Kim, K., and Rhee, S. G., Reversing the inactivation of peroxiredoxins caused by cysteine sulfinic acid formation, *Science, 300*, 653 (2003).
183. Bulteau, A. L., Ikeda-Saito, M., and Szweda, L. I., Redox-dependent modulation of aconitase activity in intact mitochondria, *Biochemistry, 42*, 14846 (2003).
184. Schuppe-Koistinen, I., Moldeus, P., Bergman, T., and Cotgreave, I. A., S-thiolation of human endothelial cell glyceraldehyde-3-phosphate dehydrogenase after hydrogen peroxide treatment, *Eur J Biochem, 221*, 1033 (1994).
185. Wawrzynow, A., Banecki, B., Wall, D., Liberek, K., Georgopoulos, C., and Zylicz, M., ATP hydrolysis is required for the DnaJ-dependent activation of DnaK chaperone for binding to both native and denatured protein substrates, *J Biol Chem, 270*, 19307 (1995).
186. Buchberger, A., Theyssen, H., Schroder, H., McCarty, J. S., Virgallita, G., Milkereit, P., Reinstein, J., and Bukau, B., Nucleotide-induced conformational changes in the ATPase and substrate binding domains of the DnaK chaperone provide evidence for interdomain communication, *J Biol Chem, 270*, 16903 (1995).
187. Tang, W., and Wang, C. C., Zinc fingers and thiol-disulfide oxidoreductase activities of chaperone DnaJ, *Biochemistry, 40*, 14985 (2001).
188. Linke, K., Wolfram, T., Bussemer, J., and Jakob, U., The roles of the two zinc binding sites in DnaJ, *J Biol Chem, 278*, 44457 (2003).
189. Goffin, L., and Georgopoulos, C., Genetic and biochemical characterization of mutations affecting the carboxy-terminal domain of the Escherichia coli molecular chaperone DnaJ, *Mol Microbiol, 30*, 329 (1998).

190. Russell, R., Wali Karzai, A., Mehl, A. F., and McMacken, R., DnaJ dramatically stimulates ATP hydrolysis by DnaK: insight into targeting of Hsp70 proteins to polypeptide substrates, *Biochemistry, 38*, 4165 (1999).
191. Li, J., and Sha, B., Structure-based mutagenesis studies of the peptide substrate binding fragment of type I Heat shock protein 40, *Biochem J, 25*, 25 (2004).
192. Bittner, M., and Vapnek, D., Versatile cloning vectors derived from the runaway-replication plasmid pKN402, *Gene, 15*, 319 (1981).

8 Publications

i. **Linke, K. and Jakob, U**., Not every disulfide lasts forever: disulfide bond formation as a redox switch, *Antioxid Redox Signal, 5*, 425 (2003).

ii. **Linke, K., Wolfram, T., Bussemer, J., and Jakob, U.**, The roles of the two zinc binding sites in DnaJ, *J Biol Chem, 278*, 44457 (2003).

iii. **Hoffmann, J. H., Linke, K., Graf, P. C., Lilie, H., and Jakob, U**., Identification of a redox-regulated chaperone network, *Embo J, 23*, 160 (2004).

iv. **Winter, J., Linke, K., Jatzek, A., and Jakob, U.**, Severe stress causes inactivation of DnaK and Activation of the redox-regulated chaperone Hsp33, *Mol Cell, in press* (2005).

Congress Contributions

i. Poster at the *2003 Molecular Genetics of Bacteria/Phages Conference* in Madison, WI, USA: **Linke, K., Wolfram, T., Bussemer, J., and Jakob, U.**, The roles of the two zinc binding sites in DnaJ, *J Biol Chem, 278*, 44457 (2003).

ii. Talk at the *9th Midwest Stress Response and Chaperone Meeting* in Evanston, IL, USA: **Winter, J., Linke, K., Jatzek, A., and Jakob, U.**, Severe stress causes inactivation of DnaK and Activation of the redox-regulated chaperone Hsp33, *Mol Cell, in press* (2005).

Acknowledgments

I would like to thank the following people very much and appreciatively acknowledge them for contributing in many different ways to make this work possible:

- Dr. Johannes Buchner, my 'Doktorvater', for his supervision and support of my Ph.D. project.
- Dr. Ursula Jakob for her outstanding mentorship and her generosity in sharing scientific and material support of her lab. Her enthusiasm and her willingness to engage in frequent discussions was an invaluable source of inspiration as I worked through the challenges of my project.
- Dr. James Bardwell for offering excellent scientific advice, opportunities for discussions and the use if his lab resources at varies points during my work.
- Dr. R. Bender, Dr. B. Bukau, Dr. C. Duan and Dr. M. Mayer for providing strains, plasmids, protocols, lab equipment or helpful discussions.
- The members of the Jakob and Bardwell labs for the wonderful time we spent together inside and outside of lab and for always being such helpful and supportive co-workers. Dr. Jeannette Winter and Anna Jatzek for their efforts to make the "Three Engel Project" a success. Tobias Wolfram and Johanna Bussemer for their help with the DnaJ zinc center mutants during their time as practical students in the Jakob lab. Dr. Jörg Hoffmann, Paul Graf, Dr. Stefan Gleiter and Lars Leichert for always having an answer to my many questions. My bench neighbor Jutta Hager for being there during the more stressful moments of my research and Caroline Kumsta for bringing much energy and good cheer to our lab.
- The lab managers Tina Kelley, Aaron Kleinjans and Christie Parish as well as the 'workstudies' for their tremendous help and efficiency in keeping the lab running smoothly.
- My friends from sailing, rock climbing and the GA Co-op who gave me the chance to experience Ann Arbor and Michigan more fully and whose company energized me for my research.
- And especially my parents for their constant support, acceptance of my need to work in distant places and their generosity in making a comfortable space for me when I returned.